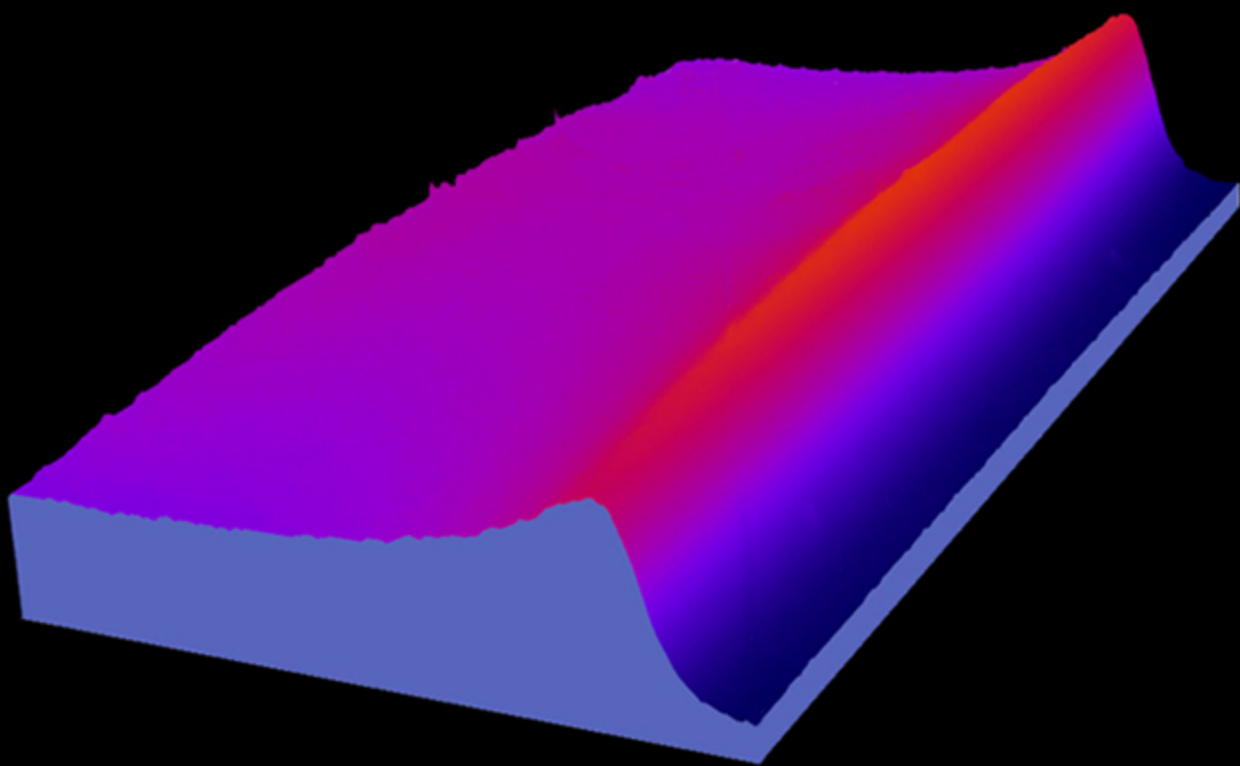


2013 ACTIVITY REPORT

TECHNICAL UNIT
DEVELOPMENT and APPLICATIONS
of RADIATION



ENEA

Italian National Agency for New Technologies,
Energy and Sustainable Economic Development

2013

ACTIVITYREPORT

UTAPRADTECHNICALUNIT

UTAPRAD DIRECTOR

Roberta Fantoni

roberta.fantoni@enea.it



SCIENTIFIC EDITORS

Roberta Fantoni

Antonio Palucci

Giuseppe Dattoli

Rosa Maria Montereali

Gian Piero Gallerano

DESIGN AND COMPOSITION

Flavio Miglietta

EXTERNAL RELATIONS

Monica Cimino

LABORATORY WEBSITE : <http://www.frascati.enea.it/utaprad/>

PUBLISHED BY : ENEA - Via Enrico Fermi, 45 - 00044 Frascati, Rome, Italy

CONTENTS

1. UTAPRAD	7
1.1 Ultrafast laser spectroscopy laboratory at ENEA Casaccia	7
1.2 Spectroscopy for food quality	7
1.3 Characterization of materials for energy and other applications	8
2. DIAGNOSTICS AND METROLOGY LABORATORY	11
2.1 Mission and infrastructures	11
2.2 Diagnostic for security	13
2.3 Diagnostics for safety	27
2.4 Environmental diagnostic related to climate changes	29
2.5 Diagnostics for cultural heritage preservation and fruition	37
2.6 Laser spectroscopic material characterization	44
2.7 Technology for energy	45
3. MATHEMATICAL MODELING LABORATORY	49
3.1 Mission and infrastructures	49
3.2 CARM Development	49
3.3 SPARC activity	52
3.4 Applied Mathematics and theoretical physics activity	54
4. PHOTONICS MICRO AND NANO-STRUCTURES LABORATORY	55
4.1 Mission and infrastructures	55
4.2 Nanostructures and spectroscopies for renewable energy	56
4.3 Luminescent radiation detectors, light-emitting waveguides and nanostructures for spectroscopy, imaging and dosimetry	62
4.4 Nanostructures assessment of SERS activity and enhancement factors for highly sensitive gold coated substrates probed with explosive molecules	69
4.5 Optical fiber sensors and nanostructures functionalised for industrial applications and cultural heritage	71
5. RADIATION SOURCES LABORATORY	75
5.1 Mission and infrastructures	75
5.2 Short-wavelength Sources and Applications	75
5.3 Optical systems for solar technologies	79
5.4 Terahertz sources and applications	83
5.5 Accelerators development	87
5.6 “Olocontrollo emulativo” technology	90
5.7 Contributions to other projects	91
6. LIST OF PERSONNEL	92
7. RESEARCH PRODUCTS	94
7.1 Patents	94
7.2 Peer review papers with impact factor (I.F.)	94
7.3 Conference presentations and proceedings, other scientific papers	99
7.4 Technical reports	107
7.5 Prizes	109

PREFACE

UTAPRAD, in its fourth year of existence, has been subjected to a few important rearrangements involving the personnel, as single and groups. At the end of 2012 and beginning of 2013 a significant turnover occurred with the entrance of 8 new permanent staff members, after the 2010 national recruitment, and other 2 by internal transfer. Additional personnel (4 units) started to work with temporary contracts on TOP IMPLART project. Meanwhile the group (5 units) dedicated to seismic microzonation joined back its historical unit (in UTPRA), and the staff of the laboratory for laser ultrafast spectroscopy in ENEA C.R. Casaccia returned to UTAPRAD, where it belonged in the former structure. Taking into account all in and out movements, and retirements in the last two years, the staff numerical consistency remained about constant, at a value slight below 100.

It is my pleasure to dedicate this issue to dr. Elisabetta Borsella, who retired in February 2013 after a long career at ENEA C.R. Frascati, in UTAPRAD (former FIS), in which she was the coordinator or the scientific responsible for ENEA of several European projects (from FP4 to FP7), becoming a renowned European expert in the field of nanotechnologies.

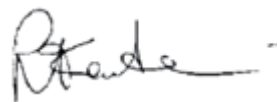
In 2013 UTAPRAD R&D activities went on mostly following the selected strategic lines for applied research projects aimed at the development and implementation of:

- Sensors and devices suitable to increase the reliability and security of systems for detection of hazardous and noxious substances, to improve food quality control systems and to promote innovation in industrial monitoring.
- Systems and instrumentation for environmental diagnostics, suitable to control marine ecosystems and gas-traces in the atmosphere, including integration and validation with satellite imagery.
- Dedicated prototypes, based on non invasive techniques, for the preservation and conservation of cultural heritage, including tools for its larger and better fruition.
- Instrumentation and apparatus for bio-medical applications, with new approaches to diagnostics, imaging and oncologic therapies.
- Technologies and methodologies for design, fabrication, characterization and functionalization of nanostructures, light-emitting micro-devices, radiation detectors and fiber optics for photonics with applications relevant to industry, bio-medicine and renewable energy.
- Research infrastructures, including the dedicated design and measurement techniques, physic-mathematical models of complex problems, needed to build up particle accelerators and broadly tunable laser sources for investigation biological systems, for material characterization and innovative technologies in micro-mechanics and micro-electronics.

In 2013 European research activities on Security at UTAPRAD have seen the final demonstration of STANDEX (with RADEX and BCT NATO projects) at a Metro station in Paris. The beginning of the new demonstration action EDEN, in which UTAPRAD coordinates other ENEA technical units, also occurred at the end of the same year. Our fluorescence lidar system for sea-waters monitoring returned after 10 years in Antarctica joining the oceanographic campaign associate to the XXIXth Italian mission funded by PNRA. Research activities addressed to diagnostics for Cultural Heritage preservation continued both at international (Italy-Japan and Italy-Serbia bilateral projects, agreement with Musei Vaticani) and national level. Outstanding international awards were achieved by UTAPRAD personnel for researches on Security system and Cultural Heritage diagnostics and Free Electron Lasers development. The Regional funded project on the development of a linear accelerator for proton therapy (TOP IMPLART) registered its first year of activity, with the construction of first modules of the machine and preliminary experiments relevant to proton beam characterization, dosimetry and

irradiation of cells at low energy (3.5 – 7 MeV). A significant effort to focus most human resources on these leading activities was carried out, which is supported by major results here described. Furthermore in 2013 a remarkable increase of qualified commercial activities (external service, measurements on demand and consultant reports) has been recorded, as mentioned in the following. Results are presented as obtained in each of the 4 Laboratories (second level macrostructure units) in Frascati and in the additional laboratory in Casaccia.

As usual, have a nice reading !



Roberta Fantoni

(UTAPRAD director)



1. UTAPRAD

1.1 Ultrafast laser spectroscopy laboratory at ENEA Casaccia

The 2013 activity was aimed at exploiting the applications of optical and laser spectroscopy in selected fields of interest for ENEA's mission relevant projects are indicated in specific cases.

Main available instrumental facilities consist of:

- Ti:sapphire femtosecond laser with cavity dumper and second harmonic generator;
- Ti:sapphire nanosecond laser with second harmonic generator;
- UV-VIS-NIR spectrophotometer with integrating sphere and specular reflectance attachment;
- FTIR spectrophotometer;
- Spectrofluorimeter with double monochromators and photon counting detection;
- Multi-excitation wavelength micro-macro Raman system;
- Dynamic Light Scattering;
- High power ultrasonic probe.

1.2 Spectroscopy for food quality

Application of spectroscopy as non-destructive test tool in the field of food qualification was exploited in two projects both coordinated by UTAGRI, aimed at assessing fruit deterioration during transportation from the harvesting site to far away markets. In the frame of "ORTOFRULOG" project, Raman and fluorescence measurements were performed in collaboration with dr. Domenica Masci and dr. Maria Sighicelli (UTAGRI) on selected fruits as tangerines, strawberries and grapes, to measure the evolution of the content of carotenoids, and of anthocyanines after inoculation of fungi. Raman measurements were performed on tangerines using a micro-Raman setup with 532 nm laser excitation,

allowing detection of the carotenoid band as a function of the fungi inoculation time and of the distance from the inoculated spot. Raman detection of anthocyanines band in grapes and strawberries was not possible because of strong background fluorescence, so their content was estimated using conventional fluorimetry, performed using a Horiba-Jobin-Yvon Fluorolog 3-22 commercial fluorimeter. As a second application, in the context of "MAGAZZINO VIAGGIANTE" project, an experimental setup for Time Resolved Reflectivity Spectroscopy (TRS) measurements was proposed, designed, and built, to optically characterize the firmness of fruits and their relative content of selected molecules. The TRS technique is based on the measurement of the time-dependence of the diffuse reflection of an ultrafast pulse by a scattering sample. In a biological sample, as a fruit, near-infrared pulses can penetrate the surface, so by measurements of the diffusely reflected pulse broadening and attenuation valuable information can be obtained, which can be put in relationship with the internal tissue structure and absorbing species content. In the experimental apparatus, the ultrashort pulse generated by a Coherent MIRA-F laser is delivered to the sample fruit using an optical fiber. The diffusely reflected light is collected by a second optical fiber placed at some centimeters from the injection point, and is detected by a photomultiplier whose output is fed to a PC card for time-correlated single photon counting (TCSPC) measurements. Preliminary measurements were performed to assess the time response of the system, or instrumental response function (IRF), and subsequently to prove its functionality on a real fruit.

Data shown in Figure 1.1 demonstrate the pulse delay and broadening effect due to propagation inside an apple tissue. Work is in progress to set up models to analyze the

experimental data; a systematic measurements run is scheduled according to the project planning.

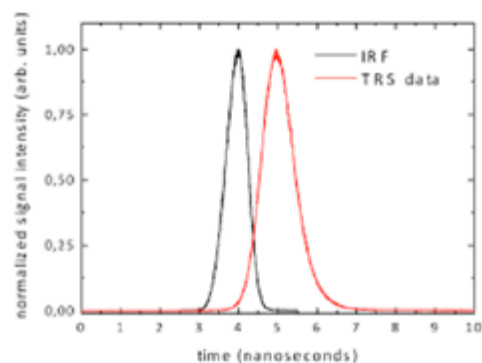


Fig. 1.1 - Instrumental response function (IRF) of the time-resolved reflectivity setup and TRS experimental data measured on a Fuji apple. Pulse delay and broadening due to propagation in the biological tissue is apparent.

1.3 Characterization of materials for energy and other applications

Realization and characterization of nanoporous electrodes for renewable energies

In the field of renewable energies, the activity was mainly directed to production and characterization of porous electrodes based on titania nanoparticles. These electrodes find wide application in photovoltaics, being one of the most intensively studied components of dye-sensitized solar cells (DSSC), and in hydrogen production by water splitting. Moreover they can be considered a model system for many other applications, as photocatalysis, sensors, and rechargeable batteries.

Nanoporous titania electrode application in DSSC was studied in collaboration with dr. Serena Gagliardi (UTTMAT-SUP), using an optoelectronic method to characterize the dynamic response of a DSSC to pulsed monochromatic excitation. An experimental setup to measure the short-circuit photocurrent transients produced by a DSSC subjected to a pulsed monochromatic beam was used, and

the time dependence of the photocurrent was analysed, obtaining the characteristic response time of the device. The dependence of the characteristic time on the excitation wavelength can be used to obtain information on the photogenerated carrier transport inside the photoanode. A charge transport model was adapted from the literature to simulate the cell response, and to help interpret the experimental data in terms of sensitizing dye absorbance and charge trapping-detrapping processes. Figure 1.2 shows the experimental response times as function of the dye absorbance, together with model results. While the model can reasonably account for the observed dependence, a better agreement in the low-intermediate absorptivity region could be obtained accounting for the details of the optical properties of the photoanode. Work is in progress in this direction. This activity was developed as a master thesis work of a student in Materials Science and Technology at the University of Tor Vergata.

The closely related topic of charge transport in pure and nitrogen-doped titania porous electrodes for water-splitting applications was also studied using a photoelectrochemical method, in collaboration with dr. Claudia Paoletti (UTRINN-IFC) and dr. Serena Gagliardi (UTTMAT-SUP). Porous electrodes were fabricated using screen-printable pastes in collaboration with dr. Rosaria D'Amato (UTAPRAD-MNF) using pure and nitrogen-doped TiO₂ nanopowders produced by laser-assisted pyrolysis in the MNF Laboratory. The current generated by the photo-assisted water-splitting process in electrodes deposited on TCO-coated glass substrates was measured in a photoelectrochemical cell as a function of the excitation wavelength; from analysis of data collected when the electrode is illuminated through the front or back side, the electron diffusion length in the electrode can be obtained. Preliminary results of this investigation do not confirm an overall positive role of nitrogen doping on electron transport. However doping is supposed to affect several properties of the material, as the electronic

band structure, defects, trapping properties, and moreover unintentional property changes could be produced by the slight differences in the synthesis procedure necessary to induce doping. Disentanglement of these various effects is necessary to assess the potential of nitrogen-doped nanophase titania for water-splitting applications.

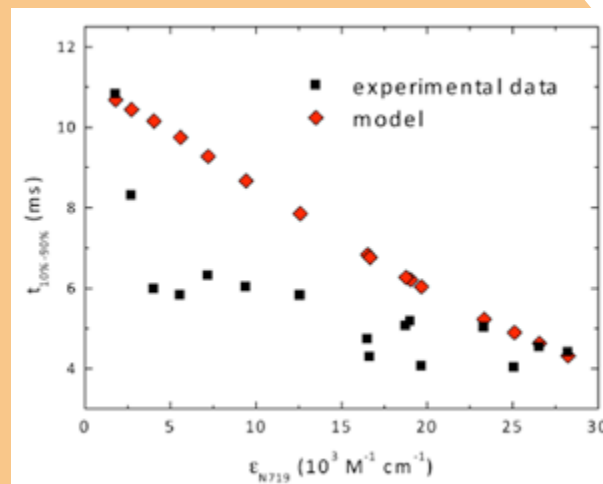


Fig. 1.2 - Experimental and modelled photocurrent response time to pulsed monochromatic light of a dye-sensitized solar cell as a function of N719 sensitizer dye absorptivity.

Use of titania nanopowders for energy saving applications based on advanced heat exchange fluids was also investigated in collaboration with dr. Flaminia Rondino (UTAPRAD-MNF), with an experimental setup aimed at measuring the thermal diffusivity in nanofluids using a purely-optical technique; details on this activity are reported in sect. 4.2.

Characterization of nanomaterials for lighting application

In the field of advanced functional materials, photoluminescence and Raman measurements were performed in the frame of international cooperation with India (Kanya Maha Vidyalaya college and Punjab Technical University, Jalandhar, Punjab) and China, (East China University of Science and Technology, Shanghai) on glasses and glass-

ceramics for applications in phosphors and light-emitting devices. Rare-earth doped materials were studied in collaboration with Indian research institutions; as an example of this activity we show in Figure 1.3 the visible emission spectra and the Raman spectra of a Dy³⁺ doped oxyfluoride glass as-prepared and after annealing at increasing times. Annealing produces nucleation and growth of nanocrystals inside the glass matrix. The Raman spectra of samples show the progressive appearance of bands due to nanocrystals; also the Dy³⁺ emission is affected by the process because the rare earth environment changes and moreover segregation of Dy³⁺ inside the nanocrystals can occur. Figure 1.3 (a) shows that the intensity ratio of the two emission bands of Dy³⁺ in the blue and yellow region

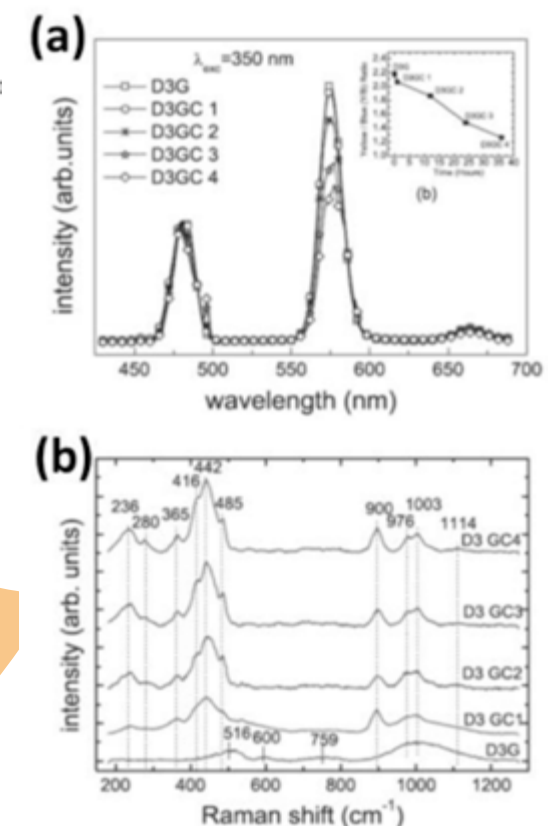


Fig. 1.3 - Visible photoluminescence spectra and Raman spectra of a Dy³⁺ doped oxyfluoride glass (D3G) as prepared and after annealing at 950 °C for 1, 12, 24, 36 hours (D3GC1-4).

changes with annealing. Therefore this study reveals the possibility to tune the color of the luminescence of the sample by changing the annealing time.

Raman spectroscopy of materials for rechargeable batteries

Application of spectroscopy to recycling of materials from exhausted lithium rechargeable batteries was exploited using Raman spectroscopy and Dynamic Light Scattering for characterization of materials contained in commercial accumulators, in a collaboration with dr. Maria Rita Mancini (UTTMAT-CHIM) in the frame of the ENEA MISE research agreements.

FTIR investigations of pigments in ancient Roman frescoes

In collaboration with the CNR Institute of Inorganic Methodologies and Plasmas, Fourier-transform infrared spectroscopy (FTIR) was applied to identification of pigments used in a Roman fresco found in the Ponti Novi settlement in the Sabina region. FTIR measurements were performed in the Attenuated Total Reflection (ATR) configuration, allowing accurate measurements using a very small amount of powder scratched from the sample. Comparison of the IR spectrum of the red pigment with the one of a red marble obtained from a quarry in the same area points out for the likely use of marble powder in the fabrication of the red pigment.

2. DIAGNOSTICS AND METROLOGY LABORATORY

2.1 Mission and infrastructures

The Diagnostic and Metrology Laboratory, included in the ENEA Frascati Research Centre, is mainly focused in the development of laser sensors for environmental monitoring applications in devoted outdoor campaigns. The implemented laser technologies are dedicated to find the state of the art in the electro-optical spectroscopic tools that are better tailored in terms of discrimination and sensitivity in diagnostic and metrology field of applications. More in details the allocated roles to the Laboratory are:

- the development of spectroscopic and optic systems for in-situ or remote (lidar systems) in sensing and metrological applications (Environment, Cultural Heritage, Security and Health);
- the development of compact and miniaturized sensors to be operated in hostile environments and space explorations;
- the development of imaging sensors for in-situ applications in different fields of interest supporting also data analysis and images release;
- the support to data merging of different active and passive optical sensors.

The competences available in the Laboratory are originated from the expertise in different scientific disciplines as laser spectroscopy, optics, active and passive sensors, terrestrial and marine biology, analytical chemistry, biology and data analysis. This know-how is fruitfully devoted to the development of sensors for scientific and industrial applications. In details the tasks and roles assigned are summarized into:

- the design, implementation and tests of compact optical systems for environmental active and passive remote sensing including harsh environments (polar and interplane-

tary explorations), Cultural Heritage and Security.

- the execution of monitoring campaigns with own instruments installed in dedicated payloads to be connected with terrestrial and/or marine autonomous robots or rovers, merging data from other sensors;
- the design, implementation and tests compact and/or imaging spectroscopic sensors for real time analysis of hazardous materials scattered in different matrices, for health applications and for the goods characterization;
- the development of optical tools for in-situ and remote sensing on demand of other UTS;
- the hardware upgrading of its own mobile laboratories for environmental monitoring (atmosphere, sea and terrestrial campaigns);
- the partnership in research activities in national and international joint ventures.

List of facilities and sensors developed by UTAPRAD-DIM during present activities are here summarized:

- Satellite oceanographic data analysis and merging laboratory
- Plant biology laboratory
- Environmental analytic laboratory
- LIBS + XRF laboratory
- Bio-electro-magnetism laboratory
- Atmospheric mobile lidar laboratory
- Molecular spectroscopy laboratory
- Artificial vision laboratory with laser scanning 3D sensor
- Lidar fluorosensor and LIF Scanning sensor

Fundings and projects

The research activities of the UTAPRAD-DIM Laboratory are mainly funded in the frame of the EC Framework Programmes FP7 SECURITY as coordinator of BONAS project (Bomb factory detection by Networks of Advanced Sensors), partner of CUSTOM project (Drugs And Precursors Sensing By Complementing Low Cost Multiple Techniques), partner of the FORLAB (Forensic Laboratory) and partner of a large demonstration project EDEN (a wide collaborative European project against CBRNE Events). Project coordinator of the RADEX project (Radar Detection of Explosives) and joining the BCT project (Big City Trial) both in the frame of the NATO Science for Peace special project STANDEX. In the same research area, partner of RAMBO (Rapid-Air Monitoring particle against Biological threats) a project funded in the frame of EDA (European Defense Agency).

In FP7 Environment theme, the laboratory participates to PERSEUS project (Policy-orientated marine Environmental Research for the Southern European Seas) and MYOCEAN (Ocean Monitoring And Forecasting) network and joined the PNRA RoME (Ross Sea Mesoscale Experiment) project during the XXIX oceanographic campaign.

Two European projects were funded by the European Research Council, CO2VOLC (Quantifying the global volcanic CO₂ cycle) and BRIDGE (Bridging the gap between gas emissions and geophysical observations at active volcanoes). International projects are also established through the Italian Foreign Office within the executive programme of cooperation in the field of science and technology with Israel in UNELAS (Underwater network of laser sensors for water monitoring) and "Study for the creation of Artistic Goods' 3D models merged with colorimetric and multispectral information" with Serbia. Furthermore at national level, the Laboratory holds research projects in the frame of MIUR and MISE (Industria 2015): IT@CHA finalized to boost the technological

innovation in maritime archaeology, joined consortia as CETMA and TRAIN, within the projects TRAMP (TRASporto in Sicurezza di Merci Pericolose), SAL@CQO (Sviluppo di un Apparato Laser per misure di spettroscopia molecolare per la Conservazione e il controllo di valori afferenti le Qualità Organolettiche dei prodotti alimentari con tecniche non invasive contro adulterazioni naturali e/o fraudolente), Incamp (Interazione del Campo Magnetico a frequenza di risonanza con enzimi e Proteine) from INAIL, or contract from EU institutions as EFDA and the project RIMA (Rete Integrata marina Mediterranea con Accesso a dati distribuiti) of Regione Liguria.

Under the theme Security the UTAPRAD DIM Laboratory has strengthened its commitment for a constructive networking with Large Industries and SMEs both at national and European level. Personnel are members of the Network of Detection of Explosives (NDE) supported by EU DG Home Affairs for short policy brief of organization of devoted conferences.

Moreover, DIM laboratory joined also the European lobby activities in IMG-S (Industrial and Research Stakeholders Group for Security), and in ENRCIP-DEMON (European Network on Critical Infrastructures - Detection of Explosive for non Aviation), at national level the Italian technological platform for Security (SERIT) and Photonics. In 2013 collaboration in existing partnerships were reinforced while the basis for new ones were created.

These actions aim on one side at ensuring a high level of cross-fertilization to fully exploit the possibilities arising from European and national funding schemes and on another side to enable market channels for exploitation of the laboratory scientific achievements.

2.2 Diagnostic for security

Rapid-Air Monitoring particle against biological threats (RAMBO)



Since 2001, due to diffusion of Anthrax spores by mail, the bioterrorism became a topic of great interest. The necessity to protect civilian population from attack of biological pathogen agents, involves the development of detectors for fast alert and identification of threats.

In this context DIM Laboratory is partner of the EDA (European Defense Agency) project RAMBO (Rapid-Air Monitoring particle against Biological threats) with the responsibility of the development of a SERS cells and of data processing. The aim of the project is the development of an advanced device for continuous monitoring of air threats particles to be detected and identified the threats in short time (<45 min) reducing the use of chemicals and reagents.

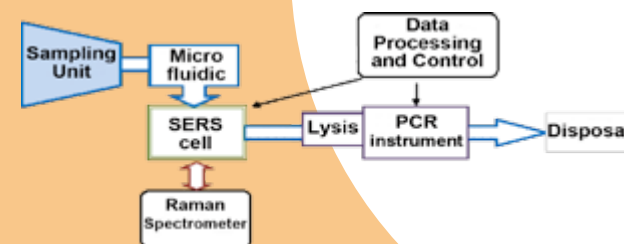


Fig. 2.0 - Concept of operation of the RAMBO sensor.

The idea of RAMBO includes the first detect-to-warn unit, based on SERS part, for the pre-alarm in air, then the second part of detect-to-threat based on real time PCR that allows the correct identification of the threats. This approach allows to start a proper response by the first responders. Figure 2.0 shows the scheme of whole device, while Figure 2.1 shows the Raman system assembled in our laboratory.

As required in the project, preparatory Raman measurements have been accomplished before

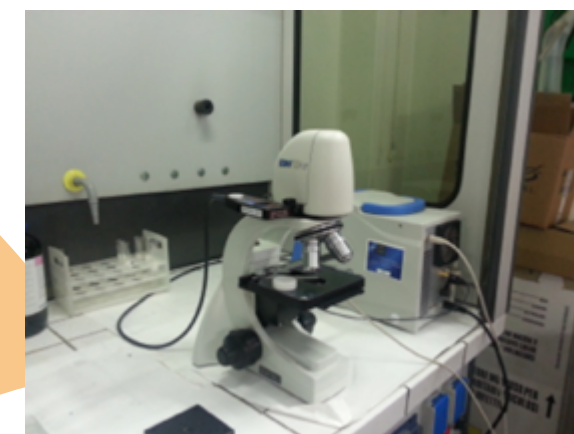


Fig. 2.1 - Raman system: $\lambda=789-1048$ nm (Raman shifts 75-3200 cm^{-1}) resolution 3 cm^{-1} . Laser source: GaAlAs diode emitting @785 nm. Tunable laser power between 3 - 300 mW. Detector, CCD with built-in thermoelectric cooler working at 10°C, with 2048 pixel (14 $\mu\text{m} \times 200 \mu\text{m}$).



Fig. 2.2 - Raman spectra of lilium spp pollen

testing Bacillus spp, by using both fresh pollens of lilium spp harvested during bloom, and on certified pollens: Populus deltoids (PD), Secale cereal (SC), Sorghum halepense (SH), Populus nigra italic (PN) (SIGMA Aldrich). A very large fluorescence emission was observed for all certified pollens. Even larger signals were obtained from lilium spp, (Fig. 2.2), apparently on the outside of the fresh pollen there is a chemical components that get lost during storage.

Safety regulations imposes to operate with simulants instead of Bacillus anthracis e.g. Bacillus atrophaeus, and Bacillus thuringiensis. SERS supports from Klarite have been implemented to enhance the Raman signal on spores and on vegetative cells. Raman spectra

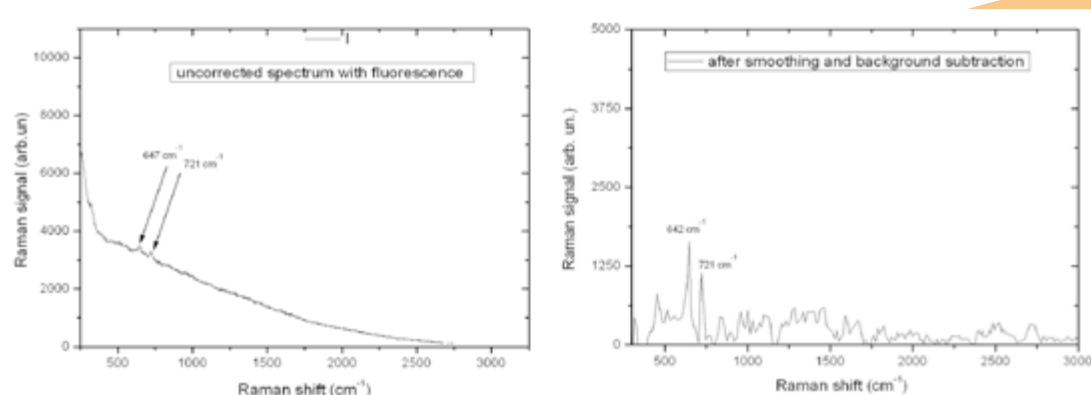


Fig. 2.3 - Uncorrected spectrum (left) and after smoothing (right) of *B. thuringiensis* vegetative cells

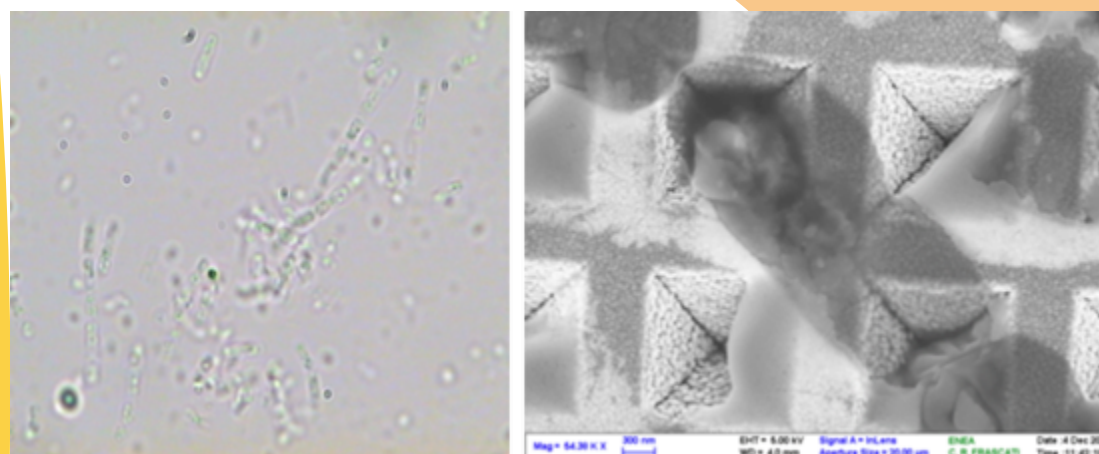


Fig. 2.4 - Vegetative cells of *Bacillus thuringiensis* at Microscope (100X) and SEM (right)

of *B. thuringiensis* vegetative cells are shown in Figure 2.3 with the respective microscope images in Figure 2.5. Two main peaks are emerging @ 647 and 721 cm^{-1} ; after smoothing and background subtraction (Fig. 2.3 right) no other relevant peaks are present. A possible interference is due to the culture medium.

Detection of drugs and precursors (CUSTOM)



The main objective of the CUSTOM project is to develop a portable device capable of detecting traces of precursor chemicals used in the manufacture of the

most dangerous drugs on the international market; the prompt and accurate detection of these chemicals strongly enhance the law enforcement also preventing their illicit uses.

In order to achieve this goal, an innovative instrument has been developed, based on a Gas Sampler feeding two sensors, namely the Laser Photoacoustic (LPAS unit) and LED Induced Fluorescence (FLUO unit), with a possibly concentrated air sample through the Drug Precursor Concentrator (PCU unit). A Master Control Board (MCB) collects the raw signals from the two sensors, provides storage in a permanent media and makes data available for subsequent analysis. The signal processing algorithms implement an accurate statistical model (MODEL) to analyze the acquired data



Fig. 2.5 - The complete CUSTOM sensor. The complete assembly in a portable case (Left). Open case, the LPAS and FLUO sensors are allocated inside (right).

and to compare them with library reference; the ultimate goal of the analysis is to define probability of presence of a predefined set of four drug precursors (BMK, Ephedrine, Safrole and Acetic anhydride).

The final version of the instrument was completed (Figure 2.5), then extensive laboratory and field tests have been started; here the major attention will be devoted to the results obtained by the control electronics, since robustness as well as an easy user interface are mandatory to achieve an elevated technological level.

ENEA has contributed to the realization of the control and power supply to provide the necessary functional support for the CUSTOM subassemblies. The design of the system is based on commercially available COTS components considering also technical aspects as: hours of operation, peak power loads, operating temperature, AC line noise. The heart of the control is the Mother Control Board (MCB) based on an ARM cortex-M3 microcontroller and a customized firmware is burned into the chip ROM flash where a Unix like real-time operating system runs. The microprocessor coordinated action upon the devices and sensors allows for sample processing, data acquisition and presentation of the results under control of the User. The final version of the board includes the

control for the sensors (LPAS and FLUO), the Pre-Concentrator unit, the air sampler and hydraulic circuit. User actions are entered via a TFT display panel with touch capability (Figure 2.6); Serial diagnostic interface (USB) and GPS device are connected as well.



Fig. 2.6 - The TFT panel display implements a user friendly interface by the definition and use of softkeys (touch buttons).

The firmware design was oriented towards the objective of maximize the system reliability, while not reducing the performances. This goal has been pursued by the use of a multi task architectural pattern dividing the software project into small and manageable individual threads. A non interruptible high privileged task takes the control of a number of individual threads each of them responsible for a specific subsystem. Within such design approach, a specific priority is assigned to each thread;

whenever necessary, privileged threads are allowed to have the highest priority to perform real-time operations and to quickly react to external events.

To have the highest sensitivity consistent with the current status of the art, a drug pre-concentrator unit was designed and realized by ENEA: its function is to absorb and concentrate drug precursors possibly present in the sampled air. As absorbent material inside the PCU, namely the syndiotactic polystyrene (sPS), was identified as cheap and robust commercial thermoplastic polymer. It has the peculiarity of having nanoporous crystal forms able to rapidly absorb apolar or poorly polar volatile organic compounds from water and air, also when present at very low concentrations. This result is achieved by means of a proper thermal treatment under the control of the MCB, which monitors all the chemical process of absorption and desorption up to the release of high concentration analyte to the measuring sensor.

Detection of explosive precursors BONAS (BOmb factory detection by Networks of Advanced Sensors)

BONAS

ENEA is coordinating the European project BONAS (BOmb factory detection by Networks of Advanced Sensors) for Security Call. The main aim of this project is to design, develop and test an innovative sensor wireless network (Figure 2.7), in order to increase citizen protection and homeland security from terrorist attacks, especially against the threat posed by improvised explosive devices, (IEDs). ENEA is in charge to support the development of two sensors, for volatile and particulate substances emitted or released in the surrounding environment. To achieve its objective, BONAS involves the realization of a lidar/DIAL remote sensor. Based on the spectroscopic research performed at ENEA in 2011 and 2012, a lidar/DIAL for the remote detection of explosive precursors has been developed. Its test has been carried out at the ENEA research center of Frascati. The lidar/DIAL was mounted in a van and operated with a portable power supply

ENEA is coordinating the European project BONAS (BOmb factory detection by Networks of Advanced Sensors) for Security Call. The main aim of this project is to design, develop and test an innovative sensor wireless network (Figure 2.7), in order to increase citizen protection and homeland security from terrorist attacks, especially against the threat posed by improvised explosive devices, (IEDs). ENEA is in charge to support the development of two sensors, for volatile and particulate substances emitted or released in the surrounding environment. To achieve its objective, BONAS involves the realization of a lidar/DIAL remote sensor. Based on the spectroscopic research performed at ENEA in 2011 and 2012, a lidar/DIAL for the remote detection of explosive precursors has been developed. Its test has been carried out at the ENEA research center of Frascati. The lidar/DIAL was mounted in a van and operated with a portable power supply

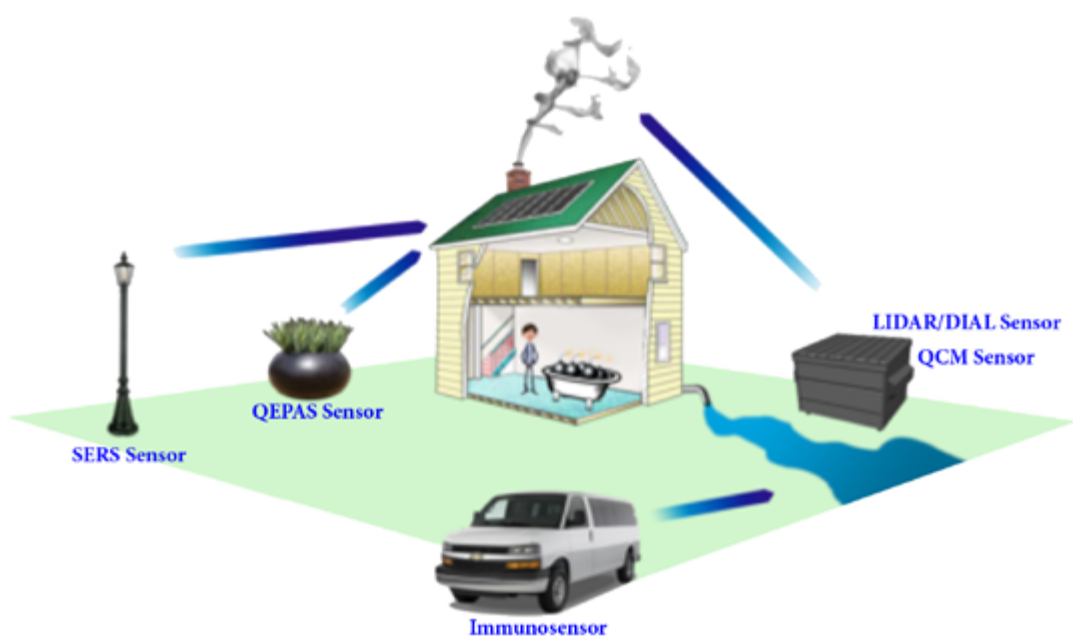


Fig. 2.7 - The BONAS sensor network



Fig. 2.8 - The lidar/DIAL (left) inside a van (right) during its test at the ENEA research center of Frascati. It was operated with a portable power supply (red box in front of the van).

(Figure 2.8). As explosive precursor, acetone was chosen. The bomb factory was simulated in two ways:

- By a 6.0-m long tunnel-shaped tent at 69.4 m from the system (acetone was poured on its floor).
- By a 2.2-m wide caravan at 75.4 m from the system (a basin full of acetone was put in it).

In both cases the system was able to detect acetone with a sensitivity of 50-100 ppm (Fig. 2.9).

The Surface Enhanced Raman Spectroscopy: evaluation of substrate amplification factor on explosive compounds for BONAS

In the framework of the BONAS project Raman Spectroscopy (RS) has been used for the detection of explosive substances and

its precursors in the presence of interfering harmless substances. Finally some properties of the Raman spectrum of explosives, suggesting their presence in the sample under examination have also been shown. Indeed the presence of more substances in a Raman spectrum is revealed by the presence of all their spectral features. This has been experimentally verified on solid powder mixtures of ammonium nitrate, a substance of concern and threatening in the class of explosives and their precursors mixed with harmless interfering of similar aspect like flour, sugar or talc. In Figure 2.10 Raman spectra of mixtures of Ammonium nitrate with these solid interferences in powder are presented: the small graphs on the left represent the Raman spectrum of each pure substance, the larger plot on the right represents the spectrum of the mixture. The spectral features of each component are clearly visible, the red peaks

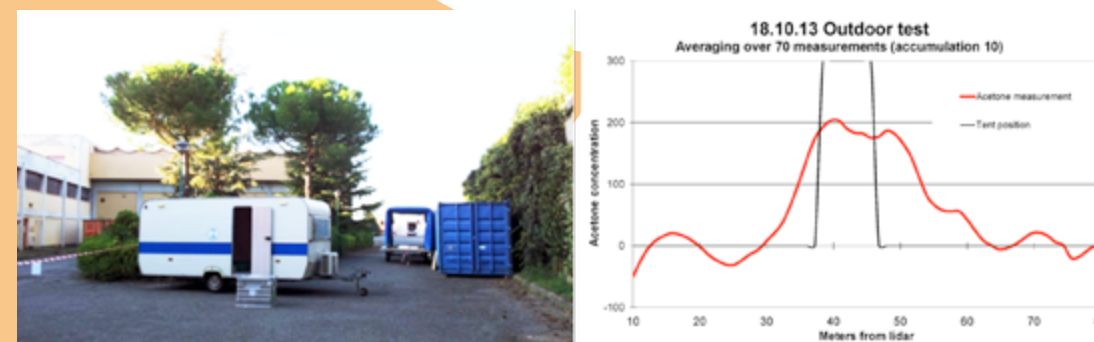


Fig. 2.9 - The Lidar test in Frascati: Left: the caravan and the tent simulating the bomb factory. The lidar/DIAL is visible in the background in the center of the tent. Right: the acetone measurement inside the tent with the range resolved concentration profile.

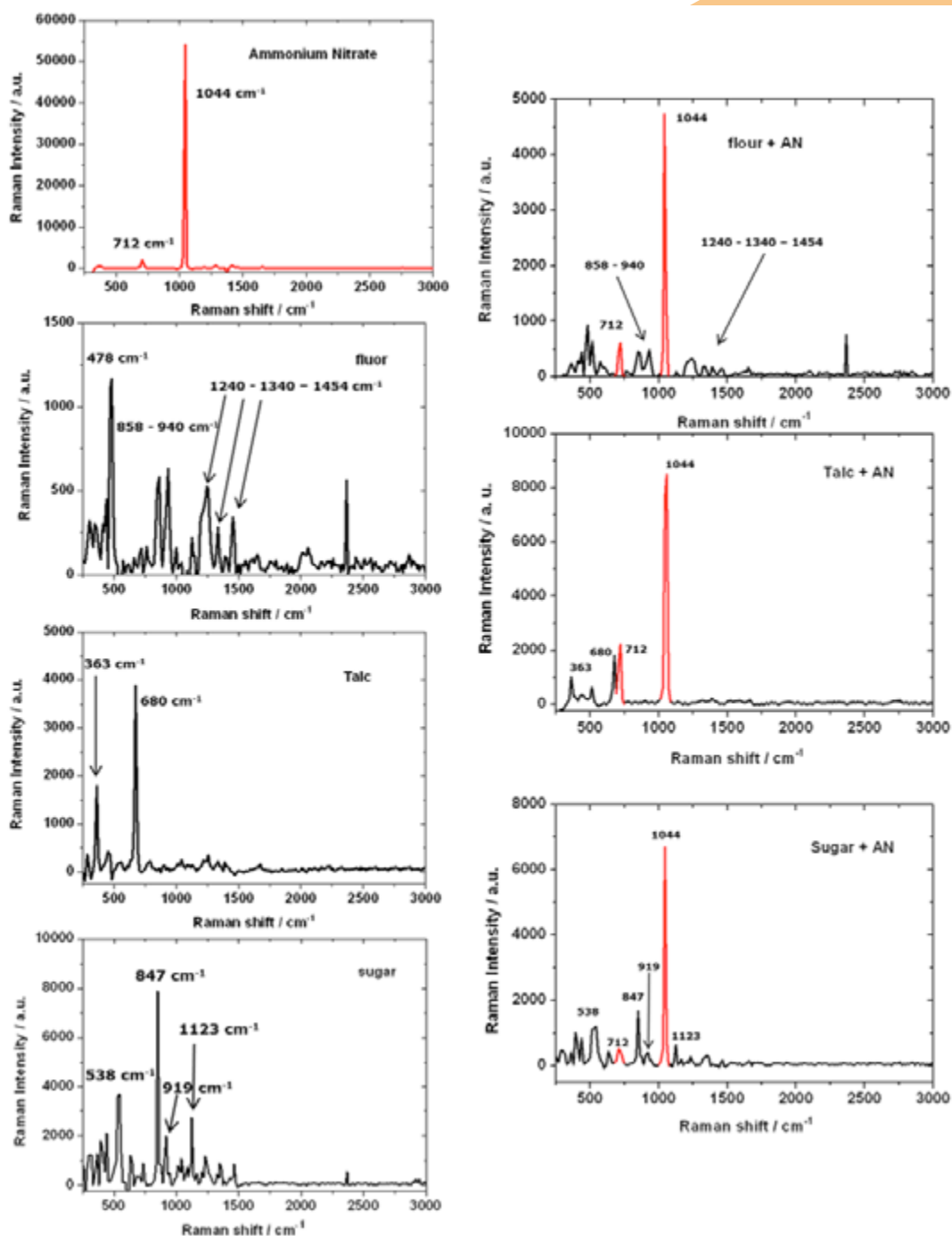


Fig. 2.10 - Raman spectrum of Ammonium nitrate (AN) mixed with flour (AN concentration: 50% in volume, 69% in weight), with talc (AN concentration: 50% in volume, 38% in weight) and with sugar (AN concentration: 50% in volume, 53.4% in weight). The main Raman modes in each mixture of AN are highlighted in red. The small graph on the left represents the pure substances.

belonging to ammonium nitrate, other features are ascribable to interfering substances.

For these measurements an integrated table-top Raman system (i-Raman from BWTEK inc.) was used, exciting the samples with a 785 nm solid state laser (linewidth < 0.3 nm) and adjustable power in the nominal range 3 - 300 mW. The detector is a CCD equipped with a built-in thermoelectric cooler working at 10° C, with 2048 pixel (14 μm x 200 μm) while the spectrometer covers the spectral range up to 3200 cm⁻¹ with 4.5 cm⁻¹ resolution at 912 nm. The collection optics is composed by a conventional optical microscope connected to the laser by means of an optical fiber with six different fields of view and resolutions. This also allows to collect the Raman spectrum from single explosives particles of micrometric dimensions after identification with the microscope because the scanned area, and therefore the sampled quantity, depends on the objective used. Different explosives detection was realized scanning samples deposited in traces on common fabrics like blue jeans, brown leather or synthetic polyester tissues, in order to simulate a fast and in-situ investigation of clothing belonging to suspicious subjects stained with

traces of explosives. The procedure started by depositing microdroplets of explosives (TNT, Urea nitrate, pentaerythritol tetranitrate, Ammonium perchlorate, and Ammonium nitrate) in liquid solution and examining the Raman signal of the residue after the solvent evaporation. Figure 2.11 left shows microcrystals of ammonium perchlorate released on polyester fabric, while Figure 2.11 right shows how it is possible to discriminate the Raman signal belonging to the underlying fabric from the signal coming from the microparticles of explosives.

FORLAB Project (FORensic LABoratory for in-situ evidence analysis in a post blast scenario)



The objective of FORLAB project (FORensic LABoratory for in-situ evidence

analysis in a post blast scenario) is to develop a portable sensor for fast screening of post-blast evidences, with the purpose of strongly reducing the number of evidences sent to the reference forensic laboratory and increasing the information provided by the

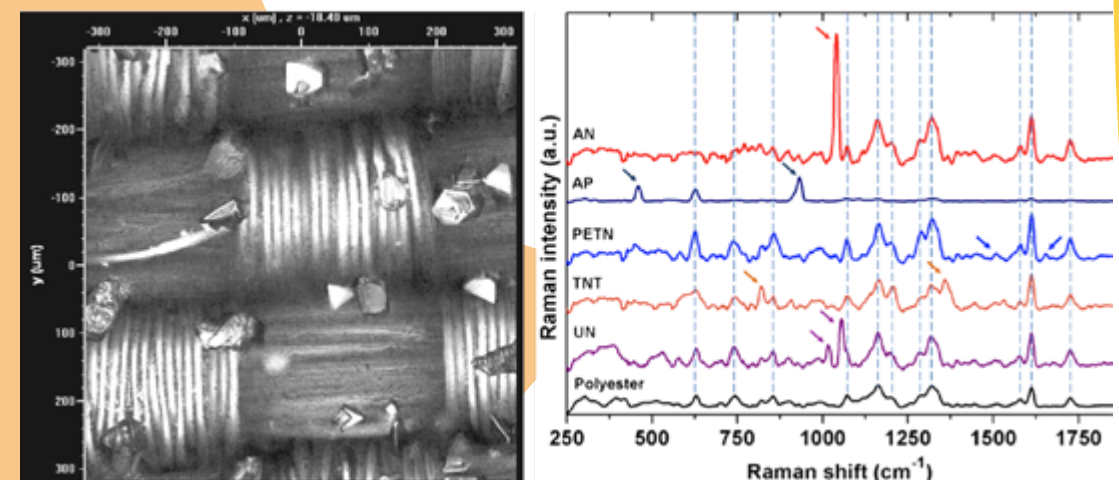


Fig. 2.11 - Left: High resolution image of ammonium perchlorate crystals on black polyester. The edge dimensions of the crystals are in the range 25-50 μm. Right: Raman spectra of AN, AP, PETN, TNT, UN on black polyester. The dashed lines represent the polyester spectral features from the background fabric while the arrows represent the identified spectral feature for each of the explosive/precursor of interest. The mass probed by laser is about 100 ng for each substance. The acquisition time is 10 s. The laser power is set between 90-180 mW depending on the sample response to the laser excitation

remains left after the explosion. The post blast scenario consists of a wide area covered by very small debris of the explosion which can be missed even by the specialist. Every detail may be crucial for the identification of the terrorist group responsible for the attack, the person who emplaced the explosive or even the person that assembled the IED. However, differentiating general debris from "clue evidences" is a hard process and a huge number of samples are usually collected in field in order to be subsequently analyzed in one of the few existing specialized laboratories.

Laser-induced fluorescence (LIF) is selected as one of the most sensitive detection schemes. The luminescence spontaneously emitted by materials irradiated with an appropriate excitation carries information about both the photophysical properties of the molecule and the chemical and physical nature of its micro surroundings. Although the LIF is not compound specific it can positively be used to discriminate among large classes of different materials including plastics, fabrics and electronic circuit PCBs. Moreover the additional capability of imaging on large areas allows for the identification and precise location of debris dispersed all around the crime scene. The LIF scanning system developed at ENEA in the second year of the project was tested in two field campaigns simulating the scenarios likely found in real life cases.

A first in field test has been organized by LCCP in Bievres (see Figure 2.12). During the training, measurements on a post – blast scenario have been performed by the LIF scanning system in order to test the system ruggedness working in real unfavorable conditions. Fluorescence images have been acquired and analyzed at conveniently selected spectral bands. After the explosion all sort of debris have been dispersed on ground as shown in left part of Figure 2.13. The fluorescence images at 370 nm and 513 nm (right side of Fig. 2.13), allow the identification and location of some plastic debris. Based on the specific feature of the spectral signature the materials relevant as post blast evidences, can be put in evidence directly on the scene and easily discriminated in false colors band images.

The second test campaign, has been organized by Astri Polska and PIAP in Poland to further test the capabilities of the screening technologies developed in the first stage of the project and to start sensor integration with other technologies (LIBS/RAMAN and 3D scanner). The main goal of the campaign was the test of the ability of the LIF scanner to work in a more complex environment, i.e. that of a post blast site where debris and shrapnel of arbitrary shape and size directly related to the explosion are diffused in large areas (more than 20m) and interleaved with background material not interesting for the analysis.

The results of an investigation conducted in the area in the explosion at a distance from 4 to 15 meters with a field of view of 6 degrees are shown in Figure 2.14 as an example of outdoor scenario. Several scans were run and the corresponding fluorescence images have been acquired, the data selected on three different bands are combined to form a single RGB false color image in order to have a better contrast between the searched plastic materials and the surrounding background



Fig. 2.12 - LIF deployment in Bievres (France)

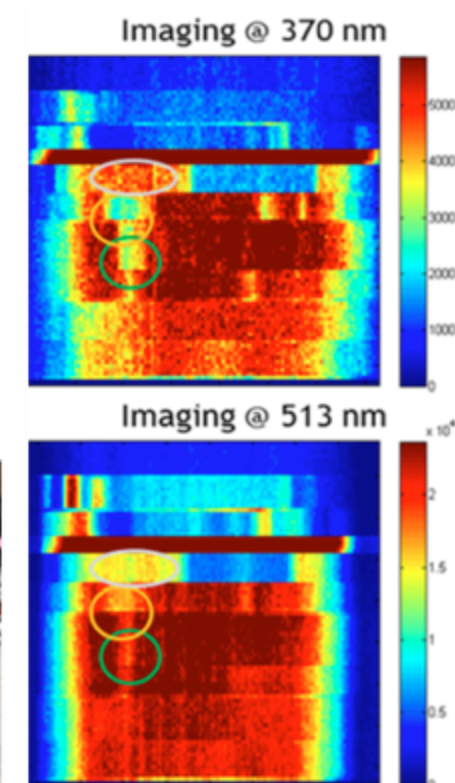


Fig. 2.13 - Area of sight for a preliminary scanning in Bievres (left side and details in the middle), and false color spectral LIF image (right side).



Fig. 2.14 - Conventional photo of the investigated area in Wroclaw (Poland) training on outdoor scenario (left side) and LIF image on a portion of the entire area restituted as three fluorescence band combination (right side).

RADEX (Raman Detection of Explosives) project



In the last decades several terroristic attacks focussed on urban transport lines occurred in different cities, which raised the needs for new reliable and effective instrumentations for explosive and precursor detections at trace levels for homeland security applications. Among the detection technologies available, Raman-based spectroscopy has gained consents as potential tool for the detection of explosives at a certain distance due to recent technical improvements. A new instrumentation was developed at the Diagnostics and Metrology Laboratory for the proximal detection of explosives (10 cm÷200 m, NATO classification). The RADEX (Raman Detection of EXplosives) system is a Raman-based technology to detect trace explosives taking in consideration the constraint of the maximum permissible laser exposure at the human cornea (3 mJ/cm² for a 266 nm laser). The expected scenario was the monitoring of dispersed explosive compounds on people, either on accessible clothes of people or on their personal objects, passing through a corridor with a high transit of people, such as a metro stations. The operational principle of the RADEX system is the following (Figure 2.15): an eye-safe laser beam is focused on the target and the Raman scattered radiation, emitted from the illuminated surface, is collected by a telescope and imaged onto the entrance of a Raman spectrometer. The radiation is then analyzed giving a spectrum suitable for the explosive detection and identification. The apparatus was developed

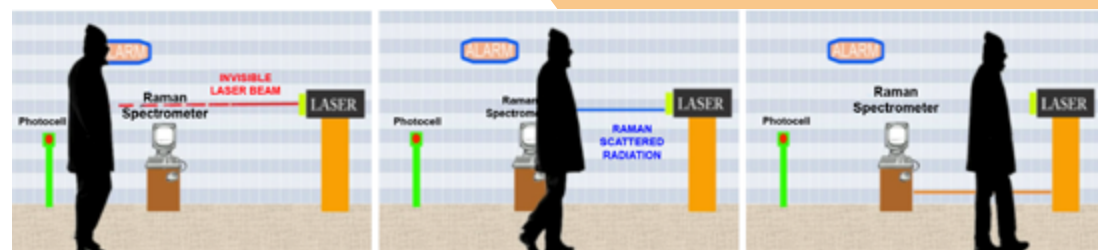


Fig. 2.15 - The operational principle of RADEX.

in the context of the STANDEX (STANdoff Detection of EXplosives) program (NATO Science for Peace and Security Program) and it was part of an explosive warning system that includes the fusion of complementary detection sensors designed to work in a mass transit infrastructure such as a metro station. The main features of the system are the use of technologies without having a physical contact with passengers and the real time response.

BCT (Big City Trials) project

The STANDEX program also included the demonstration of the system ability to automatically and discreetly detect and localize a hidden explosive in a mobile carrier in real conditions of use, during a realistic phase of tests, in the Bibliothèque Francois Mitterand metro station (the Big City Trials project). The trials were performed by using real traces of explosive materials and with environment conditions similar to those that can be encountered in a metro station. This choice was made to ensure that the technology was compatible with the hard environment conditions met inside large public transport stations, to validate the detection performances in an operational environment and to assess the potential capabilities of the prototype to work together with the other instrumentation integrated in a complex alarm system. The RADEX prototype was placed in the footbridge of the BFM metro station as shown in Figure 2.16 looking into the direction opposite to the passenger flow with the laser placed at the specified height of 1.15 m from the ground. The corridor was delimited in order to guide the passengers in direction of the instrument.

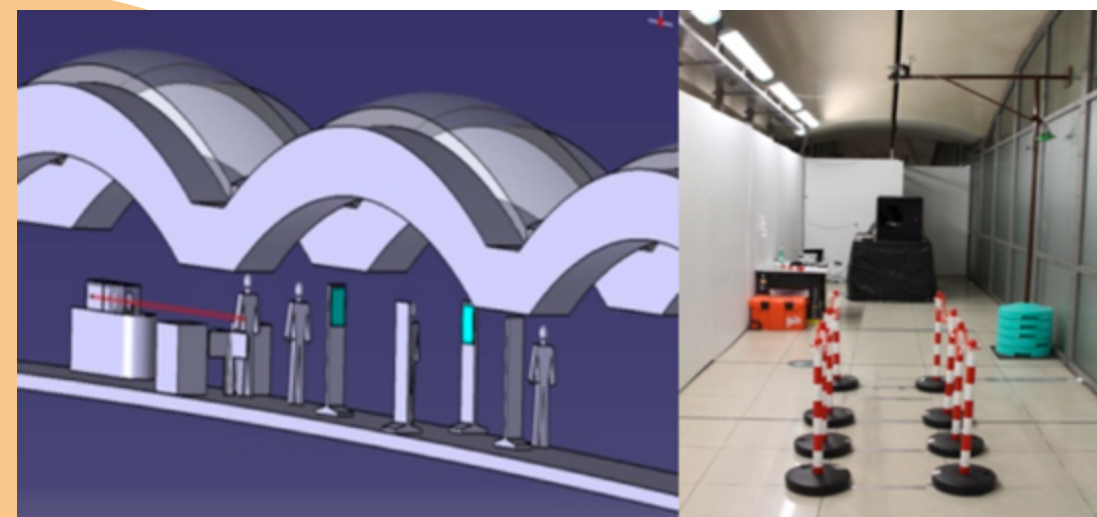


Fig. 2.16 - 3D model of the Layout of the RADEX system on the footbridge and the RADEX set-up during the trials.

At the end of the delimited corridor optical sensors were used to simulate a gate needed to synchronize the laser emission with the transit of a passenger. An on-line data analysis algorithm was implemented for the acquisition software in order to identify in real time the substances. A preprocessing is performed to clean the spectra from noise, background and, eventually, fluorescence. The recognition of peaks involves processes like filtering, transform and mapping. The identification of

species on the basis of the recognized peaks is always based on the minimization of a kind of distance in a suitable space between the spectrum under recognition and a reference data base. The layout of the acquisition software provide the following information to the operator (Fig. 2.17) : real time image from the videocamera of the instrument, the camera snapshot of the analyzed person, the acquired Raman spectrum, the logging data and the analysis results.



Fig. 2.17 - Layout of the acquisition software and the first ver-sion of the web server with details of an incident report

The developed software is user friendly for the operator, since only few preliminary steps are needed for the daily calibration and the response given is threat or no threat indicated with a red or green signal, respectively. During the trials the following energetic materials were tested: ammonium nitrate, urea nitrate, TNT, PETN. Different fabrics (naturals and synthetics) were used as substrate for the deposition of energetic materials. Samples of traces of explosives on fabrics were prepared by the Fraunhofer Institute for Chemical Technology ICT using a piezoelectric Nano-PlotterTM (PNP, GeSIM, Germany). The PNP can deliver a precise number of droplets on a well define surface. This method provides a more uniform surface coverage with the analyte also for low surface densities (down to few $\mu\text{g}/\text{cm}^2$) as requested by the project.

The implemented software allows for the use of the apparatus either stand-alone or in a more complex warning system, where the information provided by several instruments developed by other project partners are collected and processed by a Data Merging and Alert System (DAMAS). Each time the DAMAS sent a "shot" command, after the identification of a suspect person, the RADEX system automatically sent an eye-safe laser shot when the potential bomber passed through the gate. The Raman signals produced by the

target area were acquired. And compared with those included in the database to figure out the presence of explosive tracers. Then, the acquired information, with the response, were sent in real time to DAMAS (Fig. 2.18).

The RADEX prototype was well integrated in the DAMAS configuration during the trials because, it acquired information on potential bombers every time a trigger was sent by DAMAS and a full report for each event was provided to DAMAS in real time. RADEX was able to detect trace amounts of energetic materials using an eye-safe single pulse laser. The detection limit depends on the type of substance (i.e. on the Raman scattering cross section, the resonance frequency and the stability of the molecules when excited with a 266 nm wavelength).

EDEN: a wide collaborative European project against CBRNE Events



On 1st of September 2013 started the 3-year European Demonstration project EDEN which marks an unprecedented effort from the European Commission to support the research and development in the field of Security. The project is

the pyramidal tip of the vast action undertaken during FP7 to secure a competitive role on a global scale to the European stakeholders involved in the whole lifecycle of managing Security (Risks Reduction, Prevention, Preparedness, Response, Recovery). In the EDEN project 36 partners from 15 different European countries collaborate to bridge the gap still existing between End-Users needs and technologies available. The focal points of the project are several demonstration actions scheduled at the end of the research activities to validate the solutions sought in the EDEN project. ENEA plays a prominent role in the project as developer of new specific tools to be validated in three different final demonstration actions. In particular UTAPRAD DIM covers the dual role of coordinator of all the ENEA activities and developer of three out of five new tools.

The first one of the three new tools entirely developed at UTAPRAD DIM builds upon the expertise in constructing 3D laser scanners for operation in harsh environment (subsea, energy fusion machines). This time the challenge will be to develop a 3D laser scanner for operation inside a nuclear reactor for accomplishing the structural monitoring of the containing chamber and of the critical infrastructures therein. The device will allow for improved inspection/vision capabilities both during

routine inspections or as a first response to assess the consequences of threatening natural events like earthquakes. The final demonstration for validate the technology is scheduled in 2015 inside the research nuclear reactor TRIGA RC1 (Training, Research, Isotopes, General Atomics - Reattore Casaccia 1) in the Casaccia ENEA Centre (UTFISST). A plot of the scenario under development for the final test is reported in Figure 2.19 where the TRIGA RC1 reactor plant sketched in a vertical profile and with the sensor deployed in the storage pool. The laser profiler consists of a passive module made of a watertight housing and carrying the laser beam transmitter and a receiving stage. The active module out of the wet environment is made up of the electronic units for system communications and data transmission. The second new tools under development at UTAPRAD DIM for the EDEN project is an integrated laser module capable to detect LIF, Raman and LIBS spectra of explosives materials even at traces level and up to a distance of 30m. This task encompasses the remarkable achievements over the last years of the Laboratory in applying separately three laser spectroscopic techniques to explosives detection. The challenge here is to integrate them for enhancing the sensitivity, the selectivity and reducing the number of false positives.

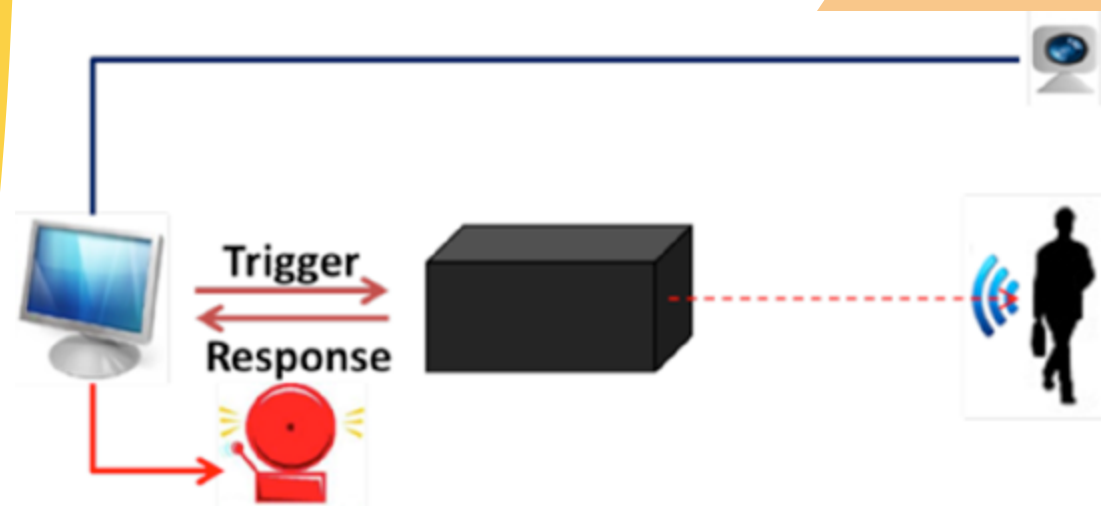


Fig. 2.18- The schematic representation of the DAMAS-RADEX communication.

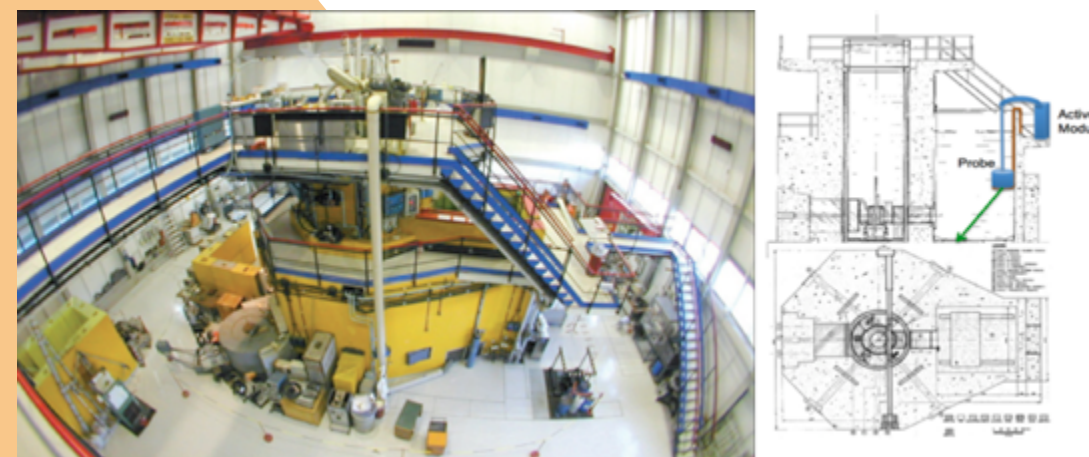


Fig. 2.19 - The ENEA TRIGA power plant for research studies. Left the nuclear reactor; Right Up: a vertical sketch of the TRIGA RC1 reactor with the laser profiler immersed in the storage pool. Down: a view from the above.

A fast switching time (less than 1s) from a technique to another has been set as system requirement together with a fully remote control and user friendly interface for non-highly trained operators. The whole assembling will be compact for installation onboard a mobile platform remotely operated (Fig. 2.20).

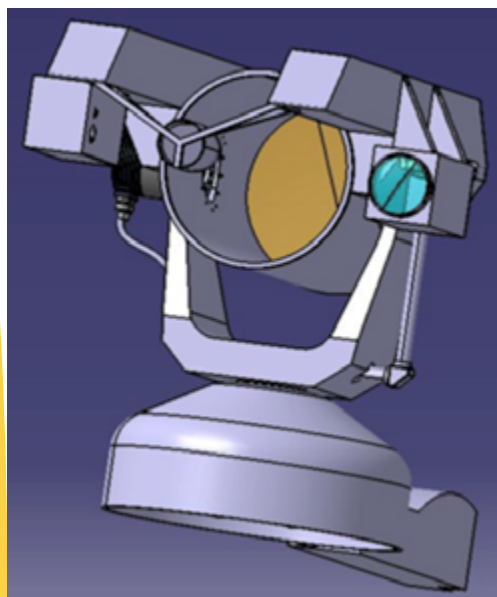


Fig. 2.20 - The first design of the combined instrument for in field measurements

The validation of this breakthrough technologies will be carried on in a properly equipped area inside the ENEA Frascati Research Centre where a suspected bag carrying explosive material will be remotely inspected with the modular laser device. An impressive planning activity is underway to build an area qualified for explosive storage and hazardous tests. This infrastructure, as a legacy of the EDEN project, will enrich UTAPRAD DIM with an up to date facility capable to attract further national and international collaborations of ever greater relevance and impact. The third tool under development at UTAPRAD DIM within the EDEN project is of completely different nature with respect the previous two and has attracted wide interest among the other project partners. It is the

development of a code to simulate how a crowd made of a large number of people (thousands) behave in critical situation. The objective of this task is to assess the risks on the safety of people crowd that is grouped in open areas to follow events such as festivals or similar and to assess whether the existing safety evacuation plans are adequate. The ultimate aim is to propose additional (reasonably applicable) measures for the security.

The code will build upon the findings of the Helbing model and will use evolutionary computational techniques such as genetic algorithms to select the best candidates for evacuation plans. As shown in Figure 2.21, the hexagonal grid technique will be adopted in order to make more robust the code. With this technique the partition of the inspected area is accomplished with hexagons rather than squares. The advantage of a hexagonal map over a traditional square grid map is that the distance between the center of each hex cell (or hex) and the center of all six adjacent hexes is constant.

By comparison, in a square grid map, the distance from the center of each square cell to the center of the four diagonal adjacent cells it shares a corner with is greater than the



Fig. 2.21 - An explicative example of the partition based on hexagon

distance to the center of the four adjacent cells it shares an edge with. The constant distance of a hex map is desirable for simulation in which the measurement of movement is a factor. The other advantage is the fact that neighboring cells always share edges; there are no two cells with contact at only one point. This tool will be validated in a tabletop demo to be carried out at the end of the project and simulating the unpredictable behavior of the crowd during a sudden radiological emergency.

2.3 Diagnostics for safety

Agro-alimentary diagnostics to protect the "made in Italy" products



The National Project MI01_00182- SAL@CQO ("Sviluppo di un Apparato Laser per misure di spettroscopia molecolare per la Conservazione e il controllo di valori afferenti le Qualità Organolettiche dei prodotti alimentari con tecniche non invasive contro adulterazioni naturali e/o fraudolente") is running the second scheduled period. In the frame of this project, non-invasive and reliable optical methods are developed in order to be employed for food safety issues as adulterated food or beverages. The natural on fraudulent adulteration deals with bacteria, viruses, parasites, mold, toxins, allergens and other contaminants. SAL@CQO presence of is aimed to develop and apply innovative easy-to-use product-instruments for Scientific research, for control authorities as well as for industry production chains where food processing requires the continuous monitoring of quality and preservation of food included in the process.

The 2013 year was dedicated both to complete the reporting and to experimental work due for the second scheduled period of the project. In more detail, new measurements were performed with the first LPAS prototype on some adulterants indicated by Italian National

Health Institute (ISS) as being of interest for the project scope, such as melamine in powder milk, methanol in beverages and N-(L- α -Aspartyl)-L-phenylalanine, 1-methyl ester, better known as aspartame. The aspartame is an artificial, non-saccharide sweetener used as a sugar substitute in some foods and beverages widely used for dietary reasons or by people suffering of diabetes. It is a methyl ester of the dipeptide of the natural amino acids L-aspartic acid and L-phenylalanine. Usually it is innocuous, but under strongly acidic or alkaline conditions, aspartame may generate methanol by hydrolysis. The methanol produced by the metabolism of aspartame is absorbed and quickly converted into formaldehyde and then completely oxidized to formic acid, which, due to its long half life, is considered the primary mechanism of toxicity in methanol poisoning. Moreover, because its breakdown products include phenylalanine, aspartame must be avoided by people with the genetic condition phenylketonuria, a rare inherited disease that prevents phenylalanine from being properly metabolized.

The second prototype was designed and realized as shown in Figure 2.22. This apparatus, differently from the previous one, can be in principle compacted in a mobile assembly even by using a relatively high power laser source (1 W of average power) instead of a laser diode. In fact the adopted CO₂ laser source is a compact one (40x11x7 cm) and emits IR radiation power 10 times lower than the analogue source in the first prototype, but still sufficient to obtain strong photoacoustic

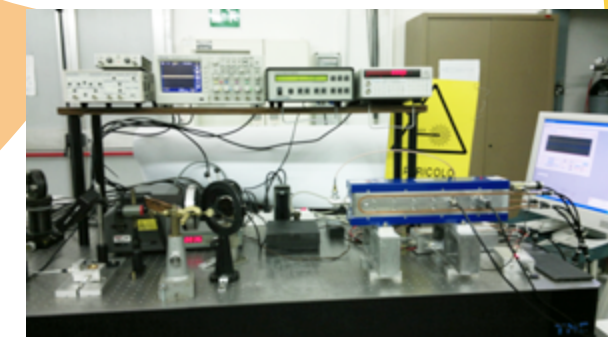


Fig. 2.22 - The SAL@CQO second step prototype.

signals from the analysed samples. It can be operated also without water cooling, nevertheless it is well stabilized by a dedicated software inserted in a feedback loop. The laser is tunable through a single screw micrometer which will be connected to a precise stepping motor aimed to a computerized remote control. The second step prototype will be used to check features to be implemented in the diode laser final prototype.

Extremely Low Frequency (ELF) weak electromagnetic fields interaction with organic molecules

ELF project (Induced Maturation And Differentiation Of Human Cardiac Stem Cells And Their Implantation in Nude Mice: A Preclinical Study For Treating Heart Attacks) finally started in 2013 being funded by Ministry of Health in 2009, under the responsibility of INAIL (ex ISPEL). The activities of our laboratory during the present year were primarily devoted to the study of the effects of weak low-frequency electromagnetic fields on the structure of biological macromolecules involved in the process of cell differentiation. At the same time, a new collaboration started with the Department of Medicine, University of Pavia, with the main aim to investigate the acceleration of certain enzymatic processes

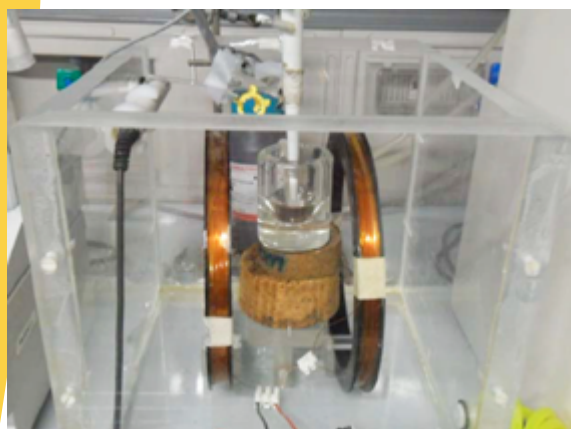


Fig. 2.23 - Helmholtz coils. Inside can be observed the "bath" where the experiment has been carried out. The bath is connected to the cryostat and maintained at a constant temperature of 37°C.

during exposure to weak magnetic fields. As first test, the speeding up of the reaction of production of amino-butyric acid (GABA) was selected, due to its skills to be the main neurotransmitter of the movement. The experimental apparatus has been developed at our laboratory (Figure 2.23) and then moved to Pavia, where experimental measurements were performed. This experiment was the subject of a thesis in Science and Technology of Drug with ENEA.

Development of techniques for tissue engineering

In collaboration with the Department of Aging and Inflammation, University P & M Curie, Paris, Indian Institute of Technology at New Delhi, India, the Regenerative Medicine Centre of Leipzig and Fondazione San Raffaele di Ceglie, on the basis of our previous results published in *Biomaterials* 2011, we built an innovative platform for tissue engineering of skeletal muscle tissue. The work of 2013 has been aimed at the functionalization of the extracellular matrix scaffold derived from the Tibialis Anterior muscle from BALB/C and BLACK 6 mice decellularized with the protocol we previously established. Several methods of functionalization were tested through chemical (polyethylene glycole) and biological (murine serum) treatments. After functionalization the scaffold was then transplanted in syngenic mice. Histological and molecular analysis allowed us to select the most suitable functionalization method able to increase in vivo myogenesis and muscle regeneration (Figure 2.24). The methodology proposed represents a promising platform to treat skeletal muscle injury non other-ways treatable. Early clinical trials are presently undergoing at the Mc Gowan Institute of the University of Pittsburg, with which we are going to establishing collaboration. A Memorandum of understanding (MoU) has been signed with the IRCCS San Raffaele Pisana/Fondazione San Raffaele and a MoU is going to be signed soon with the Indian Institute of Technology of New Delhi. Other biological investigations

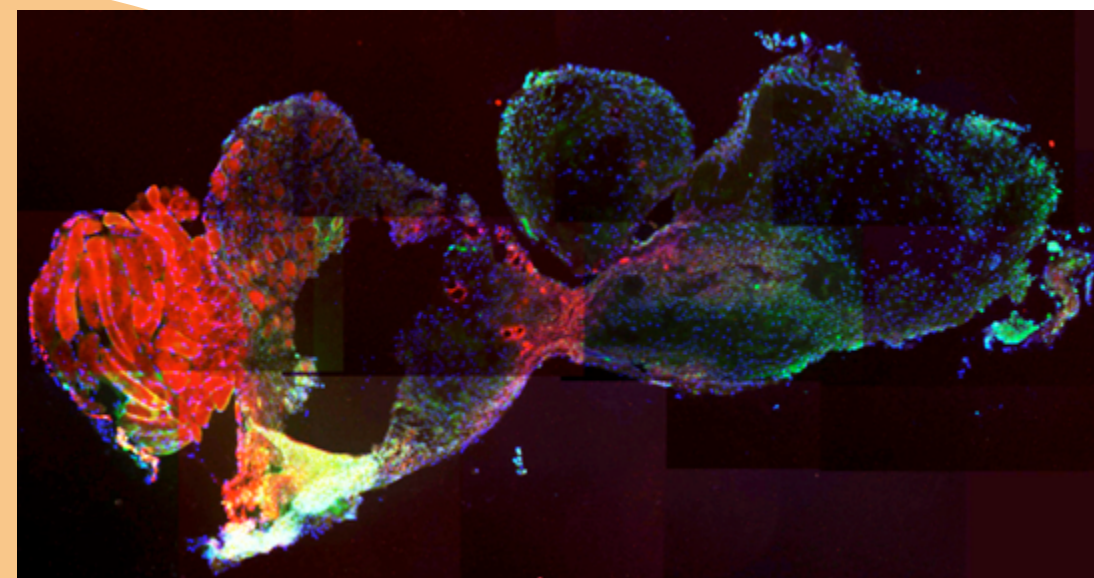


Fig. 2.24 - Immunofluorescence images for myosin (red), laminin (green) and nuclei (blue). The presence of regenerating myofibers is evident, thus demonstrating that this scaffold is able to recruit stem and progenitor cells that in such a niche are able to differentiate in mature skeletal muscle cells which will regenerate the muscle tissue.

on the effect of in vitro cells were carried on in cooperation with UTBIORAD.

2.4 Environmental diagnostic related to climate changes

The 2013 research activity of passive satellite oceanography data analysis and merging with active laser monitoring equipment were focused on remote sensing of the ocean color and SST (Sea Surface Temperature) and on field experiments to support remote sensing calibration/validation (CAL/VAL) activities. These activities were executed in the framework of two main projects: PERSEUS (Policy-Oriented Environmental Research in the Southern European Seas), a research project that assesses the dual impact of human activity and natural pressures on the Mediterranean and Black Seas and the RITMARE Flagship Project, one of the National Research Programs funded by the Italian Ministry of University and Research. A third project, RIMA (Rete Integrata marina Mediterranea con Accesso a dati distribuiti) just started at the end of 2013.

PERSEUS



The main goal of the activity performed by DIM laboratory, as partner of the PERSEUS project, was to apply bio-optical algorithms to ocean color data in order to study the phytoplankton assemblage evolution at different spatio-temporal scales in Mediterranean Sea. In this context, the determination of bio-optical algorithms, that allow to get qualitative and quantitative information about PSCs, PFTs or PSD from satellite data, provided an important instrument for a synoptic observation of the Phytoplankton community structure and its spatial and temporal variability, in order to improve the knowledge about the ecological and biogeochemical dynamics connected with it. Different models have been tested to identify several PSCs and PFTs from ocean color data based on physical, biological and ecological approaches. These three models were used to study the spatial distribution and temporal variability of three dominant PSCs in the Mediterranean Sea during the SeaWiFS

mission from 1998 to 2010 (with minor gaps due to failure of the SeaWiFS sensor during the last part of its lifetime). The two ecological models were first validate against in situ data using a Mediterranean subset of the SeaBASS dataset (see Fig. 2.25). Preliminary findings indicate that the first model tends to slightly underestimate the concentration of nanoplakton chlorophyll and overestimate the concentration of picoplankton chlorophyll. In the second model the nano plankton underestimation is less evident as well as the picoplankton overestimation. A second test based on our reformulation of the multiple regression analysis of the relation between pigment biomarkers, deduced from HPLC analysis, and concentration of pico, nano and micro plankton revealed, at least for the Mediterranean Sea, an opposite situation that favors the used of the Brewin respect to the Hirata model. Thanks to the internal laboratory characterization a specific activity of field measurements continued to produce a new dataset dedicated to the validation of satellite estimates of PSC. Measurements

done during cruise WMED BIOOPT 2012 were analyzed using HPLC and the cruise BIOOPT 2013 was performed to increase the significance of our dataset. Contemporary to the CAL/VAL activities an analysis of the time series of SeaWiFS derived PSC was performed. Figure 2.26 gives an overview of the preliminary results for two specific areas of the Mediterranean Sea. PSC satellite data for the period 1998-2010 are distribute with monthly frequency at spatial resolution of 1.1 km. gosweb.artov.isac.cnr.it a specific folder PERSEUS. Partners are provided with a shared username and password to access the PERSEUS directory. Figure 2.27 is an example of PSC products provided by ENEA for the PERSEUS web site.

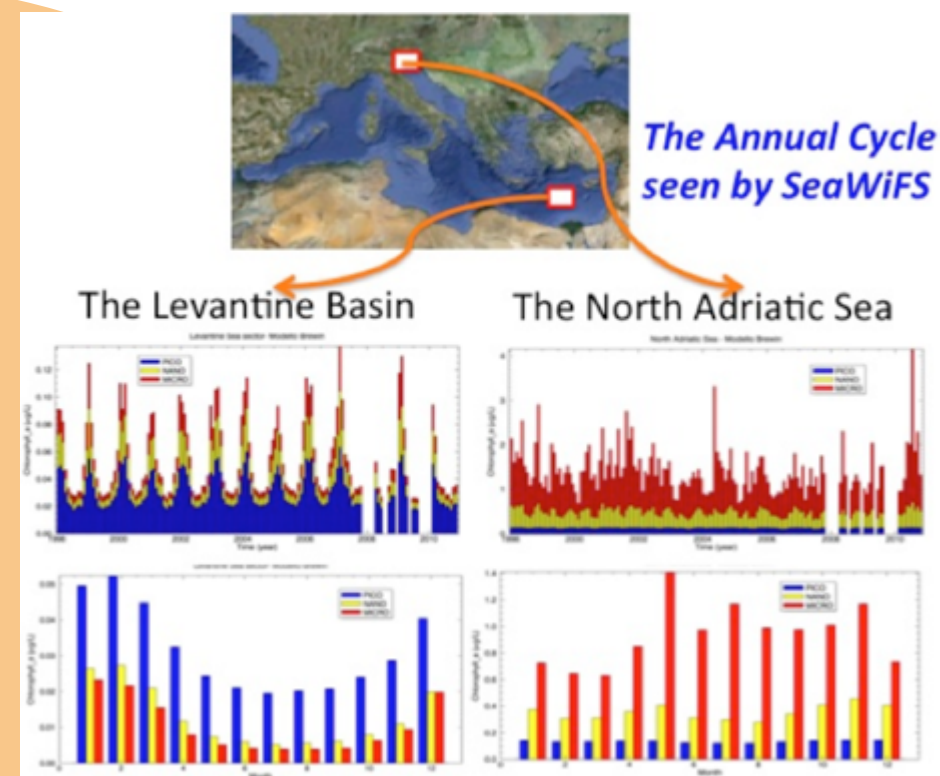


Fig. 2.26 - PSC time series in the Mediterranean Sea.

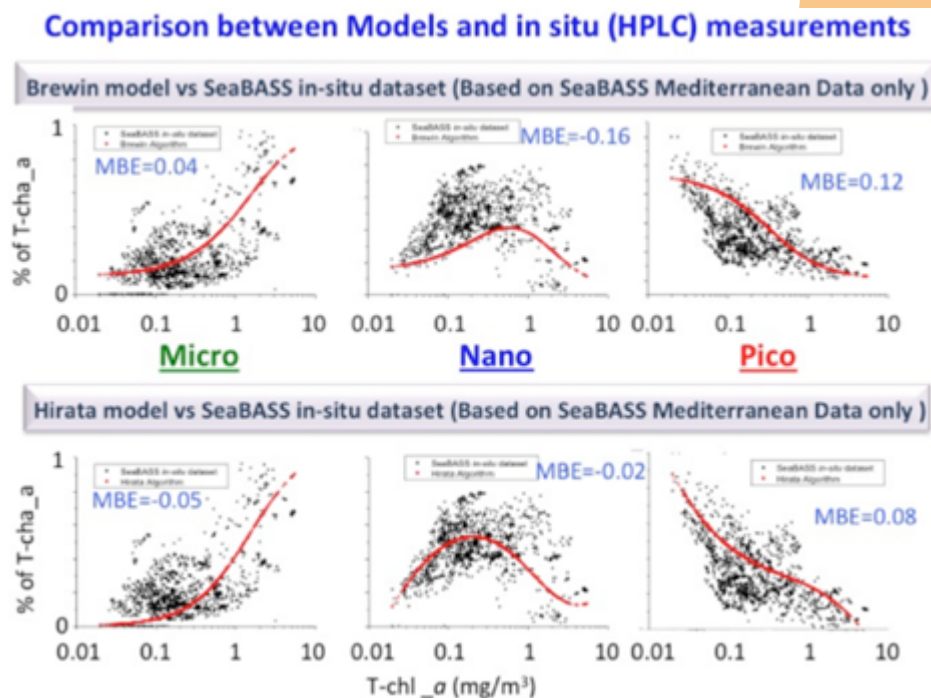


Fig. 2.25- PSC Validation in the Mediterranean Sea.

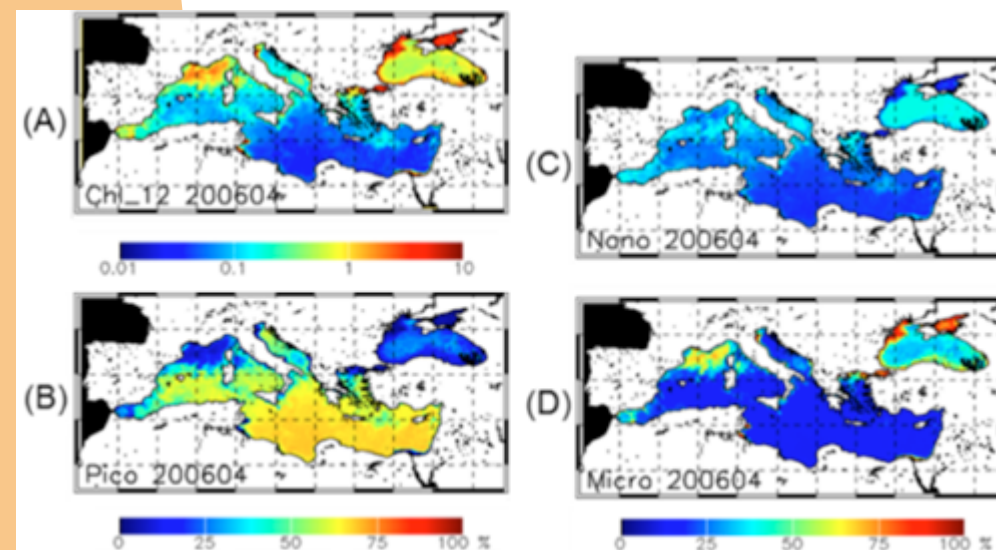


Fig. 2.27 - (A) Chlorophyll concentration on April 2006 ($mg\ m^{-3}$), (B) percent of Picoplankton. (C) percent of nanoplankton, (D) percent of microplankton

RITMARE



The role of DIM laboratory as part of the Italian RITMARE project (CNR leadership) was to design and implement a new Lidar system to continuously measure ocean ecosystem parameters from ship. The project started in 2012 and will continue until the end of 2014. During 2013 our activities concentrated on the implementation of the optical microsensors of the lidar and on field cruises to test the preliminary version of the lidar system.

Figure 2.28 shows the record of measurements made during BIOOPT 2013 with the current version of the lidar. DIM Laboratory holds also a HPLC (high performance liquid chromatography) facility for the determination of pigment composition in order to reach the following objectives:

- Validation of Ocean Color satellite data for the determination of pigment phytoplankton distribution.

- Validation of in situ data SeaTech fluorometer for the determination of Chlorophyll (Chl a) profiles.
- Determination of phytoplankton size dimensional classes and functional groups.
- Validation of Chl a Lidar fluorosensor and CASPER spectrofluorometer data.

Both instruments have been developed in ENEA for the real-time monitoring of Chl a in water. Analysis of samples collected during the WMED BIOOPT 2012 and WMED BIOOPT 2013 campaigns have been performed in our laboratory. Surface HPLC records of Chl a have been correlated with MODIS Chl a data. MODIS data have been calculated using the global algorithms and for this reason values are slightly overestimated. As it is shown in Figure 2.29 below the correlation between the two data sets is excellent. The Chl a HPLC data have also been used to calibrate the SeaTech fluorometer on ship board used to measure fluorescence profiles.

The fluorometer voltage output (V5) is linked

to the Chl a concentration by the following relation: $[Chl\ a] = 10V5$. The accordance between the HPLC and fluorometer data is very good as it is shown in Figure 2.29.

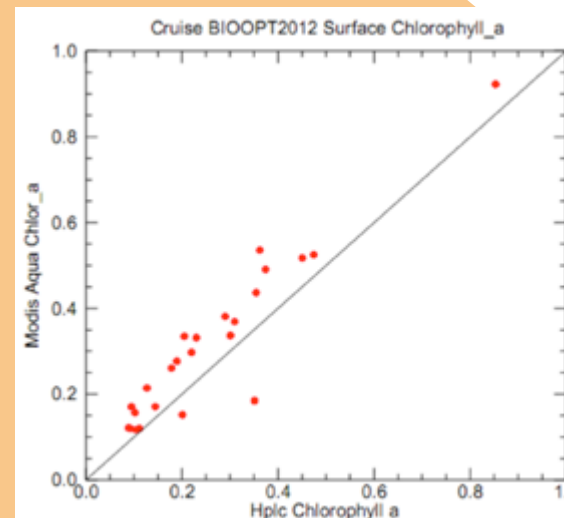


Fig. 2.29 - MODIS Chl a data vs. HPLC

RoME – Ross Sea Mesoscale Experiment



UTAPRAD-DIM participates with its electro-optics instruments POLI and CASPER to “RoME – Ross Sea Mesoscale Experiment”, a project approved by PNRA (2013 call). Thanks to lidar fluorosensor POLI and laser spectrofluorometer, deployed during the oceanographic campaign of RoME (January-February 2014), thematic maps and depth distributions of CDOM, chl-a, phycocyanin, phycoerythrin, carotenoids, tyrosines and tryptophans will be released. Merging these data and satellite radiometers imagery, the bio-optical characterization of Antarctic waters will be performed with an unprecedented spatio-temporal resolution and coverage, leading to an accurate determination of primary productivities and phytoplankton size classes.

Spectrofluorometric characterization of natural waters

The accurate monitoring of natural waters (aquifers, rivers, lakes, seas and oceans) is a key action for environment protection, ecosystem safeguard and life sustain. Laser sensing can be very effective in significant measurements of the bio-optical parameters in natural waters. In 2013, the spectrofluorometer CASPER (Compact and Advanced laser SPECTrometer for Riade) realized and patented by our lab in previous years has been deployed in marine campaigns supporting calibration validation activities of ocean color satellite radiometers (Fig. 2.30).

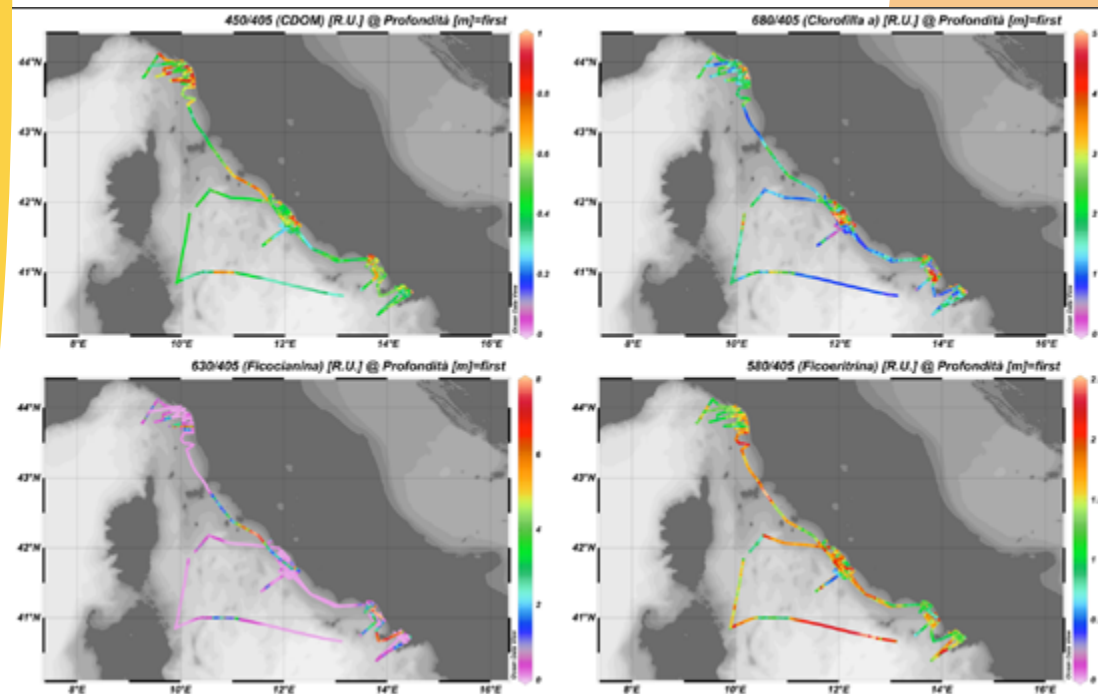


Fig. 2.28 - Along track, real-time LIDAR measurements during BIOOPT 2013.

RIMA



The Region of Liguria has recently approved the project RIMA (Rete Integrata marina Mediterranea con Accesso a dati distribuiti) with the main contractor the Liguria Cluster of Marine Technology (DLTM) formed by an aggregation of institutions and companies.

The RIMA project aims to develop an innovative computer system (software and technology) for the management of the access and to the forecast data and will promote the development of technological platforms to optimize data acquisition and archiving.

In DLTM, the ENEA Santa Teresa Research Centre is represented by UTMAR, UTAPRAD-DIM will contribute with the development of a next generation lidar for the monitoring of

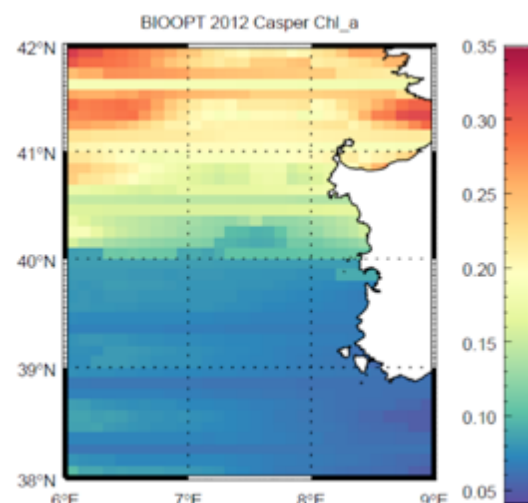


Fig. 2.30 - Biomass distribution as measured by the CASPER during the Sardinia coast campaign.

The breakthrough of SOMBRERO is the use of UV and blue LEDs instead of lasers, thus reducing size, weight and cost. In 2013, the waterproof case of SOMBRERO has been completely redesigned, in order to increase its water resistance. The system has been calibrated in the lab ($R^2=0.997$): its chlorophyll-a sensitivity is better than 0.05 $\mu\text{g/l}$ (Fig. 2.31). Just before the end of 2013, the system underwent the successful final test in the Albano Lake (Fig. 2.32).

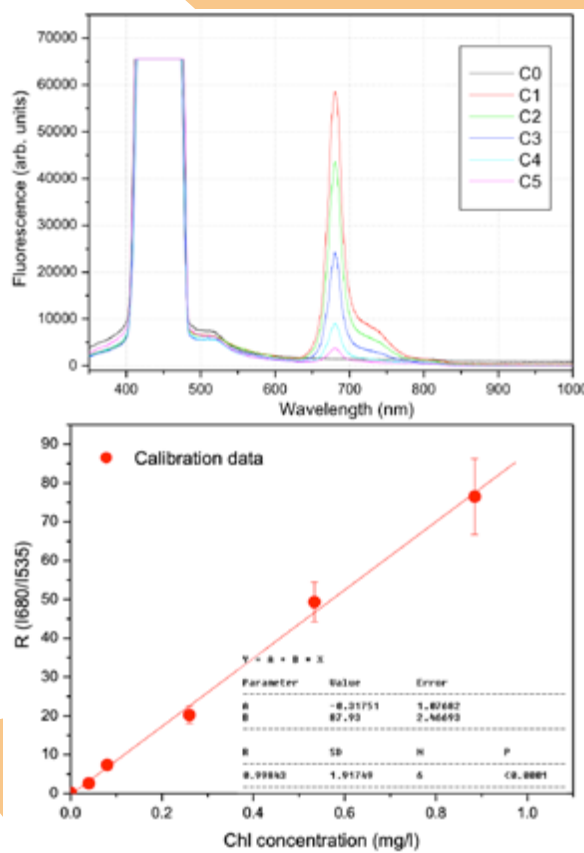


Fig. 2.31 - (top) Spectrum of Milli-Q water (C0) and chlorophyll-a solutions (C1 – C5) measured by SOMBRERO at five known concentrations. The water Raman scattering is peaked at 535 nm as expected. The emission at 680 nm (and 730 nm) comes from the chlorophyll fluorescence. The pigment concentration is proportional to the 680-to-635 ratio. (bottom) Calibration of SOMBRERO with the five known concentration mentioned above.



Fig. 2.32 - SOMBRERO spectrofluorometer (right) and during the test in the Albano Lake dipping it from a pier (left).

Lidar measurement of volcanic plumes

The true magnitude of CO₂ emissions from volcanic activity is poorly constrained, limiting our understanding of the natural carbon cycle. CO₂-sensitive lidars could be used to measure the distribution of CO₂ in a volcanic plume, thereby allowing volcanic CO₂ fluxes to be measured directly.

UTAPRAD-DIM participates as partner to two ERC research projects (CO2VOLC and BRIDGE) and as subcontractor to a PON project (VULCAMED; INGV Sezione Palermo as main contractor) aimed at producing such instruments, based on the differential absorption lidar (DIAL) technique. Our laboratory is involved in the realization of three DIAL systems (airborne for CO2VOLC and ground-based for BRIDGE and VULCAMED) for the lidar measurement of volcanic plumes. While CO2VOLC and BRIDGE started in 2012, VULCAMED is in its very early stage.

DIAL measurement of carbon dioxide in volcanic emissions is a great challenge, mainly because the laser transmitter should have a linewidth narrower than 0.05 cm⁻¹. Moreover, it is required wavelength tunability and nearly

simultaneous transmission of two differently absorbed wavelengths. All these requirements cannot be achieved by off-the-shelf lasers so an extensive market research has been performed.

Eventually:

- A fiber laser has been chosen for CO2VOLC.
- A Nd:YAG-pumped dye laser, followed by difference frequency mixing and optical parametric amplification, has been chosen for BRIDGE.
- A Nd:YAG-pumped optical parametric oscillator has been chosen for VULCAMED.

Each technical solution has advantages and drawbacks: it has been tried to maximize the advantages for each project measurement scenario.



The laser source for CO2VOLC has been delivered and is now under test. Moreover, it has been investigated the effect of a volcanic liquid water cloud on a lidar signal towards the development of a DIAL that measures volcanic CO₂ concentrations.

The BRIDGE system (Fig. 2.33) has some remarkable features:

- 10 pm stability corresponding to 0.25 and 0.2 cm⁻¹ stability at 1570 and 2070 nm, respectively;
- dynamic mode option;
- piezo wavelength control;
- Visible and UV emission, this latter with the second harmonic generation (optional).

The longitudinal mode spacing of the dye laser resonator is 0.018 cm⁻¹. Its linewidth is 1.2 pm which corresponds to 0.03 and 0.025 cm⁻¹ at 634 and 703 nm, respectively. This means that two longitudinal modes will be

UNELAS



The Scientific, Industrial and Technological Cooperation between Italy and Israel approved the project UNELAS – Underwater network of laser sensors for water monitoring. The partners

are the Satellite and Wireless Communication Laboratory of the Ben Gurion University of the Negev (BGU), Israel and our laboratory.

Built on the complementary experiences on underwater optical wireless communication (Israel) and bio-optical characterization of natural waters by light-induced fluorescence (Italy), UNELAS aims at demonstrating the deployment of an underwater sensor network for coastal zones monitoring.

The Israeli group has developed an underwater optical communication device, based on its wireless technology to transfer the information from the submersible sensor to the processing center above the sea surface. The Italian group has developed and patented SOMBRERO, an underwater spectrofluorometer.

emitted. Unfortunately, the mode structure is not predictable nor constant over minutes: this means that during a lidar experiment energy could be distributed in unknown and unequal parts in the two modes, causing a serious problem due to the narrow bandwidth of the CO₂ absorption lines. In order to overcome this difficulty, the laser manufacturer developed the dynamic mode option (patent pending): a piezo changes the resonator length of the dye laser between every shot, thus modifying the longitudinal mode structure for successive laser pulses. Hence the spectral shape for successive laser pulses is statistically distributed (in our case 50% of the energy is emitted in each mode) and artifacts due to the longitudinal mode structure are suppressed.

Piezo wavelength control allows just one laser system to fire at λ_{ON} and after 1/10 of second at λ_{OFF} . This is achieved as follows:

- the rotatable Littrow grating is mounted on a tilt piezo; with this tilt piezo the wavelength between successive Nd:YAG laser shots is changed so that one shot is fired at λ_{ON} and the other one at λ_{OFF} ;
- although the piezo is fast enough for a 10 Hz repetition rate, the two nonlinear crystals inside the IR unit cannot be moved so fast; therefore two more nonlinear crystals have to be mounted, the first one after the standard mixing crystal and the second one after the standard amplifier crystal; these two new crystals have to be mounted with a slightly different angle in order to produce λ_{OFF} : this is achieved by a special mechanics allowing the adjustment of the new crystal to the slightly different angle with a micrometric screw.

The visible and UV emissions of the system could be used for the spectroscopic

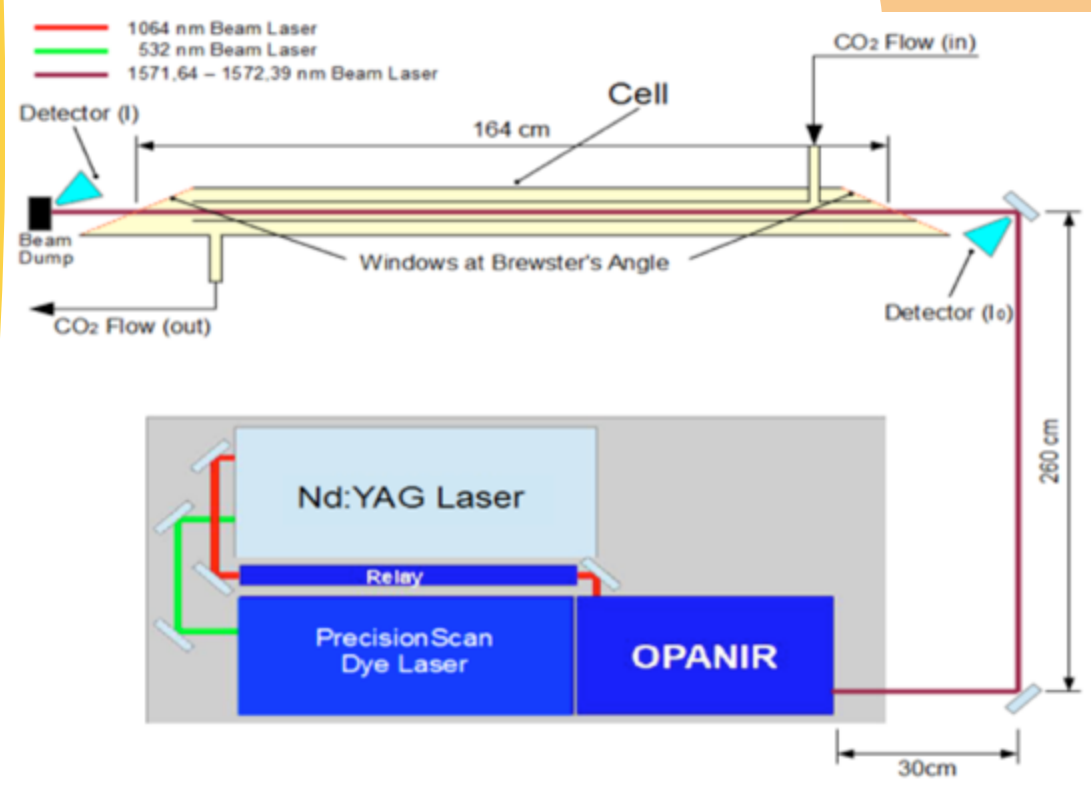


Fig. 2.33 - Sketch of the complex laser system including the CO₂-filled absorption cell used for calibration purpose.

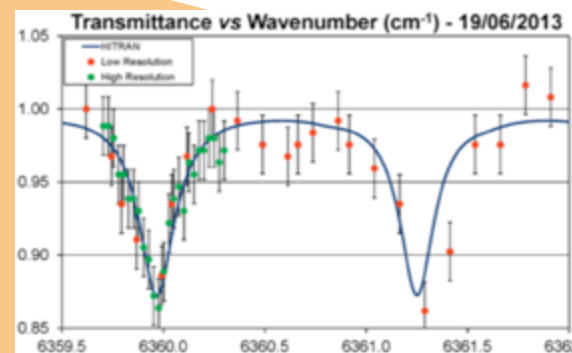


Fig. 2.34 - Transmittance measured in a CO₂-filled absorption cell. Points: experimental measurement. Line: HITRAN data.

measurement of other species (e.g. SO₂, another key molecule of volcanic plumes). Currently, the procurement of the main components (laser system, telescope, detector modules in the 1.6 and 2.1 μ m spectral regions, analog-to-digital converter) has been completed. The laser system has been tested in our lab and results with a CO₂-filled absorption cell confirm the specification provided by the manufacturer (Fig. 2.34).

The final mechanical frame where the lidar system will be hosted has been designed and is in advanced stage of realization (Fig. 2.35).

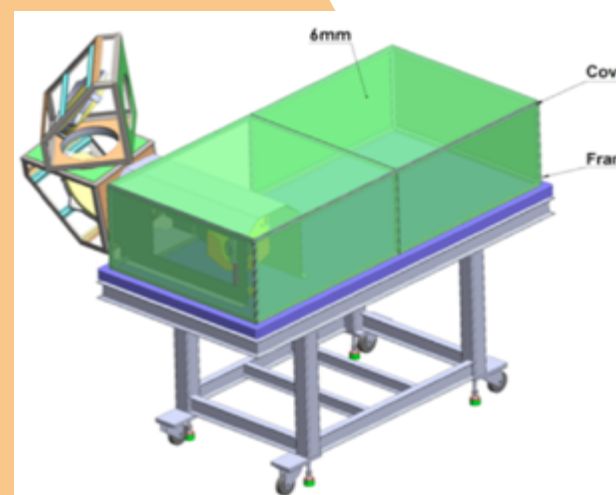


Fig. 2.35 - Mechanical frame of the BRIDGE lidar system (on the left two steering mirror to aim it to the target).



VULCAMED started in the 2nd half of 2013, nevertheless the laser source for the transmitter has been specified and the system lay-out will be delivered in early 2014 to INGV.

2.5 Diagnostics for cultural heritage preservation and fruition

IT@CHA project: an innovative subsea 3D laser scanner



The aquatic environment, and most notably the subsea ambient, is hardly accessible to optical instruments for imaging.

The presence of water gives rise to absorption and scattering processes of the optical radiation which poses limits to the quality of the images and the operative range of the devices themselves. Further technological challenges are associated with the need for the device to be submersible and housed in a watertight chamber, the delivering of power supply, the data transmission and communications.

As far as attention is restricted to conventional 2D imaging techniques for acquiring still images or videos, many progresses have been made and today excellent and well performing devices are available off-the-shelf. The same cannot be said about 3D imaging technology: in this case underwater applications lag largely behind the well-established achievements in developing devices for terrestrial environment. This is in contrast with the ever growing demand from industrial players of improved inspection techniques for assessing the integrity of critical subsea infrastructures. Another driver which is strongly emerging for 3D vision in underwater is related to archaeological applications and to the heightening of the social awareness of the oceans. In the last decade, UTAPRAD DIM has been carrying a R&D activity for developing a

laser based system for underwater 3D imaging with the potentiality to extend the operative range of the technique and its accuracy.

The efforts have been focused on the amplitude modulation technique, which has been proven both theoretically and experimentally an optimal choice for enabling efficient rejection of the unwanted contribution coming from the laser radiation backscattered by the water column. As a part of the IT@CHA project, 2013 has been devoted to consolidate the path towards the realization of a device qualified at Technology Readiness Level 7.

The new sensor has been integrated with an ancillary system made of two subsea cameras for simultaneous stereoscopic vision. In addition a watertight housing of reduced weight and dimension has been manufactured and equipped with two optical windows (Fig.2.36).

A cutting edge solution has been developed for data transmission and based on a fibre optic connector and two active transmission modules converting a radio frequency electrical signal into an optical one.

Other technological improvements include a novel optical scheme for signal detection aiming at enhancing the field of view of the device, more robust and faster motors for vertical and horizontal scans, a compact computer to be allocated aboard the housing for fully and reliable remote control. The main advantage of the technical solutions adopted is the possibility to leave aboard of the support vessel most of the electronics for the system control and communications thus reducing the complexity of the submersed part of the device.

This means relevant benefits in terms of reduced load when it comes to deploy the system on a ROV for inspection missions. The guiding paradigm in the design and realization of the sensor has been the adoption of first class and innovative choices in every part, from mechanics to electronics, from optics to engineering. A multidisciplinary task which

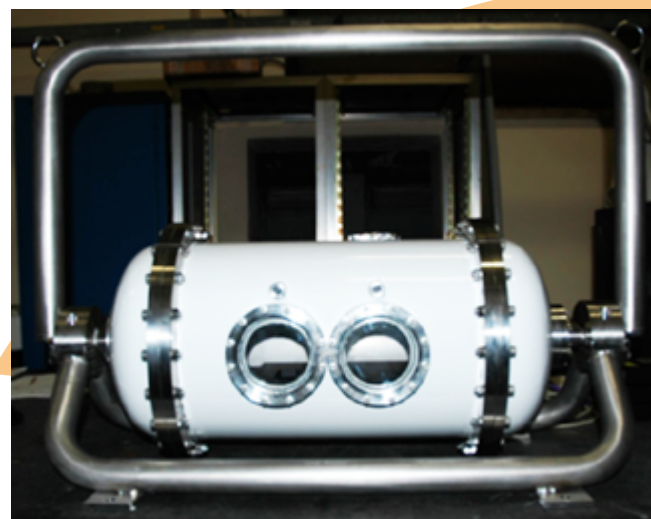


Fig.2.36 - A view of the watertight housing of the submersible 3D laser scanning system. Above the two optical windows, are visible the two cameras for stereoscopic vision.

has meant a wide scale commitment for the DIM researchers and for the technical staff. The system is now under testing in laboratory where accurate calibration procedures are underway for optimizing performances prior to test the device in the field.

3D digitisation by the RGB-ITR colour laser scanner prototype for non-invasive remote monitoring of artworks

In order to meet the demanding requirements of restorers and experts in the field of cultural heritage, the ENEA UTAPRAD-DIM laboratory has recently designed and developed the RGB-ITR (Red Green Blue - Imaging Topological Radar) system (Figure 2.37). It is an innovative Amplitude-Modulated (AM) 3D laser scanner with both accurate (submillimetric) range finding and nativecolour imaging capabilities not affected by external light sources. The instrument was already described in previous activity reports (e.g. 2012 report) and in papers published on international journals.

In 2013 the device has been employed in several field campaigns for the 3D colour digitisation of artworks, among these San



Fig. 2.37 - RGB-ITR laser-radar system assembled in a tower configuration during the field campaign by Santa Caterina della Rosa dei Funari Church (May 2013).



Fig. 2.38 - RGB-ITR 3D color model of the Bandini Chapel with the Assumption altarpiece frescoed by Scipione Pulzone (oil on slate by the a secco technique, 1585, San Silvestro al Quirinale Church, Rome).

Silvestro al Quirinale Church (Rome, May 2013) and Santa Caterina della Rosa dei Funari Church (Rome, May 2013).

Inside these churches the 3D colour digitisation of the two major masterpieces (altarpieces named Assumption and Assumption of the Virgin) by the Italian Counter-reformation painter Scipione Pulzone was funded within the scientific collaboration between ENEA (PON IT@CHA) and the Superintendence for the Historical, Artistic and Ethno-anthropological Heritage of the Lazio region.

These RGB-ITR 3D colour models have been presented during the exhibition "Scipione Pulzone (1540 ca. - 1598). Da Gaeta a Roma alle corti europee", inside the "Museo Diocesano" (Gaeta) since 27th of June till 27th of October 2013.

Figure 2.38 shows the RGB-ITR 3D colour digitisation of the Bandini Chapel with the Assumption altarpiece (1585, San Silvestro al Quirinale Church). Some details of this work are reported in Figure 2.39 where the overlapping regions of the different slates used as support for the fresco are clearly detected by the RGB-ITR data recorded at various meters of distance from the artwork.

Alterations of the altarpiece represented by swellings due to chemical/physical agents (e.g. pollutants) and various restoration works are also observable by the RGB-ITR modelling of the fresco, acquired in a remote, punctual and non-invasive way, especially in the areas of slates overlapping.



Fig.2.39 - Details of the Assumption altarpiece recorded by RGB-ITR concerning the overlapping areas of the different slate supports used for the painting. The high resolution and the high detail accuracy of the RGB-ITR images can be clearly observed.

The capability of the instrument of detecting zones and colour degradation is also evident, demonstrating its role in the preservation studies of artworks.

Figure 2.40 shows the RGB-ITR digitisation of the Assumption of the Virgin altarpiece (1598, Santa Caterina della Rosa dei Funari Church, Solano Chapel). These 3D digitisations represent the starting point in order to perform a colorimetric and structural analysis over the years for evaluating the conservation state of the artworks.

The above-mentioned masterpieces were investigated also by LIF scanner (Laser Induced Fluorescence system): its results (reflectance data) were registered and superimposed on the 3D-coloured digitisation, collected by RGB-ITR, obtaining a multi-sensorial 3D model of the artworks shown in Figure 2.41.

This integration presents several advantages.

- accurate localization of the surface damage of the artworks;
- implementation of an efficient method for a point-by-point remote colorimetry with the ability to optimize the colour infor-



Fig. 2.40 - RGB-ITR color model of the Assumption of the Virgin altarpiece frescoed by Scipione Pulzone and his school (oil on canvas by the a secco technique, 1598, Solano Chapel, Santa Caterina della Rosa dei Funari Church, Rome).

- mation from digital images and models acquired;
- demonstration of the significant improvement of diagnostic capabilities by companing single wavelength high resolution reflectance data with hyperspectral images.

During the period July - October 2013 an in-situ campaign was carried out in the



Fig. 2.41 - Overlap of reflectance images with RGB-ITR 3D color models: Bandini chapel (left), Solano chapel (center). Yellow numbers mark pixels where data reported on the right were collected representing the ratios from reflectance spectra recorded by the LIF scanning system at the working wavelengths (B = 440nm, G = 532nm, R=650nm) in comparison with B/R and G/R monochromatic ratios from the RGB-ITR at the same wavelengths.

Orvieto Dome for the remote diagnosis of the pigments and structural monitoring. The RGB-ITR was applied for the investigation of possible colour deteriorations and cracks status caused after the LAquila earthquake (6 April 2009). The study has been mainly focused on a crack considered to be critical located in the last arch (height = 17m) on the right side of the altar. The same analysis will be performed in the next years on the same arch in order to evaluate possible temporal changes in the cracks size, indicative of the Dome instability and potential structural damages. During all the first campaign, three RGB-ITR calibration curves were acquired illuminating by the lasers a Lambertian certified white target (Spectralon STR-99-020): this method ensures the reusability of the RGB-ITR data for further comparisons not only in terms of structure stability, but also for studying possible temporal alterations of the pigments.

The RGB-ITR has been also successfully employed in the acquisition of 3D colour models of three Serbian icons and drape within the Scientific and Technological collaboration (2013 - 2015) for the Technologies applied to the Cultural Heritage Preservation between Italy and Serbia. The collected data are still

under investigation. Future efforts will be addressed to improve the integration between LIF and RGB-ITR systems, permitting the development of an effective and cutting-edge technique for artwork monitoring and remote colorimetry that allows the experts to plan the restoration work, saving time and avoiding some drawbacks of the classical "naked-eye" approach, such as subjective and emotive state, influence of external light sources, use of scaffolds, etc..

Finally, an important three-year Framework Agreement for Scientific Collaboration (updatable for another three years) between ENEA and Vatican Museums was ultimately signed during 2013 aimed to apply most innovative technological developments to the conservation of cultural heritage.

Application of LIF technique in the field of Cultural Heritage

Laser Induced Fluorescence (LIF) has found, in the last years, widespread application to the field of the study and the characterization of Cultural Heritage materials. Thanks to its unique properties to be a non destructive and non invasive remote technique, with no sampling requirements, based on transportable

or portable instruments that can provide first results in real time, LIF has been widely applied to the individuation of damages or specific materials on frescos, mural paintings and large architectural surfaces. At Diagnostic and Metrology Laboratory of the UTAPRAD Unit two prototypes of LIDAR fluorosensor have been developed for LIF measurements: the first is a punctual scanning system, the second one allows a line by line scan of the investigated surface. Both the apparatus can be used also to record, remotely, reflectance data in the whole spectral range between 200 and 900 nm, useful also for a colorimetric reconstruction of the artworks.

Reflectance measurements on Renaissance artworks

Two immovable masterpieces by Scipione Pulzone named "il Gaetano" have been investigated by the LIF line scanning. The artworks are two paintings of the Assumption of the Virgin Mary that the author realized respectively on slate and on canvas in two churches in Rome (San Silvestro al Quirinale, Bandini chapel and Santa Caterina dei Funari, Solano della Vetera chapel) in the second half of XVI century by using the a secco technique. From the remote reflectance measurements different kinds of images have been obtained: RGB image from raw data, RGB image from complete spectral information, IR image. An example is shown in Figure 2.42 for the paint of Santa Caterina de' Funari. This campaign has given also the opportunity to attempt



Fig. 2.42 - Comparison among RGB image obtained from raw data (left), RGB data from the whole visible spectrum (centre), IR image (right).

a software overlap between the data of the RGB-ITR prototype and the data of the recent line LIF scanning system. An example of the obtained results has been already shown in Figure 2.41.

LIF measurements on Serbian icons

Tree icons, part of the Serbian Cultural Heritage have been scanned by both the LIF apparatus of the Laboratory.



Fig. 2.43 - One of the Serbian icons scanned by LIF apparatus.

The first obtained results have highlighted the presence of a very low fluorescence signal due probably to the conservation conditions: a dark patina, probably due to candle smoke, is detectable on the whole surface of both the artwork. Moreover, for the icon shown in Figure 2.43, the LIF data have revealed a strong disomogeneity between the face of Christ and the rest of the paint. This result is particularly interesting since such pigment difference has not been detected by naked eye or by microscope so far.

LIF application to contemporary artworks

So far, just a very few papers deal with the application of LIF to the study of contemporary artworks. In the contemporary art there is a strong diversification in terms of used techniques and materials. The latter are often fragile or perishable, but relatively new and their behaviour with aging is not yet verified. A right comprehension and interpretation of fluorescence data are, then, a challenge. Four artworks by Gastone Novelli, of the National Gallery of Modern and Contemporary Art of Rome, have been investigated by a compact LIDAR fluorosensor punctual scanning system developed at the DIM Laboratory for LIF measurements. The experimental activity has been divided in three steps.

The first step has been the characterization of materials commonly used in contemporary artworks. In the second step, the non-invasiveness of the LIF technique has been checked prior to its application on the works of art. For this reason specimens of various materials have been irradiated with laser at 266 nm and monitored with traditional colorimetry, remote reflectance and observations under the stereomicroscope. In the third step, four artworks by Gastone Novelli: "Dice meraviglioso" (1959), "Potrebbe uscire" (1959), "Gesto respinto" (1959), "Le cose nell'uovo" (1958), stored in the Galleria Nazionale d'Arte Moderna e Contemporanea

(Rome), have been investigated by LIF technique, using the portable instrument above mentioned. Fluorescence measurements have been carried out on the front and back of each work and in support some samples have been taken on the rear face of the four works and have been characterized by Micro-Raman spectroscopy. The analyses performed have highlighted the ability of the LIF technique in chemically characterizing and identifying materials, also thanks to the database built with several reference materials. Moreover, information on the artistic technique has been provided to the conservators and to the historians of art together with the knowledge of the conservation state of the studied artworks by Gastone Novelli. The collected data and the relative elaboration have provided fluorescence images, false colours images, punctual spectral information, highlighting large differences not detectable by naked eye. In particular, the use of different classical materials mixed with modern plastic diluents, that gave rise to more marked mechanic resistance properties of the surfaces, has been revealed.

In Figure 2.44 a picture of the artworks "Gesto respinto" (on the left) is compared with a fluorescence image filtered at 365 nm (on the right) obtained for this painting by LIF. The observed image distortion is due to the geometric arrangement of the system and it can be easily corrected by Photoshop.

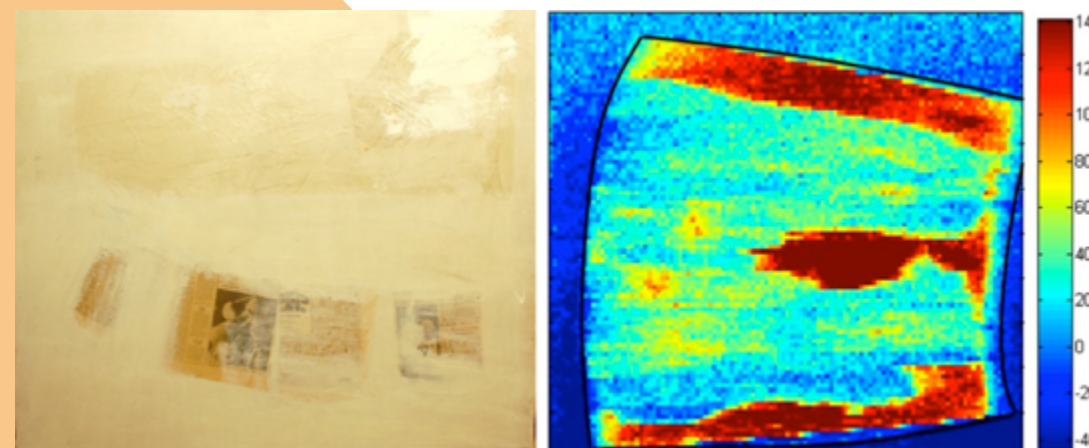


Fig. 2.44 - Left: Picture of the artwork "Gesto respinto". Right: fluorescence image filtered at 365 nm of the painting.

2.6 Laser spectroscopic material characterization

Ultra-sensitive LIBS analysis of liquids in small volumes

ENEA has an internationally recognized expertise in LIBS analysis of liquids and materials inside liquids. Here, we report some results of an extensive experimental work aimed to obtain ultra-sensitive LIBS analysis of liquids in small volumes. This issue is of an utmost importance for different applications, including medical and biomedical, environmental monitoring, quality control in industry, food control and security. LIBS measurements on liquids have very high detection threshold, typically > 1ppm, and also for this high energies (>100 mJ) of one or two coupled lasers are required. The process of laser induced plasma formation is inefficient because a great amount of the input laser energy is expended for liquid evaporation and inherent mechanical effects such as liquid droplet expulsions or their explosion. The most efficient LIBS method on liquids

regards sampling of a liquid jet with two high energy lasers, but this requires a complex instrumentation, the sample volumes larger than 100 ml and washing of the liquid circuit when changing the sample. We developed a method for sampling of single liquid droplets with volume in order of only 10 μL, and by applying relatively low energy (in order of 10 mJ) of a single laser source. Here, we exploit a presence of a substrate as a mean for lowering of the plasma formation threshold and additional plasma heating. The droplet thickness on a solid support is always larger than 0.5 mm, and a laser pulse with sufficient energy to form the plasma disintegrates the droplet, causing splashing on nearby optics which prevents further measurements. Our innovation consists in deformation of a liquid droplet into a liquid film of controllable thickness, either by a mechanical energy or an external electrical field. Such deformation increases an efficiency of the plasma formation and its intensity, eliminates the droplet disintegration and allows the sampling over many laser shots (up to 50). A comparison between sampling a droplet without and with its controlled deformation is shown in Figure 2.45. In this process, a choice of the substrate materials is essential for lowering of the necessary input laser energy and for obtaining highly stable LIBS signal from one shot to another. As a final result, we obtained highly sensitive LIBS measurements on a single droplet, with the estimated detection limits in order of 0.001 ppm (Fig. 2.46). A patent procedure is currently pending for the method and instrument for sensitive LIBS analysis of single liquid droplets.

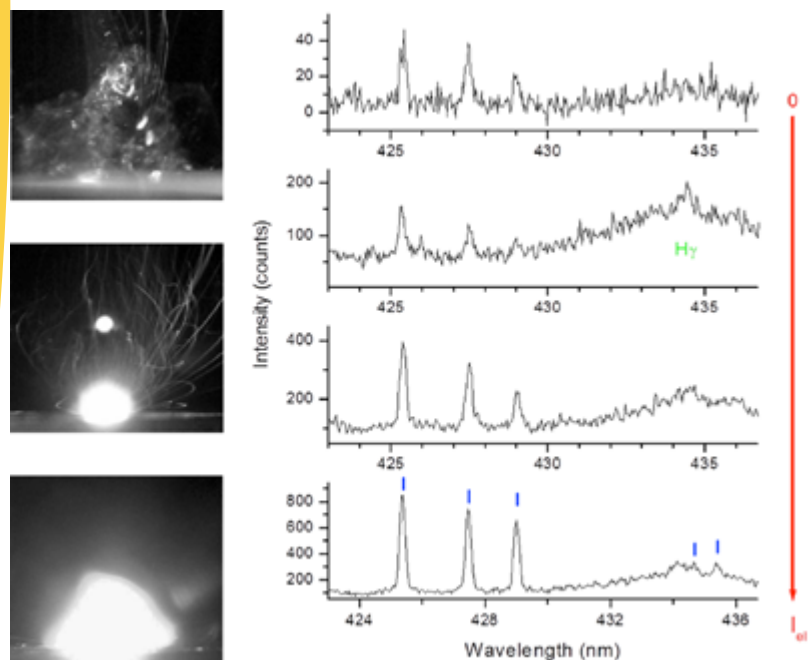


Fig. 2.45 - Photographs of the plasma (left) and the single shot LIBS spectra (right) from chromium in water solution: the droplet thickness decreases downward.

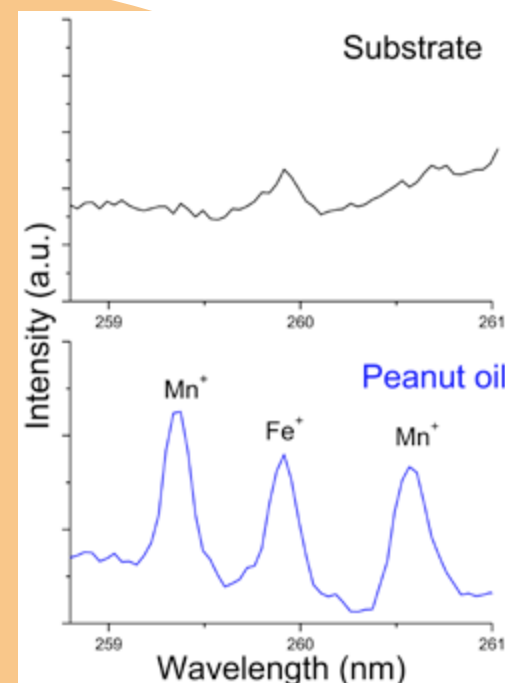


Fig. 2.46 - Detection of Mn and Fe in peanut oil droplet by applying a single laser shot; the reference values from literature are 1-22 ppb and 7-35 ppb, respectively.

LIBS as an internal ENEA's technological service

LIBS laboratory provides also an internal service for material characterization to other ENEA's groups. Here we report an example of characterization of some components of high-vacuum chamber. The scope of the measurements was to identify the material and the deposited layer at the surface, the latter necessary to tag the source of the contamination. Although the component was considered based on an aluminium alloy, LIBS measurements revealed that the base material was Molybdenum, containing following minor or trace components: Si, Al, Ca and La (Fig. 2.47). A presence of Lanthanum was surprising, however, four characteristic La lines were clearly detected and with intensity ratios corresponding to NIST database. The surface contamination on the internal chamber's part had dark color, and it was supposed to be due to Fe or Si deposition during recently performed experiments. However, the LIBS stratigraphy

show that the main element in the deposited layer is Germanium, which emission is absent already after the second laser shot applied at the fixed position (Fig. 2.47 bottom). During the crater drilling by the successive laser shots, the intensity of the ionic lines (Mo⁺) increases due to increased temperature of the confined plasma. These measurements allowed to the end-user to identify clearly the contamination source.

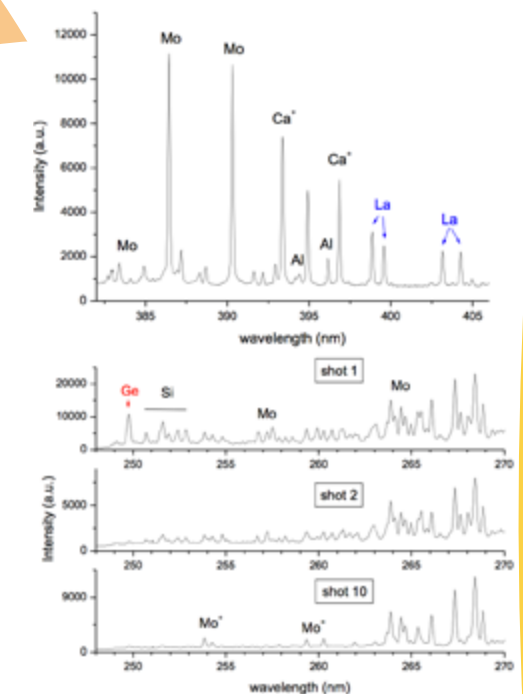


Fig. 2.47 - Top- Identification of the base material; Bottom - depth profiling of the contaminated area and identification of the contaminant (Germanium).

2.7 Technology for energy

In Vessel Viewing and ranging System for ITER

The "In Vessel Viewing and ranging System" (IVVS) is a laser radar sensor for viewing and ranging able to perform a survey of the status of the first blanket wall and plasma divertor facing components in ITER reactor and to make erosion measurements of the vessel during the plasma discharges. The activities of designing and testing of the probe components

have been completed in the 2013 by means of the Fusion for Energy (F4E) Grant F4E-GRT-282 (RH) for the full compatibility of the IVVS probe with the geometrical constrains of the access port and the ITER working conditions: high temperature (120°C), very high magnetic field (8T), ultra high vacuum (UHV), neutron and gamma fluxes (5kGy/hour and integrated dose up to 10MGy). The IVVS prototype developed at ENEA UTAPRAD-DIM Laboratories in cooperation with UTFUS-ING is a high-performances amplitude-modulated laser radar working in the near infrared region (820nm). The probe steers the laser beam through a fused-silica prism attached to the mechanical axes whose rotations allow the scan of the desired area. Two optical encoders accurately measure the angular position of the prism allowing the reconstruction of high-resolution range and intensity images. Several tests on critical components like piezoelectric motors, optical



Fig. 2.48 - Top: piezo-motor test assembly on the CALLIOPE Facility. Bottom: insertion of the tested components in the TAPIRO neutron channel

encoders and fused-silica optical samples have been completed at the CALLIOPE (UTTMAT) and TAPIRO (UTFISST) facilities, located at the ENEA Centre in Casaccia, in order to verify their behavior under gamma and neutron irradiation (Fig. 2.48). New tests on IVVS probe have been completed at UTFUS-ING in 2013 exploiting facilities at ENEA Frascati, in order to verify the compatibility of the critical components to magnetic field and vacuum for typical ITER working conditions. Further erosion tests have been also carried out on a reference aluminium alloy plate placed at about 4m of distance from the IVVS laser radar. The metallic plate was eroded on four different areas (engravings) with various depths (2.1mm, 0.5mm, 0.3mm, 0.1mm) in an attempt to simulate the possible erosion processes of the ITER vessel. Thereafter, several scans of the target were performed placing the metallic plate at different orientations with respect to the direction of the incoming laser beam (inclination angles of 0°, 20°, 45° and 60°) for acquiring high-resolution, reliable, accurate 3D models of the investigated target with different laser powers up to 20mW and modulation frequencies of about 500MHz. A comparison between the plate loss of weight opportunely evaluated by means of the IVVS laser radar and measured by a high-accuracy balance before and after the erosion has been performed showing a maximum percentage error less than 10% in optimal working conditions. A new IVVS version has been obtained by using a new version of the laser source having better performances, especially in terms of stability, allowing to achieve a range resolution of about 40 micron and pixel integration time of 3ms. In Figure 2.49 the

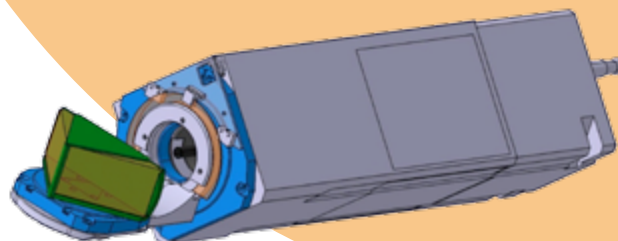


Fig. 2.49 - Final version of IVVS probe

final version of the IVVS probe is shown. A new design of the optical configuration has allowed to maintain a high collection efficiency of the signal, though the lateral dimensions of the probe have been decreased at the values 150mm*150mm.

LIBS detection of H and D in ITER-like tiles superficial layers

The cooperation with the ENEA UTFUS-TEC, followed up in 2013 in the framework of the EFDA Task WP11-ETS-DTM - 01-05 "dust and tritium management". The optimization of the experimental parameters for a LIBS system to be implemented in situ and remote sensing was completed in view of the design of an apparatus to be installed in the next fusionistic ITER machine. As part of the Italy-Poland collaboration in the same area of activity, in November 2013 a Laser-Induced-Breakdown-Spectroscopy (LIBS) investigation of metallic sample of fusionistic interest was performed at the Institute of Plasma Physics and Laser Microfusion (IPPLM - Warsaw) laboratories. In this test was evaluated the potentiality of a double pulse LIBS technique to increase the experimental sensitivity. The results obtained, and still being processed, have demonstrated the increase of the atomic emission spectroscopy using the double-pulse technique, in which two temporally close ($\Delta t \approx 300$ ns) laser pulses are employed, the first ablating a small fraction of material from the sample surface and forming a microplasm of ions reproducing the atomic composition of the sample, the second reheating this plasma in order to increase its spectroscopic signal. In Figure 2.50 the temporal evolution of the spectroscopic signal is shown. As an example of signal enhancement in Figure 2.51 the spectroscopic region around 657 nm is shown, where the H α and D α lines of the Balmer series of hydrogen and deuterium are observed, as markers of the presence in traces of these two isotopes on the sample surface. Also observed in this spectral range are two ionic emission from carbon, arising from the sample surface, made of this element for 50% in atomic concentration.

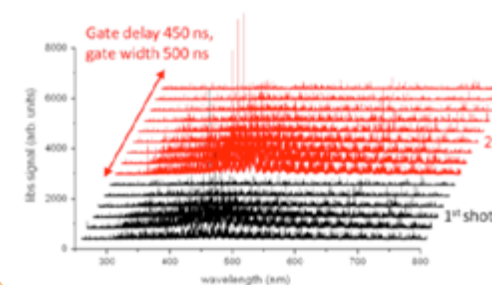


Fig. 2.50 - Temporal evolution of the double pulse LIBS spectroscopic signal. In black the spectral emission arising from the induced microplasma, in red the effect of the second shot reheating the microplasma and enhancing the spectroscopic signal.

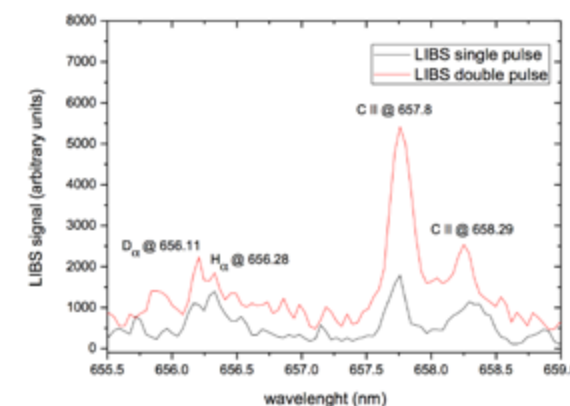


Fig. 2.51 - Double-pulse (red line) vs single pulse LIBS (black line) on samples of fusionistic interest.

Energy storage: ProGeo project

The accumulation of electricity from renewable sources through the transformation of surplus into "electro-fuels" is becoming one of the most competitive means of energy storage. The demonstrative plant, ProGeo 20 kW, funded by the private firm PLC System, has been completed with the manufacture of the main innovative components and their connections. The pressure and temperature tests will be completed by April 2014 and the green-methane production will start later.

R&D hydrogen recovery by membrane processes

The CO₂ produced is expected to be roughly 90% in the methanation reactor. At this stage, it is also possible to separate the portion of H₂

that does not react with the CO_2 and send it back to the reactor, saving power and resulting in the overall process being more efficient. The development of adequate nano-structured membranes is, as a result, expected to enhance the quality of the process, making it possible to separate off a small portion of the hydrogen suspended in a flow composed primarily of CO_2 and CH_4 . This membrane technology is a cleaner approach to providing higher efficiency and more reliable processes for the recovery of fuels such as hydrogen. Certainly, advanced materials must be designed to enhance the current permeability/selectivity ratio through mechanisms running from H_2 -selective to reverse H_2 -selectivity separations (Fig. 2.52).

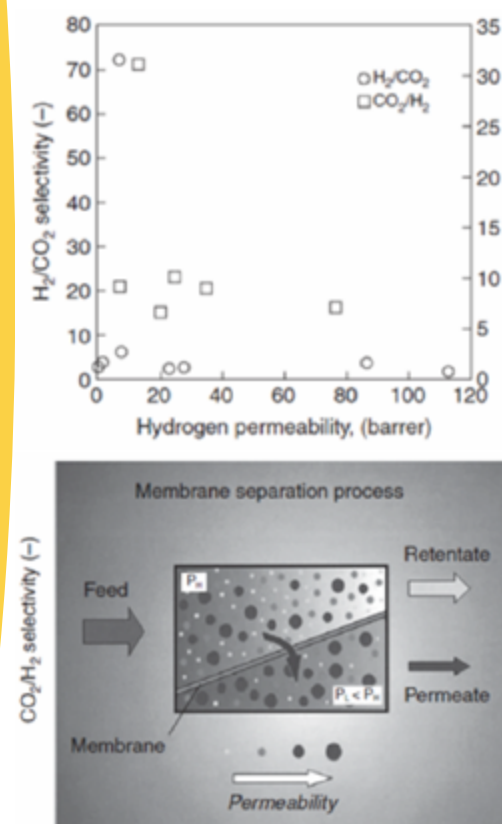


Fig. 2.52 - (a) Hydrogen permeability vs H_2 -selectivity and reverse H_2 -selectivity; (b) schematic representation of membrane gas separation.

Engineer and optimizing R&D

The methane reactor is the core of the system and its careful design allows the achievement of a very high conversion level in a very small space. An essential point is the gas pressure drop when passing through the catalyst inside the reactor itself. In order to design and to optimize a compact methane reactor, with high gas flow and moderate pressure, it was necessary to simulate the pressure drop in a proper mock-up. In Figure 2.53 it is possible to verify that the selected catalyst in the identified geometry of the reactor could produce a mean pressure drop of about 1 bar.

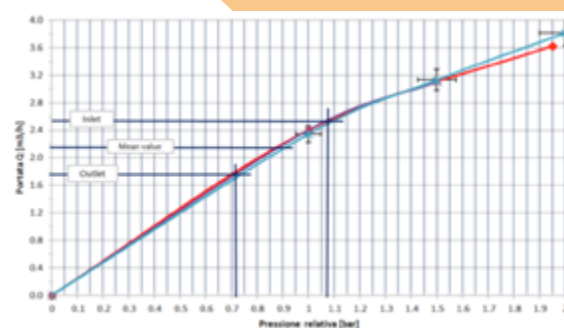


Fig. 2.53 - Simulated pressure drop in the methane reactor.

During the methane reaction we have a molar reduction of the reacting gases and the pressure drop changes along the axis of the reactor itself. Other characteristics are going to be evaluated on trial (catalyst thermal conductivity, etc.) in order to define a proper geometry to assure the lowest differences of the main reaction parameters. The storage is a primary element in the further development and distribution of renewable energies. Thus the various technologies involved – membrane processes, catalysts, storage and fuel cells, etc. – must be integrated and integrally linked to rational distribution and use of these energy sources.

3. MATHEMATICAL MODELING LABORATORY

3.1 Mission and infrastructures

Main objectives of the laboratory are to develop advanced Mathematical Methods for the study of the classical and quantum optics and for modeling the transport of charged particle beams, to study and modeling of complex and quantum optics, and for modeling the transport of charged particle beams, to study and modeling of complex systems, including biological systems.

Competences available in the Laboratory are originated from expertise in different scientific disciplines as charged beam dynamics and transport, accelerators, RF structures, lasers, free electron lasers, optics and resonators, mathematical modeling.

UTAPRAD-MAT is currently involved in the development of the SPARC free electron laser test facility at LNF-INFN.

The activity of UTAPRAD-MAT during 2013 has been developed along the following directions:

- Free Electron lasers (FEL)
- Design of electron Sources
- Applied Mathematics and Theoretical Physics

Funding and Projects

The research activities of the UTAPRAD-MAT Laboratory were mainly funded in the frame of National research programs (MIUR) as partner of collaboration (SPARX) addressed to FEL development including the collaboration with INFN on SPARC LAB activities.

The ENEA Fusion Technical Unit (UTFUS) in collaboration with the Radiation Sources Laboratory (UTAPRAD-SOR) and the Theoretical Physics Laboratory (UTAPRAD-MAT) have set up a joint Task-Force for the

for the preliminary design and a prototype realization of a CARM to be tested on the Frascati Tokamak (FTU).

3.2 CARM Development

During the year 2013 the scientific activity for the design of a new source of high-frequency (> 250 GHz) high power (~ 500 kW) radiation for applications in the field of nuclear fusion, such as heating and plasma diagnostics and “current drive”. The theoretical analysis has been directed towards the understanding of the relevant theory as closest as possible to the theory of ordinary Free Electron Laser operating with magnetic undulators. The obtained results have opened the possibility of describing these devices in terms of simple and reliable formulae which allow a very fast design of the entire system.

In a CARM (Cyclotron Auto-resonance Maser) device a moderately relativistic e-beam is injected in a cavity where an axial magnetic field drives the electrons along an helical path (Fig. 3.1). Coherent emission towards a mode of the cavity occurs whenever the resonance condition

$$\omega = \Omega + k_z v_z \quad 1)$$

is satisfied. In the previous equation

$$\Omega = \frac{eB}{m\gamma}$$

is the relativistic cyclotron frequency, v_z is the electron longitudinal velocity and k_z is the field wave vector, linked to the phase velocity by the identity

$$v_p = \frac{\omega}{k_z} \quad 2)$$

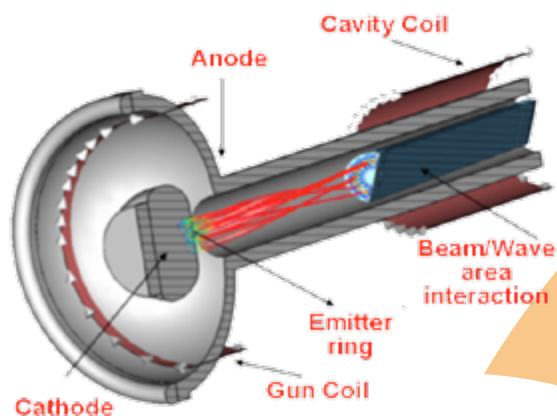


Fig. 3.1 - The CARM component, from the electron gun to the interaction region

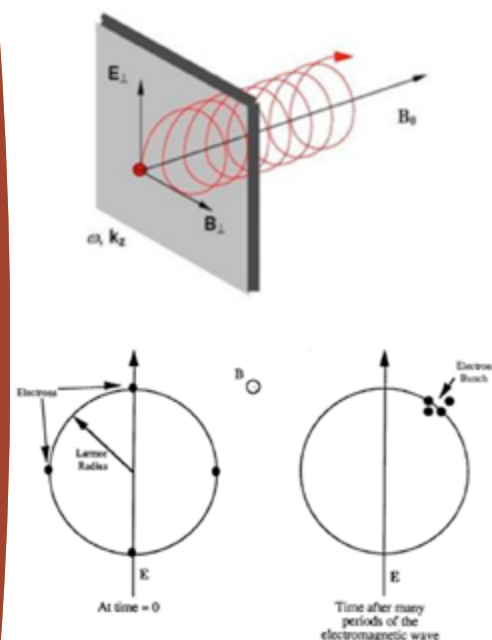


Fig. 3.2
 a) Cyclotron trajectories inside the interaction region;
 b) Schematic view on the Bunching mechanism, referred to the electron reference frame

The emission process occurs via the bunching mechanism, schematically depicted in Figure 3.2, along with the electron trajectories inside the interaction region. The interaction with the cavity mode electric field determines an energy modulation which transform into a density modulation and coherent emission

occurs when the electrons are modulated on a scale comparable to the mode wavelength.

In these devices the auto-resonance is guaranteed by the fact that any variation of ω is compensated by a suitable modification of the longitudinal velocity. This effect is in turn responsible for the intrinsic high efficiency of these devices. The CARM theory can be reformulated by using the same language and formalism of FEL theory, to this aim we will take advantage from the wealth of scaling relations currently exploited for the design and the optimization of the undulator based FEL devices. The core of our strategy is that of analyzing the CARM theory and find a one to one correspondence with the physical quantities entering the description of a FEL.

The following set of variables is sufficient to describe the CARM dynamics

$$w = \frac{\gamma_0 - \gamma}{\gamma_0}, \delta_0 = \left(1 - \frac{\beta_z}{\beta_p}\right) \left[1 - s \frac{\Omega}{(1 - \beta_z^2)^{3/2}}\right], \delta = \frac{2}{\beta_z^2} \left(1 - \frac{\beta_z}{\beta_p}\right) w, \quad (3)$$

$$\Delta = \frac{2(1 - \beta_z^2)}{\beta_z^2(1 - \beta_z^2)^{3/2}} \delta_0, \xi = \frac{\beta_z^2(1 - \beta_z^2)^{3/2} \cos z}{(1 - \beta_z^2)^{3/2} c}$$

$$F_s = \frac{4|d|}{\gamma_0 m_e c^2} \frac{(1 - \beta_z^2)^2}{2\beta_z^2(1 - \beta_z^2)^{3/2}} [CJ] \Pi$$

Regarding the electron kinematic quantities we will use β_z and β_\perp to indicate the (initial) longitudinal and transverse reduced velocities respectively, while γ stands for the relativistic factor and

$$\beta_p (= \frac{v_p}{c})$$

for the phase velocity term. The coordinate of propagation, namely the longitudinal coordinate, is z . The symbol Π denotes the TE mode field amplitude and $[CJ]$ is a contribution depending on the geometry of the cavity where the interaction occurs, in

the case of a cylindrical cavity it is given by a suitable combination of Bessel functions, the index s stands for the s -th harmonics.

Furthermore δ_0 is the frequency detuning and the condition $\delta_0=0$ corresponds to the resonant interaction. The previous variables can be embedded to provide a set of equations resembling the pendulum like equations and in the small signal regime the field growth can be derived from the integral equation, resembling that of the ordinary FEL

$$\frac{d}{d\xi} F = \frac{i}{2} (b\Delta - 1) I \int_0^{\xi} (\xi - \xi') F(\xi') e^{i\Omega(\xi - \xi')} d\xi' + i \frac{I}{2} \int_0^{\xi} [F(\xi') e^{i\Omega(\xi - \xi')}] d\xi'$$

This approach has allowed the derivation of the field growth along the cavity axis, according to what has been reported in Figure 3.3

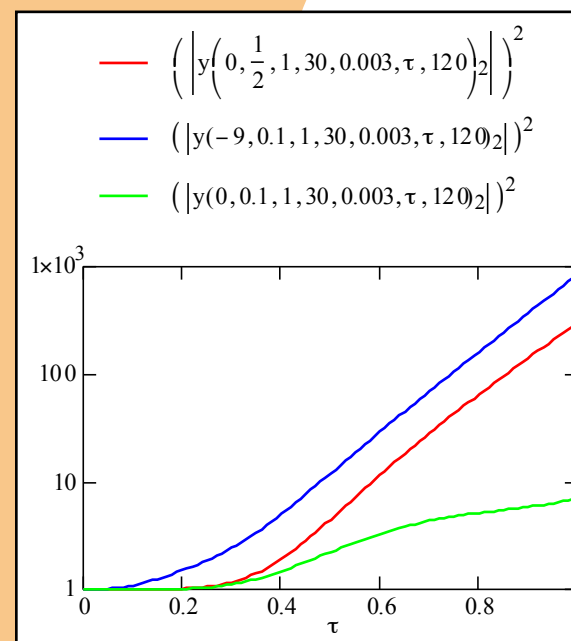


Fig.3.3 - Normalized CARM intensity evolution vs. τ for values reported below

a) $v = 0, b = \frac{1}{2}, \chi = 1, \alpha = 3 \cdot 10^{-3}, g_0 = 30$

b) $v = -9, b = 0.1, \chi = 1, \alpha = 3 \cdot 10^{-3}, g_0 = 30$

The obtained numerical results have been shown to be compatible with the analytical formula (see Fig. 3.4 for the comparison)

$$F(z) = \frac{F_0}{9} \left[3 + 2 \cosh\left(\frac{z}{l_g}\right) + 4 \cos\left(\frac{\sqrt{3}}{2} \frac{z}{l_g}\right) \cosh\left(\frac{z}{2l_g}\right) \right] \quad (14)$$

Where l_g is the gain length

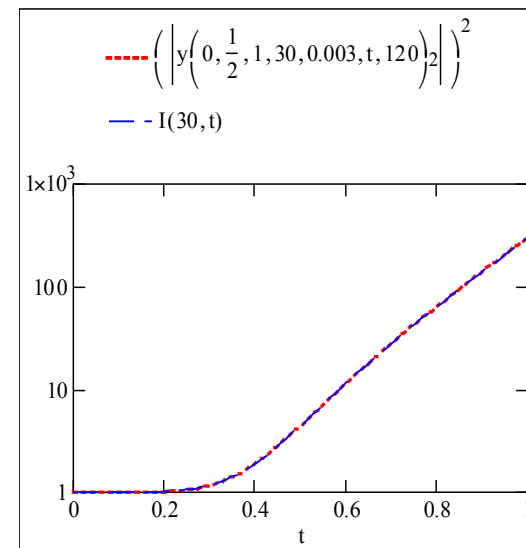


Fig. 3.4 - Comparison between analytical (blue) and numerical (red), results at $b = \frac{1}{2}, v = 0$

The extension to the non-linear regime will allow the inclusion of the saturation effects and the relevant analysis is in progress.

The design of cavity and of the gun geometry have been improved.

As matter of fact the results of this refinement have provided the longitudinal spread and spot shape inside the cavity, reported in Figure 3.5.

analytical treatment. A significant result of the theoretical analysis has been the prediction of overlapping effects between the operating modes, a result which has been checked in the experiment (see Fig. 3.7).

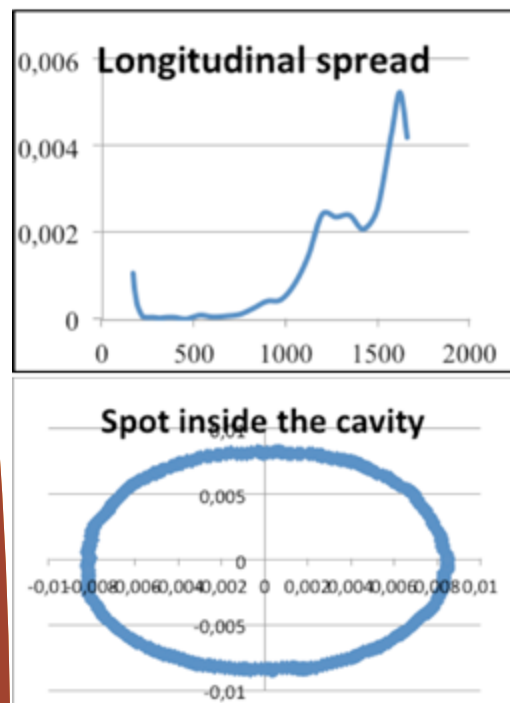


Fig. 3.5 - Calculated longitudinal spread (top) and spot inside the cavity (bottom).

3.3 SPARC activity

Particular attention has been devoted to the understanding of the SPARC dynamics operating with two different frequencies (λ_2 and λ_1). In particular different configurations have been analyzed either from the theoretical and experimental point of view. In Figure 3.6 we have reported the mode growth and the relevant comparison between numerical and

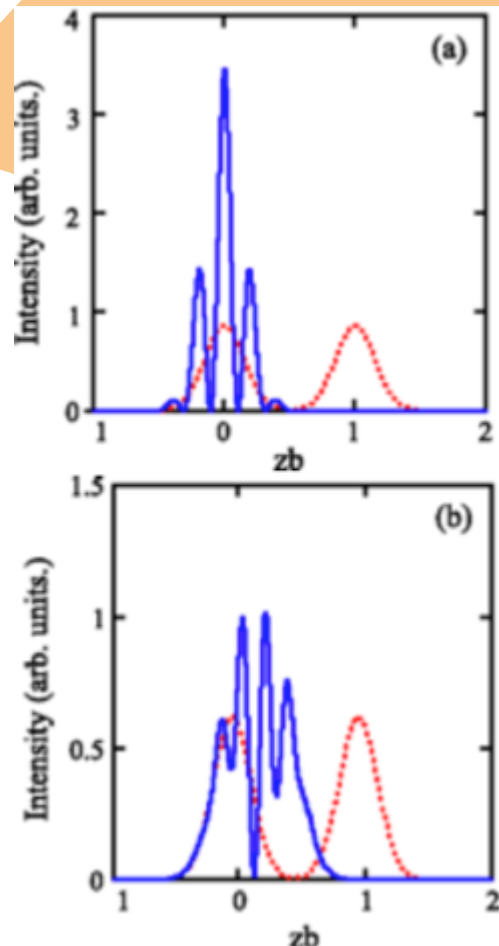


Fig. 3.7 - Calculation of overlapping effects between operating modes.

In Figure 3.7 the field power evolution (PROMETEO simulation) of the two peaks, along the physics undulator coordinate $z(m)$, for different detuning conditions: (a) $\lambda_2 - \lambda_1 = 107.3nm$, (b) $\lambda_2 - \lambda_1 = 30.3nm$, (c) $\lambda_2 - \lambda_1 = 10.3nm$ is shown.

Dimensionless intensity versus zb , packet coordinate normalized to the bunch length. The red dotted curve refers to the radiation produced by two identical bunches separated by a rms bunch length. The blue curve shows (a) completely overlapping bunches and (b) bunches with distance $db \approx 0.4\sigma_z$. The numerical analysis reported in Figures 3.6 and 3.7 suggests that the two operating fields at different wavelengths exhibit a kind

of mutual bunching, which becomes more significant with decreasing frequency shift. The importance of the bunch separation is further stressed in Figure 3.8 where the presence of spikes is observed with varying distances between the two electron bunches. The experimental data collected by FROG detector, reported in Figure 3.8, have reproduced the behavior predicted by the theoretical analysis (sim.). An important upgrading of the SPARC control system has been developing a software application that implements a new approach to matching no longer based on the periodicity of the Twiss parameters of the beam along the undulator, but on the optimization of the gain function. The software has been implemented on the

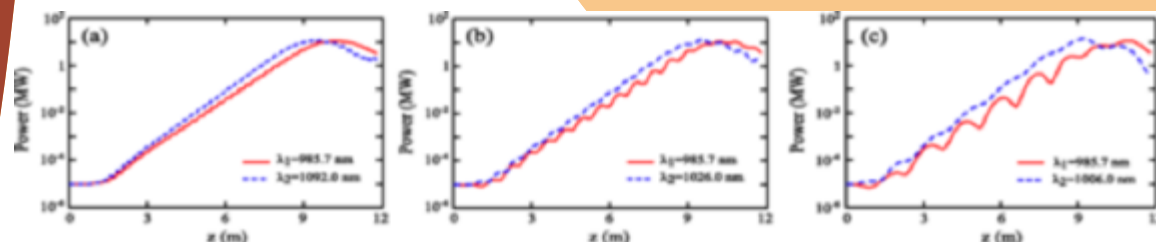


Fig. 3.6 - Comparison of numerical and analytical treatment for SPARC mode growth.

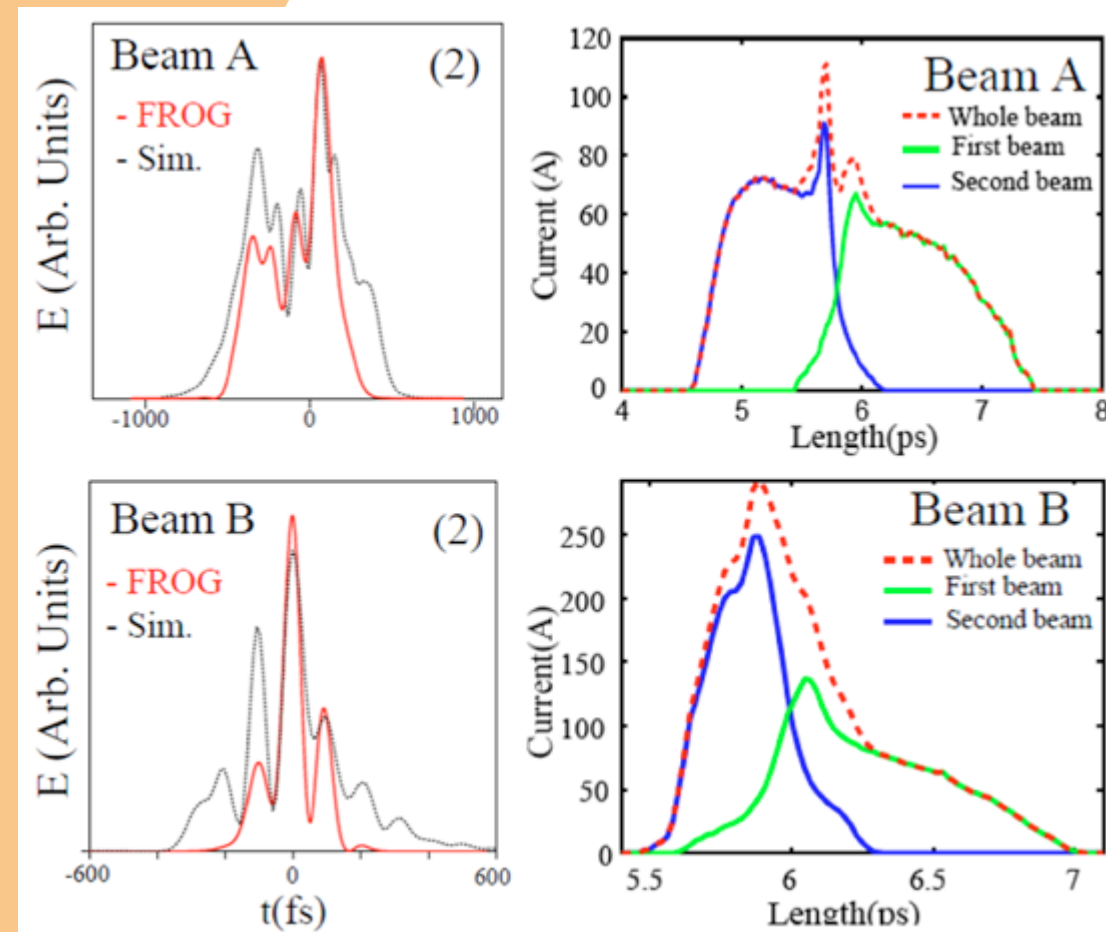


Fig. 3.8 - FROG images from the SPARC experiment of Optical pulse intensities and corresponding electron bunches temporal shapes

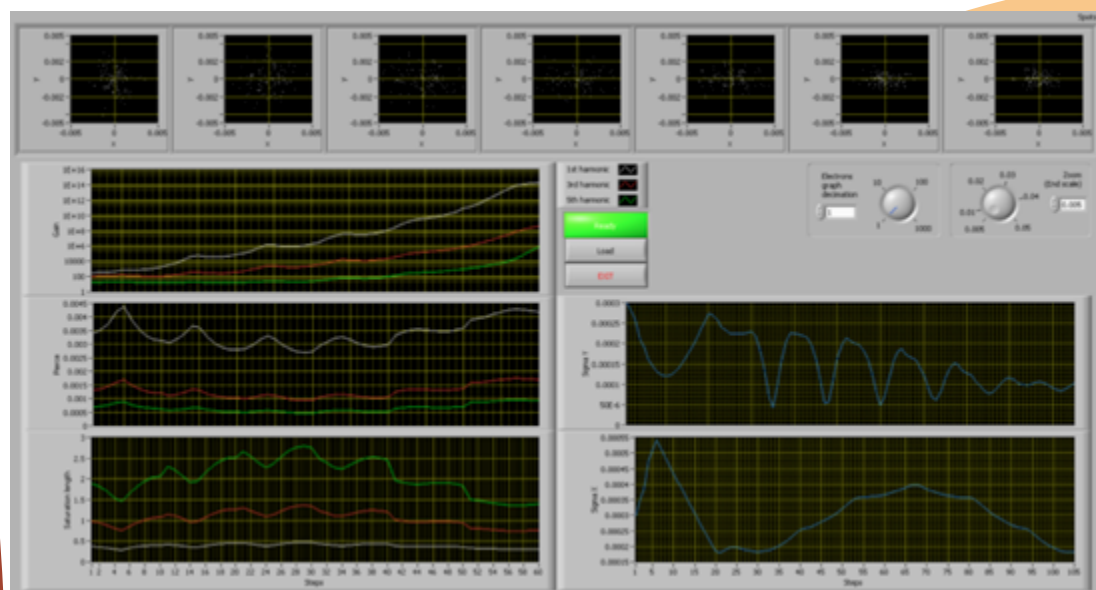


Fig. 3.9 - Sparc Transport beam control panel

control system of the SPARC experiment, an idea of the various panel controls managed by this new software is reported in Figure 3.9.

3.4 Applied Mathematics and theoretical physics activity

The collaboration with the university of Paris Sud, Paris XIII and the Polish Academy of Sciences, has been pursued on the activities related to the study of symbolic methods and to their application about integration techniques and solution of differential equations for the problem of anomalous transport. Within this context the laboratory has obtained new and important results within the context of the analysis of photoluminescence (PL) decay. The analysis of the related phenomena has been developed using an analysis based on the solution of fractional Fokker-Planck equations, yielding the Levy Stable distribution for the PL decay which has been able to disclose a close agreement between analytical and experimental results as shown in Figure 3.10.

Analogous methods of solution have been employed for the analysis of the solution of entirely new families of quantum relativistic

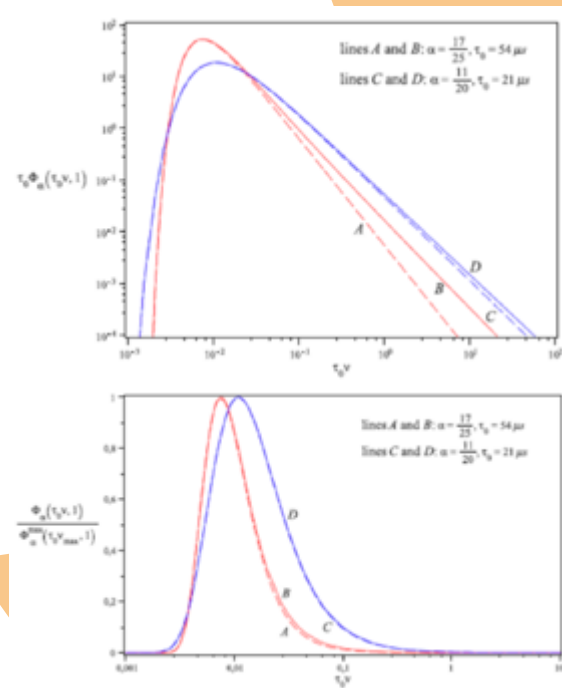


Fig. 3.10 - Effective decay rate vs. frequency

equations, of Dirac and Klein- Gordon type.

Within such a framework new techniques have been developed to treat problems in relativistic quantum field theory.

4. PHOTONICS MICRO AND NANO-STRUCTURES LABORATORY

4.1 Mission and infrastructures

Photonics and nanotechnology have been recognised by the European Commission among the Key-Enabling Technologies (KETs) of the European program Horizon 2020 (2013-2020). They play an important role in the R&D, innovation and strategies of many industries and are regarded as crucial for ensuring their competitiveness in the knowledge economy.

The major challenges in the modern world, solution for energy, health, environment, information and communication technology (ICT), safety and security, are driven in their development by the generation, guiding, amplification, manipulation and detection of photons, the basic unit of light.

In the last decades, important advances in the field of nanotechnologies enabled major breakthroughs in various scientific domains, due to the possibility of controlling and tuning the physical properties of materials at the nanoscale (electron confinement).

One of the main objectives of photonics, the R&D of technologies for miniaturization of novel light-emitting devices and optical sensors, includes functionalisation with nanomaterials, control of interfaces at nanoscale and engineering of semiconducting-metallic-dielectric multi-layered media. Their spatial dimensions should be below the typical wavelength of the used electro-magnetic (e.m.) radiation for fully exploitation of light-matter interactions and photon confinement effects.

At ENEA C.R. Frascati, in the Technical Unit for the Development of Applications of Radiations, the Photonics Micro- and Nano-structures Laboratory (UTAPRAD-MNF) carried out R&D activities on synthesis, characterisation and functionalisation of nanomaterials (nanopowders, nanowires, nanotubes, etc.) together with the study,

realization and characterization of novel light-emitting micro-devices and solid-state radiation detectors. It is deeply involved in the development of monitoring systems based on fibre optic technology, and works both to develop new type of optical sensors and novel and efficient practical solutions to use and apply type of sensors whose usage is well assessed.

Applications in scientific fields and industrial sectors - high-energy physics, biomedical imaging, diagnostics and dosimetry, cultural heritage, structural monitoring, etc. -, as well as in innovative energy production systems, including nuclear ones, are explored.

In 2013, the activities focused on:

- development of synthesis processes of Si-based nanostructures and electronic characterization of interfaces, for scientific research and technological applications in the fields of photonics, electronics and energy, e.g. solar cells and energy storage devices;
- development and optimization of laser assisted pyrolysis synthesis for nanopowders production. Their characterization by morphological and physical-chemistry analysis are carried out together with investigation of their functional properties, e.g. biocompatibility and in vivo and in vitro luminescence, thermal properties of several composites, etc;
- study, realization and optical characterization of novel solid-state luminescent radiation detectors based on point defects in dielectric (lithium fluoride, LiF) crystals and thin films grown by thermal evaporation on amorphous and crystalline substrates. They found applications in micro and nanotechnologies, photonics, energy, biomedical diagnostics and dosimetry;
- advanced optical investigation of lumines-

scint materials through laser confocal microscopy and absorption and photoluminescence spectroscopy, for the development of miniaturized solid state light-emitting devices, like organic light-emitting diodes (OLED), solid-state lasers and amplifiers in waveguide configurations, planar optical microcavities and distributed gratings;

- study on the enhanced sensitivity of Raman/SERS spectroscopy in different configurations. This technique is also used to analyze traces of energetic materials;
- development of interferometric techniques and benches based on distributed optical fibre sensors for static and dynamic monitoring of infrastructures, in particular in large civil engineering works, cultural heritage and seismic prevention.

Available infrastructures include well equipped laboratories and advanced instrumentation for nanomaterials and thin films synthesis, light-emitting micro-devices developments and their characterisation:

- evaporators for the growth of dielectric, metallic and organic thin films;
- plants for laser assisted synthesis of nanopowders (LUCIFERO), nanowires and carbon nanotubes;
- electron spectroscopy laboratory;
- optical spectroscopies and confocal laser microscopy laboratories;
- interferometry and fibre optical sensors laboratories.

Funding and projects

In 2013 UTAPRAD-MNF carried on R&D activities within the frame of public funded national and regional research programs of industrial research, mainly supported by MIUR (Ministero Istruzione, Università e Ricerca), MiSE (Ministero dello Sviluppo Economico), Regione Lazio, in collaboration with Italian universities, research institutions and industries. Private funded industrial projects devoted to develop innovative industrial products with high technological

content are also carried on.

In the seventh framework programme FP7, UTAPRAD-MNF participated to EU projects, mainly on Theme 4, NMP – Nanosciences, Nanotechnologies, Materials and New Production Technologies – in collaboration with scientific and industrial partners.

In H2020 UTAPRAD-MNF joined the EU COST Action-MP1203 (Advanced spatial and temporal X-ray metrology), in the domain MPNS, Materials, Physical and NanoScience.

Technical contacts are frequent and fruitful with several small and medium companies operating in the field of optical components, spectroscopy, microscopy, lasers, and vacuum evaporation systems.

4.2 Nanostructures and spectroscopies for renewable energy

Synthesis of nanostructured silicon for lithium batteries anodes

This activity was recently started in the framework of the agreement between ENEA and Ministero dello Sviluppo Economico (2012-2015), AdP ENEA-MiSE, activity RSE (Ricerca di Sistema Elettrico), A4 Project: Advanced Systems for Energy Storage. Silicon charge capacity is about 12 times higher than graphite, which is the commonly used material for commercial lithium batteries anodes. For this reason, the synthesis of silicon electrodes consisting of silicon nanostructures is believed to have the potential to remarkably improve the storage capacity. Si nanostructures have been demonstrated to better withstand the well known pulverization process that afflicts bulk silicon due to the cyclic intercalation of the Li ion in the Si lattice during the charge/discharge cycles. In this view, the work has been focused on the growth of Si nanowires (SiNW) on a cheap substrate such as stainless steel with the aim to achieve a high surface density and give an estimate of the surface specific weight. The nanowires have been grown by Chemical Vapour Deposition (CVD) on a surface functionalized by Au. To

achieve nanowire growth it is necessary using a metallic catalyser that promotes the Vapour-Liquid-Solid (VLS) mechanism. If the metal is deposited in form of nanometric islands, the VLS reaction induces the accumulation of Si atoms from the gaseous precursor (Si_2H_6) on the Au island which forms an eutectic alloy which is liquid above 370°C . As shown in Figure 4.1, the fast Si accumulation results in a supersaturation of the liquid alloy which causes nucleation and columnar growth of Si.

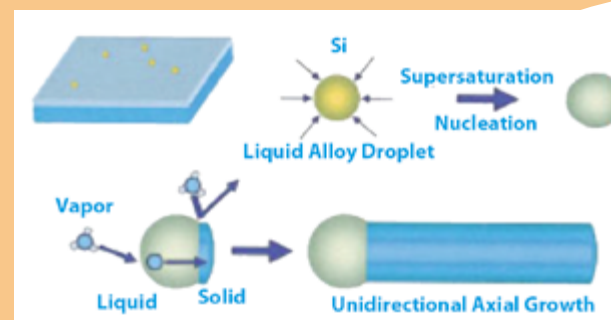


Fig. 4.1 - VLS growth mechanism.

Si NW have been grown on stainless steel 304 sheets $30\mu\text{m}$ thick. The substrates were mounted on a pyrolytic boron nitride (PBN) heater and outgassed up to 650°C before Au functionalisation. Au was evaporated by Physical Vapour Deposition (PVD) by means of a simple Knudsen cell. The average Au thickness was estimated by X-Ray Photoelectron Spectroscopy (XPS) of the order of 1nm. NW density, diameter and length are determined by at least 5 parameters: substrate temperature T , precursor gas pressure P , gas exposure time t and morphology of the metallic islands. With the aim of achieving a NW density suitable for Li batteries anodes, we have identified the best operating ranges for these parameters by assuming a constant Au quantity and morphology. An example of obtained Si NW layers is shown in Figure 4.2. SEM (Scanning Electron Microscopy) pictures in Figures 2a, 2b and 2c show SiNW/steel with average length of about $10\mu\text{m}$ and grown at $P=40\text{Pa}$ and $T=618^\circ\text{C}$, 636°C e 668°C , respectively.

The average diameter is 80 nm at 618°C and is observed to increase to 120 nm at 636°C and to 240 nm at 668°C . The diameter increase is accompanied by a density decrease which

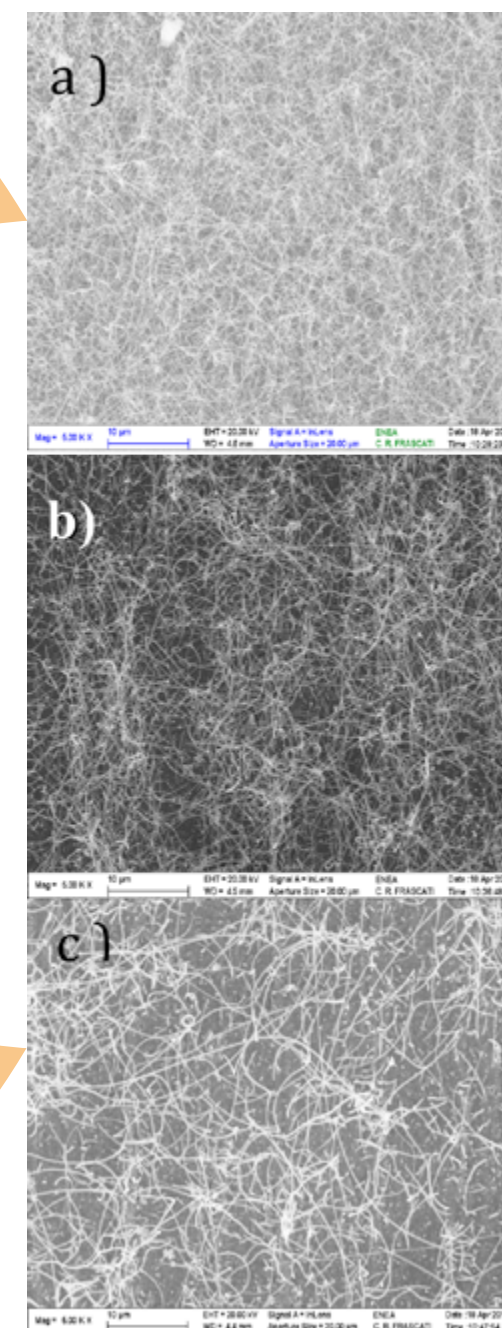


Fig.4.2 - SEM pictures of CVD grown SiNW on 304SS at different temperatures; a) $T=618^\circ\text{C}$; b) $T=636^\circ\text{C}$ and c) $T=668^\circ\text{C}$.

can be explained by a possible formation of bigger Au islands on the surface due to enhanced aggregation induced by the higher temperature. The estimate of the average density (mg/cm^2) of the nanowire layer is crucial for extracting the specific capacity (mAhg^{-1}) of the battery anode. From the analysis of the SEM pictures it is apparent that the NW density is at least $1\text{NW}/\mu\text{m}^2$. By assuming a 100 nm mean diameter and 15 μm mean length, a surface density of $100\ \mu\text{g}/\text{cm}^2$ is obtained. From these simple assumptions it results that, for our optimally grown samples surface, densities of the order of a few hundreds of $\mu\text{g}/\text{cm}^2$ should be expected. This range is accessible by analytical precision balances. Two balances with 0.001 mg and 0.01 mg resolution have been used to determine the NWs weight. Substrates were weighed before and after deposition and the resulting weight was taken as the mean value of a series of measurements. Sources of additional weight are the Au layer and Si deposited on the rear of the sample, which have been estimated to be 2 μg and 63 μg , respectively. The uncertainty on the weight was determined to be $\pm 50\ \mu\text{g}$. SiNW/steel sample, shown in the Figure 4.2a, has a weight of 520 μg . In this case the estimated NW weight is $460 \pm 50\ \mu\text{g}$.

X-Ray Photoelectron Spectroscopy (XPS) studies of solar cells materials and interfaces

$\text{Cu}_2\text{ZnSnS}_4$ (CZTS) has received increasing attention in the last few years, as an environmentally friendly material for photovoltaic applications. CZTS-based solar cells have obtained so far a record efficiency of 9.2%, but a deeper knowledge of the material's physical properties might bring further improvements. Several issues are still to be addressed. For example, it is known that a Zn-rich and Cu-poor composition is the best choice for photovoltaic applications but it is still not clear how the composition influences the material's optical properties. With this aim, several CZTS thin films grown by varying the composition of the starting layered precursors

were analyzed by XPS in order to determine the composition of the absorber material CZTS and the nature of the back interface with the Mo layer. Results indicate a Zn enrichment at the back interface and point to Mo sulfide formation.

Spectroscopic and mass spectrometric investigation on nitroaromatic compounds

Nitroaromatic compounds are relatively rare in nature, but are widely used in the chemical industry for the production of dyes, resins, pesticides, herbicides, explosives, and other useful materials such as polyurethane foams. In particular, chemical moieties substituting H atoms of benzene and larger aromatic rings are generally known to have significant effects on the chemical properties of the aromatic compounds, through their ability to either withdraw or donate electrons to the p-conjugated system. These observations triggered the birth of an area of study of the relationships between structure and aromatic properties. In this context, in collaboration with CNR-ISM, core-ionization energies (IEs), measured by XPS at GasPhase Beamline of Elettra, Trieste, represent a more direct probe of the ability of aromatic molecules to accept positive charge at a specific site, as they are related in a strict quantitative way to the screening of photoinduced core holes by means of the displacement of the valence electronic density in a positively charged ionized state. For example, in Figure 4.3, the C(1s) core-level spectra of the ortho-, meta- and para- nitrotoluene isomers measured at a photon energy of 382 eV are shown together with the results of the theoretical predictions. The presence of competing electron-donor and -attractor groups such as CH_3 and NO_2 , respectively, together with highly accurate experimental and theoretical estimates of C(1s) core shifts, represents a fruitful chance to reach the heart of well-established text. Moreover, a new ion-mass spectrometer apparatus has been realized for photoionisation and photofragmentation

experiments and available at the Circular Polarization Beamline at Elettra Sincrotrone, Trieste. The new experimental set-up consists in an ionization region equipped with a set of ion optics, that transport the ions produced by ionization via synchrotron radiation in a

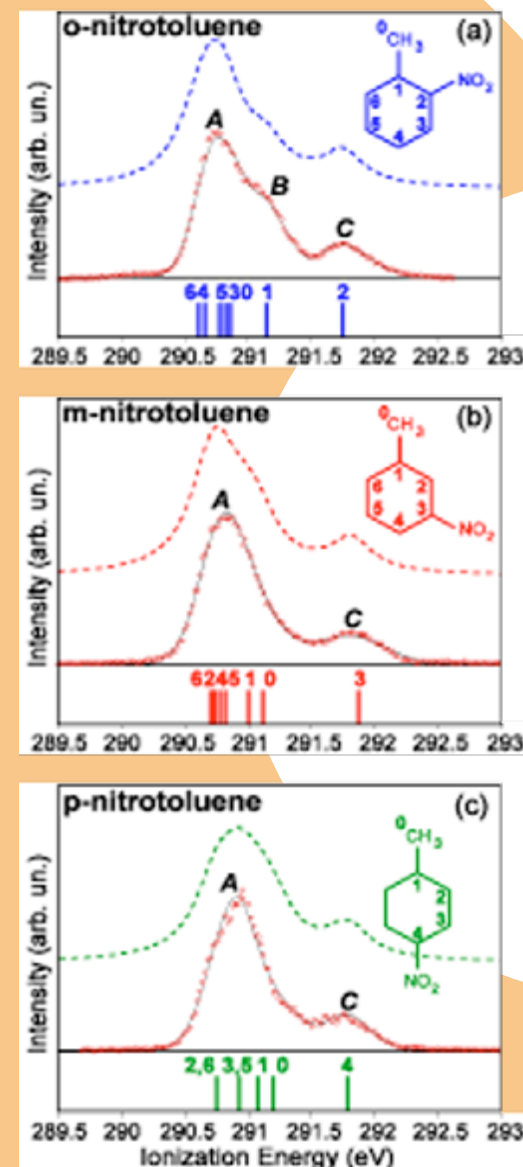


Fig. 4.3 - C(1s) XPS spectra of o- (a), m- (b), and p- (c) nitrotoluene. Experimental measurements (open circles) have been fitted with Gaussian lineshapes (full black lines). Dashed lines represent convolutions of Gaussian peaks centered on the 0-6 bars (0-4 in the case of para-nitrotoluene), corresponding to the theoretical estimates of C(1s) XPS lines.

quadrupolar spectrometer equipped with a channeltron detector. Taking advantage of tuneable synchrotron VUV radiation in the range from 8 to 12 eV, the photoionisation and photofragmentation thresholds of nitrotoluene isomers were measured.

Laser synthesis of SiC, TiO_2 , SiO_2 nanoparticles for nanofluid coolants and their characterization

Heat transfer fluids are of major importance to many industrial sectors, including transportation, energy supply and production, as well as electronics; improvement of their efficiency can lead to effective energy savings in these areas. In particular, nanoparticle (NP) suspensions (nanofluid, NF) have attracted considerable interest due to some experimental observations of enhanced thermophysical properties such as thermal conductivity, thermal diffusivity, and heat transfer coefficients over the base fluids. At UTAPRAD-MNF, the set-up LUCIFERO exploits CO_2 laser pyrolysis technique for production of developmental quantities of nanopowders. In this synthesis technique, the condensable products result from laser induced chemical reactions at the crossing point of the laser beam with the molecular flow of gas or vapour-phase precursors (Fig. 4.4). By fine tuning of the process parameters, NPs of high purity, selected dimensions and different chemical characteristics and properties have been produced, among them Si, SiC, SiO_2 , TiO_2 and C nanopowders with dimensions from 5 to 80 nm, reaching a productivity till 80g/h. The FP7 EU Project NanoHex "Enhanced Nanofluids Heat-Exchange", having as objective the development of high performance NF coolants achieved by dispersing and stably suspending in base fluids a limited amount of NPs (metallic or nonmetallic) with typical size on the order of 10 - 250 nm, was successfully concluded. Pyrolytic NPs of TiO_2 and SiC were dispersed in water and in ethylene glycol and thermal



Fig. 4.4 - Picture of the set-up LUCIFERO

conductivity, heat exchange coefficient and viscosity were tested on the obtained NF by using conventional methodologies (at the University of Birmingham-UK and the Royal Institute of Technology-SW) and by applying them in two different demonstrators for the cooling of Data Centers and Power Electronic Components (realized during the project by Thermacore Europe Ltd-UK and Siemens AG-Germany). The relative thermal conductivity of the water based NFs was found in substantial agreement with the prediction of the Maxwell model. Moreover, thermal diffusivity (D_{th}) measurements of NF based on pyrolytic titania (TiO_2) NPs were performed at UTAPRAD lab. in ENEA C.R. Casaccia using an optical technique known as Forced Rayleigh Light Scattering (FRLS). This technique permits to detect optically the dynamics of a time-dependent phase grating (period Λ) created inside a weakly absorbing sample by the interference of two coherent "writing" beams produced from a high power pump laser. The grating relaxation time t_g is related to the sample thermal diffusivity by the expression:

$$(1) \quad t_g = \frac{\Lambda^2}{4\pi^2 D_{th}}$$

In order to measure the grating decay time t_g , a low power beam is shone into the sample at the Bragg angle φ and diffracted by the grating.

The thermal conductivity k of the sample can be then determined if the sample density and specific heat are known, by the relationship $D_{th} = k/\rho c_p$. For NF based on NP produced in the LUCIFERO plant, the conductivity enhancement was calculated using the thermal diffusivity values measured by FRLS technique and shown in Figure 5 as a function of titania volume fraction (ϕ_p). The data (solid symbols) exhibit a rather linear relation with a maximum 6% enhancement for 0.6% volumetric loading of titania. This experimental evidence has been interpreted by comparing our experimental results with the recent aggregation model of Prasher, which allows to evaluate the effective thermal conductivity of colloids containing aggregates with fractal structures in terms of their morphology and size. According to this theoretical approach, we have chosen to fit the experimental data using the Prasher's model with df as free parameter. The best fit (see solid line in the Fig. 4.5) is obtained for a fractal dimension value approximately equal to 2.1, which is a reasonable value for pyrolytic nanopowders. As shown in the figure, the good agreement between the experimental and predicted data highlighted the crucial effect of the morphology of the pyrolytic aggregated titania NPs on the thermal conductivity enhancement.

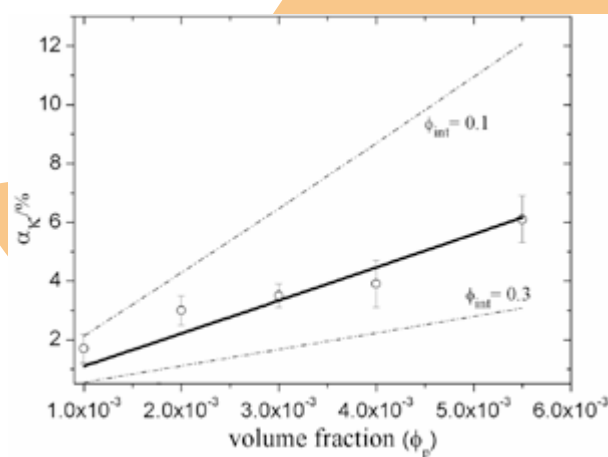


Fig. 4.5 - Comparison of experimental data (symbols) with those predicted by Prasher' model using the fractal dimension as free parameter.

TiO_2 nanopowders for development of porous semiconductor electrodes

In the renewable energies field, TiO_2 is widely investigated as electrode in photoelectrochemical devices, like cells for hydrogen production by water splitting, or dye-sensitized solar cells (DSSC). For efficient operation of these devices, optimization of electron transport in the working electrode is of the utmost importance. Impurity doping is one of the strategies to achieve this goal, and, in particular, N-doping was reported to effectively increase the electron collection efficiency in DSSC. Titania nanoparticles were synthesized in the LUCIFERO set-up by laser pyrolysis of an aerosol of titanium (IV) isopropoxide (TTIP) $Ti[OCH(CH_3)_2]_4$ mixed with either ethylene or ammonia (NH_3) as reaction sensitizer. When NH_3 was used, nitrogen was incorporated in the NP as a consequence of partial dissociation of NH_3 and the level of N concentration can be varied by changing the process parameters. In particular, a decrease of the TTIP flow and an increase of the pressure in the chamber led to increased N concentration in the produced powders due to the higher relative concentration of N radicals in the reaction zone. From the structural point of view, the average crystallite size of samples produced with ethylene as sensitizer was of about 10 nm, the crystalline phase being approximately 30% rutile and 70% anatase. When ammonia was used as sensitizer, the average crystallite size resulted to be of about 15 nm and the crystalline phase was mostly anatase, probably due to the lower flame temperature. NPs are characterized by means of XRD (X-Ray Diffraction), SEM, Raman and Diffuse Reflectance spectroscopy, performed at UTAPRAD lab. in ENEA C.R. Casaccia. In cooperation with UTMAT and UTRINN, a set of TiO_2 porous electrodes using pure and N-doped pyrolytic nanopowders were prepared by screen-printing. The electron transport in the electrodes was characterized by a photoelectrochemical method in order to extract the electron diffusion length L_{diff}

during operation in a water-splitting cell. The results show that L_{diff} in electrodes containing pyrolytic NPs compares well with that of the commercial standard. Assuming the visible absorption of NPs as an estimate of the amount of the incorporated N, L_{diff} resulted to decrease with increasing N content. Work is in progress to understand if this result is directly related to the effect of doping or rather to the different morphology and properties produced by the change in synthesis conditions necessary to vary the N incorporation. Pyrolytic nanoparticles of pure TiO_2 were also used as the active material for manufacturing composite anodes for lithium-ion batteries and compared with TiO_2 nanoparticles commercially available and TiO_2 nanotubes obtained from electrochemical synthesis, which appear the most promising materials to synthesize anode materials with high capacity and cyclability.

Synthesis and characterization of carbon nanoparticles for energy storage

In rechargeable lithium batteries, nanostructured carbons are investigated as anode materials and especially as key components for building advanced composite electrode materials. In Li-ion batteries, storage occurs primarily in the non-carbon components, while C acts as the conductor and as the structural buffer. Through the elegant design of hierarchical electrode materials with nanocarbon networks, both the kinetic performance and the structural stability of the electrode material, which lead to optimal battery capacity, cycling stability, and rate capability can be improved. Carbon nanopowders were synthesized in the LUCIFERO set-up by means of the laser pyrolysis of C_2H_4 (ethylene). Ethylene was chosen as precursors for high content of C/mol (85.7%), because it absorbs the laser radiation at 944 cm^{-1} and has a low firing threshold of the flame and energy of dissociation. Depending upon the chosen

pressure, temperature and laser power density, the laser pyrolysis of ethylene can produce tars, carbon black or even diamond-like materials. Different experiments were performed by varying the flow of the hydrocarbon as well as the laser power density and working pressure, in order to obtain turbostratic or graphitic structure and reach a productivity more than 5 g/h. The powders were characterised by BET (Brunauer-Emmett-Teller, IR (infrared) and Raman spectroscopy at UTAPRAD lab. in ENEA C.R. Casaccia (see sect. 1.5), showing that the C nanoparticles are structurally heterogeneous, namely there is coexistence of amorphous and turbostratic carbons. Preliminary test of the electrochemical properties of pyrolytic C nanopowders, in cooperation with UTRINN, evidences the requirement of more homogeneous structures.

4.3 Luminescent radiation detectors, light-emitting waveguides and nanostructures for spectroscopy, imaging and dosimetry

Versatile solid-state lithium fluoride fluorescent detectors for X-ray imaging

Lithium fluoride imaging detectors in forms of crystals and thin films for extreme ultraviolet radiation, soft and hard X-rays, based on photoluminescence (PL) of aggregate electronic defects in LiF, are under development for imaging applications with laboratory radiation sources, e.g. laser driven plasma-sources and conventional X-ray tubes, as well as large-scale facilities, e.g. synchrotrons and free-electron lasers (FEL). Among their peculiarities, noteworthy ones are their very high intrinsic spatial resolution (standard 250 nm, intrinsic below 100 nm) across a large field of view ($> 1 \text{ cm}^2$) and wide dynamic range. Moreover, they are easy to handle, as insensitive to ambient light and no development process is needed. Colour centres (CCs) can be permanently produced in LiF by X-rays and efficiently emit light in the

visible spectral range under selective optical excitation at room temperature (RT). After X-ray exposure, the latent images stored in the LiF plates are read by fluorescence optical microscopy techniques. At UTAPRAD-MNF, the Solid State Laboratory participates in the EU COST Action-MP1203 (Advanced spatial and temporal X-ray metrology), in the domain MPNS, Materials, Physical and NanoScience. Research contacts are under way with the DIPROI (Diffraction and Projection Imaging) beamline at FEL-X FERMI (Sincrotrone Elettra, Trieste) dedicated to diffraction coherent imaging with soft X-rays.

Enhanced photoluminescence of lithium fluoride thin-film X-ray imaging detectors

LiF thin layers can be thermally evaporated in the form of polycrystalline thin films and their PL response can be tailored through the choice of a reflecting substrate and control of their growth conditions. At ENEA's Frascati Solid State Laboratory, optically transparent LiF films of different thickness were thermally evaporated on different substrates, under controlled conditions of substrate temperature and evaporation rate in order to realize vertical multilayer structures able to increase the collection efficiency of the PL signal emitted by CCs during the optical reading process in a fluorescence microscope, and, consequently, the sensitivity of the LiF-film radiation detectors. This behaviour has been experimentally demonstrated by comparing the PL intensities coming from two LiF thin films grown in the same evaporation run on a glass and a Si(100) substrate, respectively, after soft X-ray irradiation in the same conditions in a laser plasma source developed at Tor Vergata University of Rome. Identical metallic meshes were placed in contact with the LiF film surface. The image stored in the LiF film detector on Si read by a confocal fluorescence microscope NIKON Eclipse 80i-C1 under Argon laser excitation at 458 nm is shown in Figure 4.6, where the dark areas correspond to the width of the nickel wires of the mesh. In the inset, the

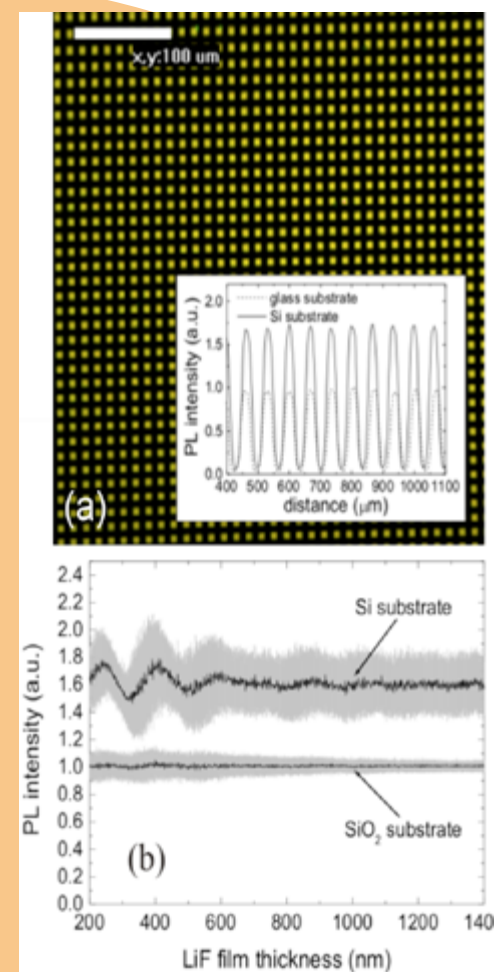


Fig. 4.6 - (a) Fluorescence image of soft X-ray contact micro-radiographies of a nickel mesh on LiF films (thickness about 1 μm) on Si substrate. In the inset, PL intensity profiles along a line of image in Fig. 6(a) and an analogous image obtained with a glass substrate. (b) Theoretical simulation of the PL intensity of a LiF film over a Si and SiO_2 substrate vs the LiF film thickness.

PL spatial profiles are shown for the colored LiF films on both substrates. The integrated PL signal measured on the LiF film on Si is higher than the one collected from the LiF film on glass and the ratio of their intensities is 1.76 ± 0.11 . These experimental results satisfactorily agree with theoretical predictions about the PL intensity radiated from an entirely colored LiF film placed over SiO_2 and Si substrates. By using a fully analytical approach, developed by Dr. E. Nichelatti (UTMAT-OTT, ENEA

C.R. Casaccia) the outcoupled PL could be theoretically estimated as a function of the film thickness; the results are shown in Figure 4.6 (b) for both the substrates. The grey bands represent the uncertainties deduced with a Montecarlo approach. An ENEA patent of high-sensitivity LiRA (LiF Radiation) film detectors fully exploiting this photonic approach was deposited.

Luminescent LiF radiation detectors combined with polycapillary optics in compact X-ray laboratory sources

A novel laboratory compact X-ray imaging system based on polycapillary semi-lens combined with a microsource X-ray tube and LiF-based detectors for contact X-ray microscopy was tested (collaboration with XLab, Istituto Nazionale di Fisica Nucleare - Laboratori Nazionali di Frascati, INFN-LNF). The polycapillary optics is composed by many bundles containing thousands of channels with the length of about 60 mm; each single channel is characterized by an average diameter of about 4 μm . First high spatial resolution fluorescence images of transmitted X-rays through a polycapillary semi-lens stored in a LiF crystal were obtained.

Figure 4.7 shows an X-ray transmission image of a polycapillary semi-lens stored by stable formation of luminescent CCs in a LiF crystal placed at the lens exit. From the fluorescence image we can easily resolve the multiple channels for effective X-ray transmission (white areas) as well as the external polycapillary walls (dark hexagons). In particular, almost each glass channel, even if it is stretched due to the melting during the lens drawing process, transports effectively X-radiation resulting in a quite uniform X-ray distribution behind the optics. The capability of LiF detectors to store images with high spatial resolution on a wide field of view allowed to obtain images of the transmitted X-rays through the entire lens and through the single channels, which is fundamental for their full characterization.

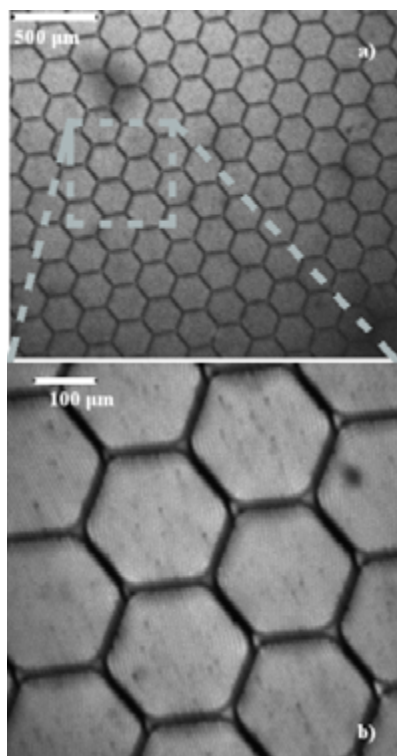


Fig. 4.7 - Fluorescence image of X-rays transmitted by polycapillary semi-lens stored on a LiF crystal placed at its exit and read by a confocal laser microscope with 4x (a) and 20x (b) objectives.

In-line X-ray lensless imaging with lithium fluoride film detectors

In-line X-ray lensless projection imaging experiments at the Topotomo beamline of the ANKA synchrotron facility with a white X-ray beam (3-40 keV) by using LiF films and crystals were performed. As the energy of X-rays increases, the absorption coefficients of materials decrease and low atomic number objects, such as biological specimens, show low contrast. Image contrast can be improved by adding phase information to the image obtained from X-ray absorption phenomena. An effective method to image phase modulation is to record the intensity modulation of the wavefront emerging from the sample at a sufficient distance from the sample itself. High-resolution X-ray images of a metallic test pattern (Xradia X500-200-30, gold mask deposited on a $(500 \times 500) \mu\text{m}^2$

Si_3N_4 window, 330 nm thick) were successfully recorded out of focus on LiF detectors. The propagation distance between the test pattern and the detector was set equal to 17.5 cm. Figure 8a) shows the image of part of the test pattern irradiated in projection mode by the broadband X-rays (exposure time 30 s) stored in a LiF film ($1 \mu\text{m}$ thick on a glass substrate) and read after irradiation by a confocal laser microscope in fluorescence mode. Although X-ray attenuation length in LiF varies between 0.02-12 mm for the used X-ray energies, intense PL images are obtained from the LiF film detector. Figure 4.8b shows the PL intensity profile (dots) along

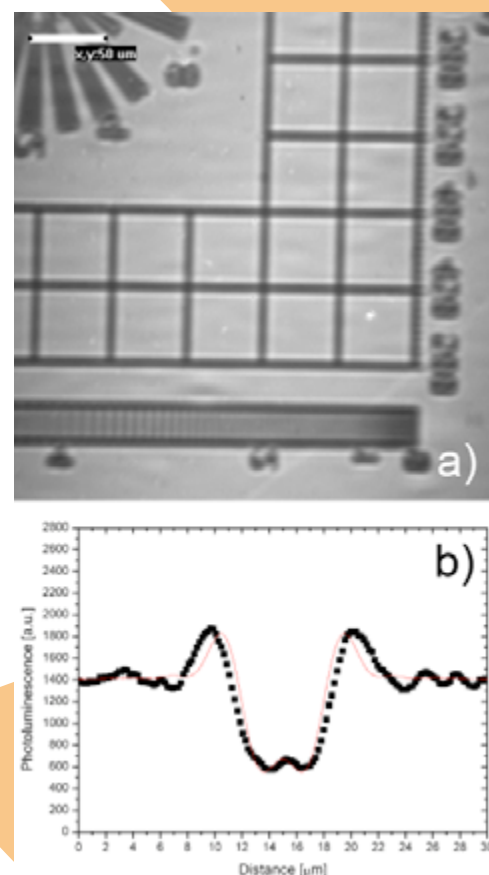


Fig. 4.8 - a) Detail of the projection X-ray image of a test pattern stored in a LiF film ($1 \mu\text{m}$ thick on a glass substrate) read by a confocal microscope in fluorescence mode. B) CC fluorescence intensity profile (dots) along the vertical red line drawn on the image stored in the LiF film (a) and corresponding calculated intensity distribution of the impinging X-rays (full line).

a vertical red line drawn on the image stored in the LiF film (Fig.4.8a). Edge-enhancement effects attributed to out-of-focus phase-contrast imaging of the Au wire of the mask ($3 \mu\text{m}$ thick and $2.5 \mu\text{m}$ wide) are evident. The theoretical X-ray intensity profiles as calculated with a computer simulation are also shown (full lines). The fairly good agreement between the CC fluorescence intensity profile and the corresponding simulated intensity distribution of the incoming X-rays suggests a linear optical response of the CCs PL in the LiF film detector in the used experimental conditions. This linear behaviour has been confirmed by the analysis of the F_2 and F_3^+ CCs PL signals detected with a CLSM system vs X-ray irradiation times (0.5-30 s). The results are very encouraging for the exploitation of solid-state LiF radiation detectors for X-ray lensless projection imaging experiments.

Solid state detectors based on luminescent point defects in lithium fluoride for proton beam diagnostics

Ion beams of different energies are widely investigated for applications to radiobiology and radiotherapy. In the framework of the TOP-IMPLART (Oncological Therapy with Protons - Intensity Modulated Proton Linear Accelerator for Radio Therapy) project, proton beams of 3 MeV and 7 MeV energy, produced by a linear accelerator (UTAPRAD-SOR) were used to irradiate LiF crystals and thin films only $1 \mu\text{m}$ thick, grown by thermal evaporation on glass and silicon substrates, in the fluence range from 10^{11} to 10^{15} protons/ cm^2 .

The irradiation of LiF induced the formation of primary (F) and aggregate (mainly F_2 and F_3^+) electronic defects, as resulted from optical absorption measurements performed by a Perkin-Elmer Lambda 950 spectrophotometer. PL spectra of LiF crystals and films were measured at RT by pumping in a continuous wave regime with the 457.9 nm line of an Argon laser, which allows to simultaneously excite the green and red emissions of the F_3^+ and F_2

colour centres. The PL signal was spectrally filtered by a monochromator and acquired by means of a photomultiplier with lock-in technique. By a fluorescence microscope Nikon Eclipse 80-i C1 equipped with a Hg lamp and an Andor NEO s-CMOS camera, it was possible to record the transversal proton beam intensity profile by acquiring the PL image of irradiated LiF. Both crystals and films showed to be versatile radiation imaging detectors, as they could store information about the proton beam intensity on a large area with high spatial resolution and revealing even subtle intensity differences. The PL images acquired by the optical microscope were also used to measure the integrated PL intensity as a function of the proton beam irradiation fluence: a linear optical response was obtained in a fluence range covering several orders of magnitude, which is dependent on the used LiF samples and the selected beam energy (see Fig. 4.9).

The sensitivity of the optical PL reading techniques and the high emission efficiency of the F_2 and F_3^+ centres, combined with the good optical quality of the thermally evaporated LiF films, provided encouraging results, which are under study in order to optimize the LiF film characteristics related to their visible PL response on selected dose intervals, for dosimetry and imaging applications in protontherapy.

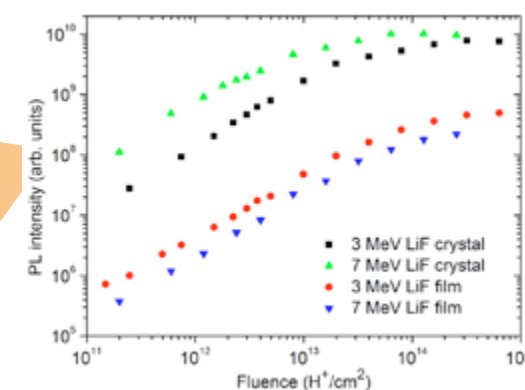


Fig. 4.9 - Integrated visible photoluminescence (PL) signal as a function of the 3 and 7 MeV proton beam fluence in coloured LiF crystals and $1 \mu\text{m}$ thick films grown on a glass substrate.

Photoluminescence of colour centres in thermally evaporated LiF films irradiated by high-energy electrons

Nowadays there is a great interest in the technological research about luminescent materials for development of solid state detectors for ionising radiations. They found application in the characterisation of intense ionising radiation sources, decommissioning and storage of radioactive waste, mapping the flux in the out-of-core regions of fission and fusion reactors, but also in life-science. LiF-based radiation imaging detectors based on LiF films assure great versatility, as they can be grown in the form of optically transparent thin films on various substrates by thermal evaporation, tailoring their geometry, size and thickness.

The main deposition conditions, such as nature of the substrate, substrate temperature, deposition rate, total thickness, etc., influence the structural, morphological and optical properties of LiF thin films and the formation efficiency of the radiation-induced colour centres. As example, the AFM image of a LiF film thermally evaporated on a glass substrate is shown in Figure 4.10.

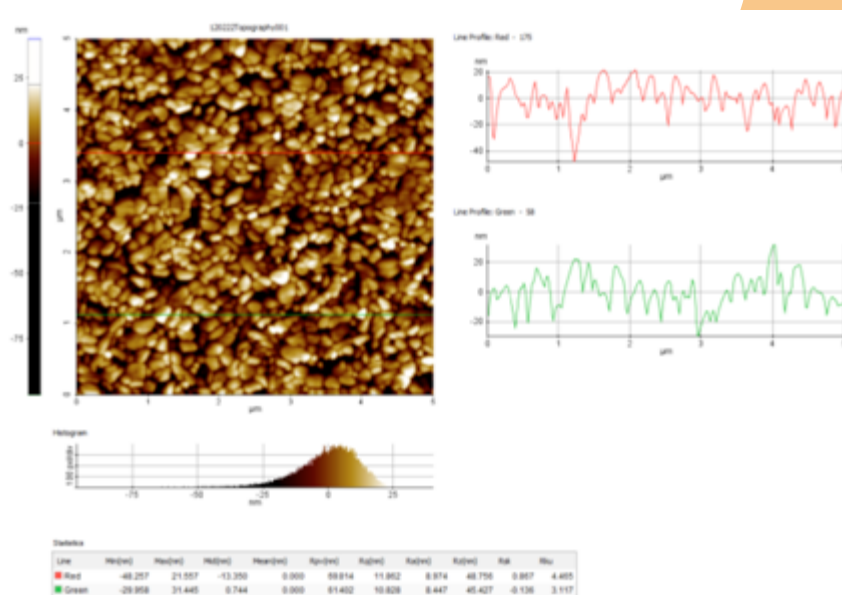


Fig. 4.10 - 2D AFM image of a 1 μm thick LiF film grown on a glass substrate at $T_s=300^\circ\text{C}$ (Courtesy of A. Rufoloni, UTFUS-COND)

LiF films of increasing thicknesses grown by thermal evaporation on glass substrates were irradiated in air at a dose of 8.4×10^4 Gy by means of the electron beam supplied by the LINAC at ENEA C.R. Frascati (UTAPRAD-SOR). For electron beam energy of 5 MeV the penetration depth in LiF is of some millimetres and the LiF films are homogeneously coloured throughout their entire thickness. As expected, at the same irradiation dose, the F_2 and F_3^+ PL peak intensities at 680 nm and 541 nm, respectively, increase linearly with the film thickness in the interval between 1.0 and 1.7 μm . One of these LiF films was characterised by the Combined Excitation-Emission Spectroscopy (CEES) technique. In this approach a large number of excitation (or emission) spectra are recorded at a sequence of emission (or excitation) wavelengths. These measurements are used to obtain a three-dimensional graph, which shows the excitation intensities as a function of excitation and emission wavelengths. This kind of representation gives a global view of all the emission and excitation peaks and allows to distinguish each emission band and correlate it to the appropriate excitation wavelengths.

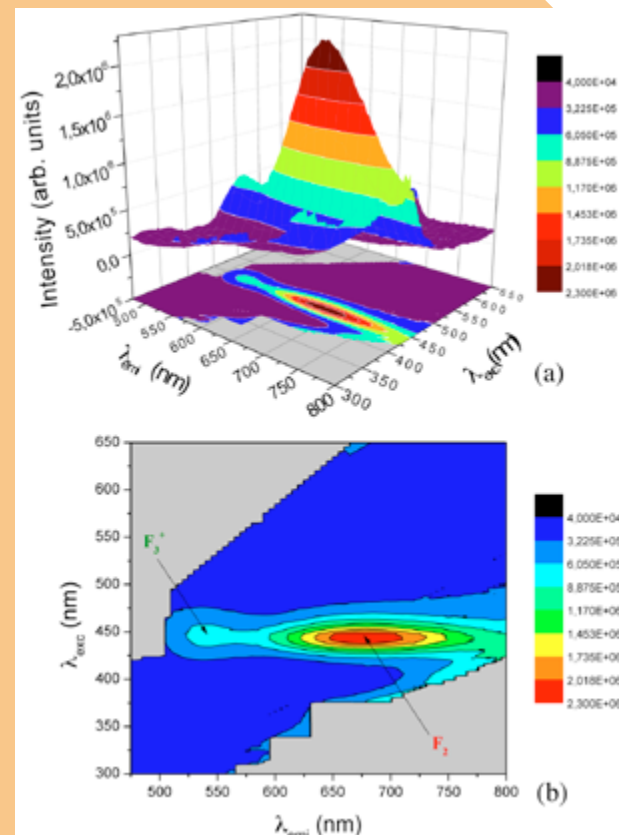


Fig. 4.11 - 3D (a) and 2D (b) representations of the PLE (Photoluminescence Excitation) spectra of a 1.1 μm thick LiF film, NLiF45 n°12, after beta irradiation at 8.4×10^4 Gy collected at RT.

Thermoluminescence of gamma-irradiated LiF crystals and thin films

Thermoluminescence (TL) is one of the most frequently used techniques in radiation dosimetry for personal and environmental use. Among the various crystalline materials utilized as TL dosimeters, LiF is the most common because of its almost biological tissue equivalence and its chemical-physical properties. Nominally pure LiF crystals,

obtained from a single crystal containing less than 100 ppm impurities, were irradiated at increasing doses by gamma-rays coming from a 60°C source at the Institute of Physics of National Academy of Science, Minsk (Belarus). Of them, seven samples were irradiated at RT in a dose range between 8.4 and 2.5×10^5 Gy, and the 8th one was irradiated at a dose of 8.4×10^4 Gy while keeping the temperature at -60°C . Optical absorption and PL spectra were measured to investigate the radiation-induced CCs and evaluate their concentrations. TL spectra in the range $50 \div 450^\circ\text{C}$ with a heating rate of 0.25°C/s were measured at the CNR-IMIP (Bari) by using a commercial automated RISØ TL/OSL-DA-15 reader. A first-order kinetics approach was used to simulate the TL spectra, and from the best-fit procedure ten glow peaks (GPs) spanning from 100 to 450°C were highlighted. The comparative analysis of the GPs intensities and the CC concentrations in function of the irradiation dose has shown that the impurities, less than 10^{18} cm^{-3} , still play a predominant role in the TL spectrum. TL measurements performed on beta-irradiated LiF thin films, grown on glass and silicon substrates, are under study.

Optical characterization of Tetraphenyl-butadiene films used as wavelength-shifters for liquid Argon detectors in Dark Matter search

The use of efficient wavelength-shifters from the vacuum-ultraviolet to the phototube's range of sensitivity in the visible is a key feature in detectors for Dark Matter search and neutrino physics based on liquid argon scintillation detection. Thin film of Tetraphenyl-butadiene (TPB) deposited onto the surface delimiting the active volume of the detector and/or onto the photosensor optical window is the most common solution in current and planned experiments. Detector design and response can be evaluated and correctly simulated only when the properties of the optical system in use (TPB film + substrate) are fully understood.

In collaboration with the Italian Institute for Nuclear Physics-Gran Sasso Laboratories (INFN-LNGS), the Yale University (USA) and Rome Tor Vergata University, PL spectra of TPB films grown on different substrates were measured for various coating thicknesses at several temperature in the range 87 ÷ 300 K. Optical reflectance and transmittance spectra of the TPB coated substrates in the wavelength range of the TPB emission were also investigated, in collaboration with UTMAT-OTT.

Advanced optical characterization of color centers channel waveguides induced in lithium fluoride crystals by femtosecond laser

Advanced optical characterization of broadband light-emitting channel waveguides directly written in LiF crystals by femtosecond (fs) laser pulses was performed (collaboration with Federal University of Technology, Paraná, Brasil and University of Roma Sapienza). The high intensity pulses allow higher order electronic transitions in the material and/or material damage, resulting in appreciable changes of the local refractive index. Fs laser pulses irradiation produces in LiF crystals F_2 and F_3^+ aggregate defects. Buried channel optical waveguides were directly written at a few fixed depths in a blank, optically polished LiF crystal with dimensions (30x10x6) mm³ focusing the laser beam inside the sample. A fluorescence image of CC active waveguides written in the LiF crystal is presented in the inset of Figure 4.12. The LiF-based waveguides were observed by a fluorescence microscope (NIKON Eclipse 80i) under blue light illumination which simultaneously excites the Stokes-shifted PL of both F_2 and F_3^+ centres. They are regularly spaced by about 200 μ m. Their brightness is due to CC light emission under optical pumping. The visible PL spectra emitted from one of the fs laser written waveguides are presented in Figure 4.12. PL measurements were performed by pumping with the 457.9nm line of an argon ion laser,

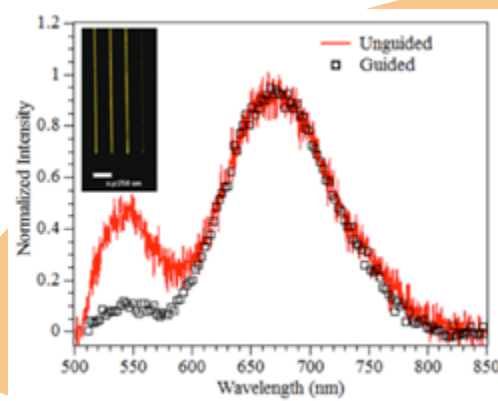


Fig. 4.12 - Normalized photoluminescence spectra obtained from a colour centre waveguide (recording energy 5 μ J/pulse, translation speed 191 μ m/s) excited by a laser at 457.9nm. Red trace is the emission spectrum collected from the top surface of the crystal (unguided fluorescence), black trace is the spectrum collected co-linearly to the waveguide axis. The inset shows a top view of a region of the crystal with four strip waveguides observed in fluorescence mode. The measured waveguide is the last one on the right.

focused on the waveguide by a microscope objective, perpendicularly to the top surface of the crystal. Fluorescence was collected by a large diameter (400 μ m) silica optical fibre and analyzed by a monochromator (Ocean Optics QE65000). The collecting fibre was positioned either pointing to the top surface of the crystal (to collect unguided luminescence) or aligned to the waveguide axis (to collect guided luminescence). The broad red and green emission bands can be attributed to the optically active F_2 and F_3^+ CCs, respectively. Regions of the LiF crystal outside the written strips does not show any PL signal, which indicates that CC are formed due to the fs laser pulsed irradiation. A different peak intensity ratio of the green (F_3^+) to the red (F_2) emission bands in the normalized PL spectra of Figure 12, which depends on the fluorescence collection geometry, was previously observed in low-energy electron irradiated single-mode active waveguides in LiF. It was attributed to the presence of more complex absorbing defects, like F_4 (four close F centres) defects, whose absorption bands, peaked at 515 and 545 nm, overlap the emission band of the

F_3^+ ones and modify the imaginary part of the complex refractive index of the irradiated guiding layer.

4.4 Nanostructures assessment of SERS activity and enhancement factors for highly sensitive gold coated substrates probed with explosive molecules

The Surface-Enhanced Raman Scattering (SERS), introduced three decades ago, is used to provide a drastic amplification of the Raman signal. The Raman signal enhancement is observed when the molecule to be studied is adsorbed on a nanosized roughened metallic surface, in particular silver or gold, and is due to resonant excitation of surface plasmons. It is known that the observed enhancement factor (EF) has a two-fold origin, one through an electromagnetic mechanism and the other having a chemical nature, i.e. being due to an increased polarisability of the molecule adsorbed on the metal as a result of charge transfer processes. To be used in a sensor system, a SERS substrate should enhance the Raman signal sufficiently to enable consistent and uniform chemical detection sensitivity across the surface, maintaining its properties as long as possible in time, and to provide a high number of sites for molecular adsorption. In the framework of the BONAS project, coordinated by UTAPRAD-DIM, we studied enhancing properties of Klarite[®] substrates, fabricated by a vapour deposition technique, in which a thin gold layer is deposited on a silicon surface with an ordered structure of inverted pyramids. The pyramidal pits were produced by chemical etching of Si surface, after definition of a mask by optical lithography. The aperture size L of inverted pyramids is aligned along the [100] direction of Si wafer and is linked by the silicon crystal structure with the scalable pyramidal void depth d through the relation: $L=2d \cdot \text{tg}(\alpha)$, where $\alpha \approx 35.3^\circ$ is the inclination to the normal of the pyramid's face for Si[100]. The cross-section view shows that the gold layer deposited onto the internal walls of the pyramids has a thickness of about 300

nm, and a nanostructured roughness of about 20 nm (Fig. 4.13).

The origin of SERS activity of Klarite surface was widely discussed in literature. On the

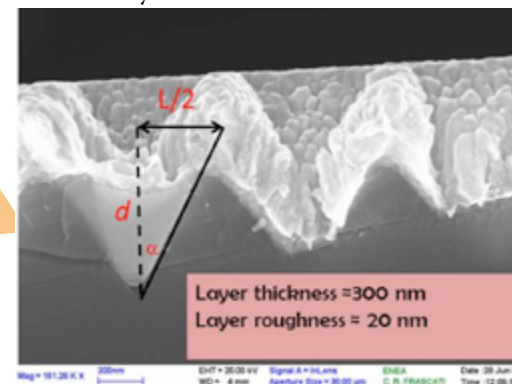


Fig. 4.13 - HR-SEM cross section view of Klarite surface inverted pyramids.

base of a theoretical approach, only localised plasmons, whose energies are related to the specific geometry, are responsible for the Raman signal amplification when the molecules are adsorbed on the pyramid's walls. As consequence, for each pump laser wavelength, it is possible to select the substrate with the void depth appropriately matched which gives the highest SERS response. To verify this model, we compared the SERS activity of Klarite substrates with different void aperture size/depth by estimating the EF of each surface. The obtained results are displayed in Figure 4.14.

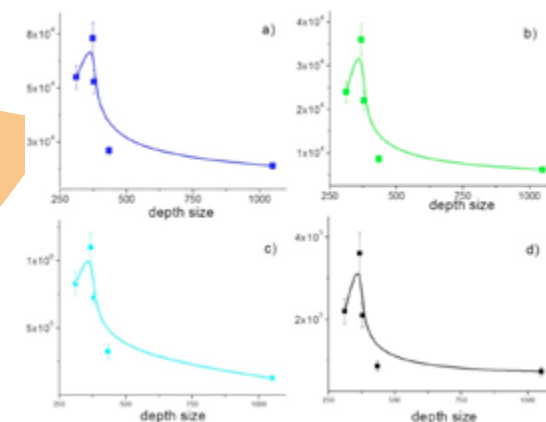


Fig. 4.14 - EF versus pit depth size plot for RDX (a), PETN (b), TNT (c), KNO_3 (d).

Because the array period is the same for each sample, we are probing only enhancement effect due to the surface plasmons. In fact the diffraction effect, which also contribute to the overall EF, depends only from the array pitch and apex angle α . The measured EF show strong maxima for a void depth of 373 nm corresponding to an aperture size of 528 nm. These SERS resonances correspond to the resonance of pump photons with the localised plasmons. Nevertheless the discussion of this behaviour is complicated because we should take into account the averaging effect from typical commercial Raman instruments, which sum over a wide range of collection angles, our measurements show an excellent agreement with theoretical predictions supporting the model of plasmons confined in the pit well. The EFs display the same resonance behaviour, but the resonance maxima range from $(1.1 \pm 0.4) \times 10^6$ for TNT to $(3.6 \pm 0.5) \times 10^4$ for KNO_3 , indicating that the adsorption chemistry also plays a role in the enhancement mechanism, which is not purely based on the electromagnetic effect.

SERS studies of functionalized carbon nanotubes

In order to utilize carbon nanotube (CNT) and their extra ordinary properties in real-world applications, CNT/polymer nanocomposites were developed and applied in different fields as energy, automotive and aerospace. However, the effective utilization of CNTs for fabricating nanocomposites strongly depends on the possibility to obtain a homogeneous dispersion of CNT throughout the matrix with a good interfacial bonding; it allows to achieve a significant load transfer across the CNT-matrix interface, improving the mechanical properties of composites. Surface functionalisation of CNTs helps in stabilizing the dispersion, prevents re-aggregation of nanotubes and also leads to coupling of CNT with polymeric matrix. However, this method also causes deterioration of intrinsic properties of CNT. Alteration of CNT properties lead

to poor reinforcement and conductivity. Hence, it becomes obvious that dispersion and stabilization are not simple issues and compromises have to be made depending on the applications.

The structural quality of pristine and functionalised MWNT (Multiple Well) is routinely evaluated as a function of the ID/IG ratio, where ID is the intensity of the 1338 cm^{-1} band, due to the lattice vibration away from the centre of the Brillouin zone, activated by the presence of disorder in carbon systems, and IG is the intensity of the 1596 cm^{-1} band, assigned to the in plane vibration of the C-C bond. Raman features associated with functional groups are often not observed in the Raman spectra due to the small quantity of the molecules attached to the nanotubes. In our studies, we have used the SERS technique to amplify the Raman signal of functional groups to record Raman spectra of nanotubes and prove experimentally the functionalisation effect. The SERS spectrum acquired from a dense layer of pristine MWNTs (curve (a) in Figure 4.15) has no significant differences in comparison with the Raman one, excited at 785 nm, if one excepts the amplification of the signal. On the contrary, when thinner films of nanotubes are used, SERS spectra show variations in intensity of some Raman lines,

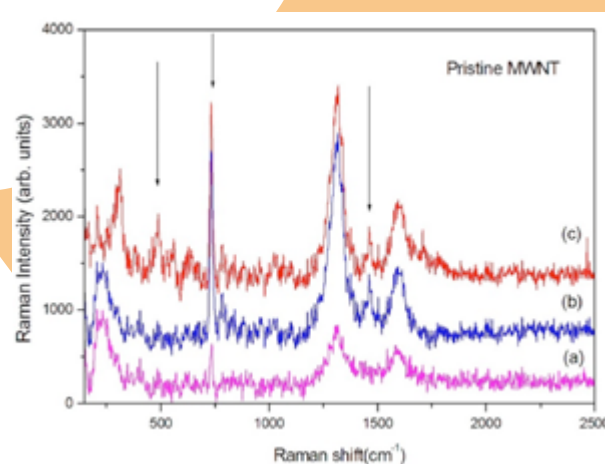


Fig. 4.15 - SERS spectra of pristine MWNTs deposited on Klarite surface. The layer thickness of deposited film decreases from curve (a) to curve (b)

peak shifts and line shape changes considered as originating from interactions between the substrate and the nanotube film. We observed a gradual increase of the “D” band, suggesting an enhanced degree of disorder, with a concomitant modification of the “G” band profile, consisting in a gradual narrowing of its low energy side. By decreasing the layer thickness, in the intermediate frequency range and between D and G bands, several sharp peaks can be detected, characteristics of C60-like molecules. This modification can be interpreted by considering the breaking of the nanotubes into species such as amorphous carbon, tubular fragments and closed-shell fullerenes. Such reactions are of chemical nature occurring at the nanotube-metal substrate interface. Thus, the increase in the Raman signal can be described as a chemical SERS effect, where the enhancement is attributed to the resonance encountered when the energy of the exciting photon matches the charge transfer transition energy. This finding is in agreement also with the small enhancement factor (about 10) that we measured for MWNTs Raman signal.

Si nanocrystals as luminescent probes for bio-imaging

Silicon nanocrystals synthesized by LUCIFERO set-up, as prepared, after chemical oxidation and post-synthesis doping with Yb, were object of additional investigation of their optical properties and biocompatibility as add-on to the former project FP6 BONSAI “Bio-imaging with Smart Functional Nanoparticles”, in collaboration with UTAPRAD lab. at ENEA C.R. Casaccia. Full exploitation of the optical properties of Si-nc for bioimaging and other applications rests on a detailed understanding of the process responsible for PL excitation and emission. In collaboration with Cà Foscari University of Venezia – Italy, we have compared the spectroscopic properties, red PL emission and luminescence decay, of the same as-prepared sample and after chemical oxidation. We concluded that PL emission

in Si nanocrystals is initiated by quantum-confined carrier interband excitation followed by relaxation to the interface defect states. Local strain and variation of the chemical environment can strongly influence the emission energies, and this could explain the sample dependent optical properties often detected on Si-nc, especially after the surface functionalisation and bioconjugation steps needed for biomedical applications.

Another fundamental part of the assessment of Si-nc for bioimaging is their biocompatibility. This was assessed in cooperation with University of Milano-Bicocca – Italy by using some specific in vitro studies that represent a relatively rapid and cost-effective way of screening in the assessment of nanoparticles toxicity. Tests were performed on different batches of samples, as prepared by laser pyrolysis, surface-oxidized and Yb-doped Si nanoparticles. We can conclude that the Si-nc are quite biocompatible in the range of concentration up to 10^3 ng/ml , used in this study as well as in other ones. An increase in the PL efficiency of these nanoparticles could make them good candidates for biomedical application.

4.5 Optical fiber sensors and nanostructures functionalised for industrial applications and cultural heritage

Optical fibre sensors

Sensors based on optical fibre technology have specific features that can make their usage of great advantage with respect to traditional sensors based on electric/electronic technology. Among them the immunity from electromagnetic disturbances, no requirement of electrical power at the sensing point, in-series cabling of multiple sensors along the same optical fibre, the measurement of different physical and chemical quantities by use of the same analysis technique of the optical signal.

Development of sensors for measurement of magnetic field

Activity is being conducted to develop a reliable low frequency, high precision magnetic field sensor. The sensor is based on use of magnetostrictive materials instrumented with fibre optic sensors. Prototypes have been produced and tested, using both Terfenol-D (a Te and Fe alloy) and Galfenol (a Ga and Fe alloy) as magnetostrictive material, and FBG (Fiber Bragg Grating) as optical sensor. The principle underlying the development of the sensor is to measure the magnetic field through the induced deformation of the material: the magnetic field drives the deformation of the magnetostrictive material which in turn is monitored by the FBG. In order to take into account the deformation of the magnetostrictive material due to thermal excitation, that would be misunderstood as due to a variation of the magnetic field, a supplementary FBG is used to monitor the temperature of the material and its signal is taken into account in working out the magnetic field measurement. Prototypes were tested with success and work is in progress to improve measurement resolution and to lower measurement error. One more important issue of the work in progress is to appreciably rise the maximum measurable magnetic field, toward the demanding values produced by superconducting magnets inside the vessel of the experimental nuclear fusion Tokamak plants. In fact, the availability of magnetic field sensor based on optical sensor technology, with their peculiar feature of electromagnetic disturbances immunity, could effectively be of help for the experimental diagnostic of the Tokamak plants.

Development of sensors for biomedical applications

FBG technology is very attractive to develop sensors for the measurement of thermal and mechanical parameters in biological applications that require to be worked out in

presence of electromagnetic interferences. Work is being performed to develop a force sensor based on use of multiple FBG (Fiber Bragg Grating) type optical sensors whose use is foreseen for monitoring the reactions to perception stimuli of patients during Magnetic Resonance Imaging procedures. Prototypes based on different designs have been produced and characterized. The basic design of all prototypes considers an optical fibre provided with FBGs to be encapsulated in a PDMS (polydimethylsiloxane) sheet. Prototypes were characterised and subjected to comparative performance test to define best design. Figure 4.16 shows a prototype of the magnetic field sensors being tested by a high field electromagnet.



Fig. 4.16 - Test of the magnetic field sensor being performed by a electromagnet employed to provide a high and uniform field in its gap. The red box contains the sensor and allows its reliable and repeatable positioning.

Functionalisation of optical fibre sensors by metal coating

Optical fibre sensor of FBG (Fibre Bragg Grating) type can be functionalized for measurement of physical and chemical parameter by deposition of various material as a coating on its surface. The coated material acts as a transducer: the FBG sensor measures the deformation of the coating due to the physical/chemical parameter. Temperature sensor with enhanced repeatability and with no appreciable increase of thermal inertia were obtained growing thin Al (aluminium)

layers on FBG by in vacuum evaporation. FBG were mounted in an axially rotating fibre-holder of the evaporation vacuum chamber in order to obtain an uniform and cylindrical-symmetry metal coating. Al was chosen referring to its high thermal expansion coefficient. The production of enhanced thermal sensors by $\sim 2 \mu\text{m}$ thin film Al coating deposition on commercial grade FBG, fully preserving the optical features of the grating, was demonstrated. The thermal expansion coefficient of the metal, much larger than the glass one, guarantees enhanced linear elongation/contraction of the FBG and thus enhanced temperature sensitivity of the sensor. The symmetric geometry of the coating and its elastic feature, quite different from the elasto-plastic one of the glass, guarantees repeatability of the elongation/contraction and thus both linearity and long term stability of the sensor. In collaboration with Sapienza University, the adopted technique is being used in combination with further coating deposition of Cu (copper) and Ni (nickel) by electro-deposition methods.

Development of innovative sensing solutions for monitoring cultural heritage

Optical fibre sensor of FBG (Fibre Bragg Grating) type can be effectively used for

structural monitoring of architectural historical complex, taking specific advantage of the unrivalled low invasive character of FBG monitoring systems. A monitoring system for opening of cracks has been developed and installed on the monumental cathedral of the city of Orvieto, the large 14th-century Roman Catholic church, constructed under the orders of Pope Urban IV. The activity is part of a large and multidisciplinary work aimed to assess the conservative state of the cathedral and its seismic vulnerability. The installed sensors perform continuous static monitoring of opening of cracks in the higher part of both the aisle walls, close to the transept. The installed monitoring system takes full advantage of the possibility to connect in series FBG sensors, being realised by one thin single optical cable running along the communication trench and interconnecting all the optical sensors. Monitoring so far performed has given significant results allowing the correlation between temperature at the masonry and cracks micro-opening behaviour, pointing out crack micro-opening cycles due to day/night temperature variations. Figure 4.17 shows the inside of the cathedral with evidence of the installed sensors.



Fig. 4.17 - Left: inside of the cathedral of Orvieto showing the balcony along the aisle walls, between the windows and the arches. Right: evidence of two sensors, barely visible as a dark bar on the white stripe of the wall.

SiO₂ and TiO₂ nanoparticles for development of nanocomposites for cultural heritage preservation

In recent times there was a surge of interest for the application of nanocomposites to restoration and conservation of artworks. In fact it has been found that the addition of inorganic oxide nanoparticles, such as silica and titania, improves the performances of materials used in the conservation field. The application of nanomaterials and nanotechnologies is enabling new functionalities that promise to improve the properties of traditional commercial products. SiO₂ and TiO₂ nanoparticles were synthesized by LUCIFERO set-up, with a special attention to the purity of the powders and low aggregation of the NP in order to obtain an homogeneous and transparent nanocomposite. The nanoparticles were produced by using liquid precursors (tetraethoxysilane (TEOS) Si(OEt)₄ and TTIP respectively) and were

dispersed in two commercial products, largely used as protective coating, Paraloid B72, an acrylic resin and Rhodorsil RC80, a silicon-based polymer.

In cooperation with UTTMAT-DIAG and UTAPRAD-DIM, the preservation properties of our nanocomposites were tested by the application on two different litotypes, very common in outdoor cultural heritage: white marble and travertine. Samples of treated stone were submitted to artificial aging processes, both in climatic chamber and in solar box, to assess and compare the performance vs. nanocomposites, by using non invasive diagnostic techniques. The results show that some properties of conservation materials can be improved by the presences of nanoparticles because they induce substantial changes of surface morphology of the coating layer (Fig. 4.18) and counter the physical damage observed during artificial weathering.

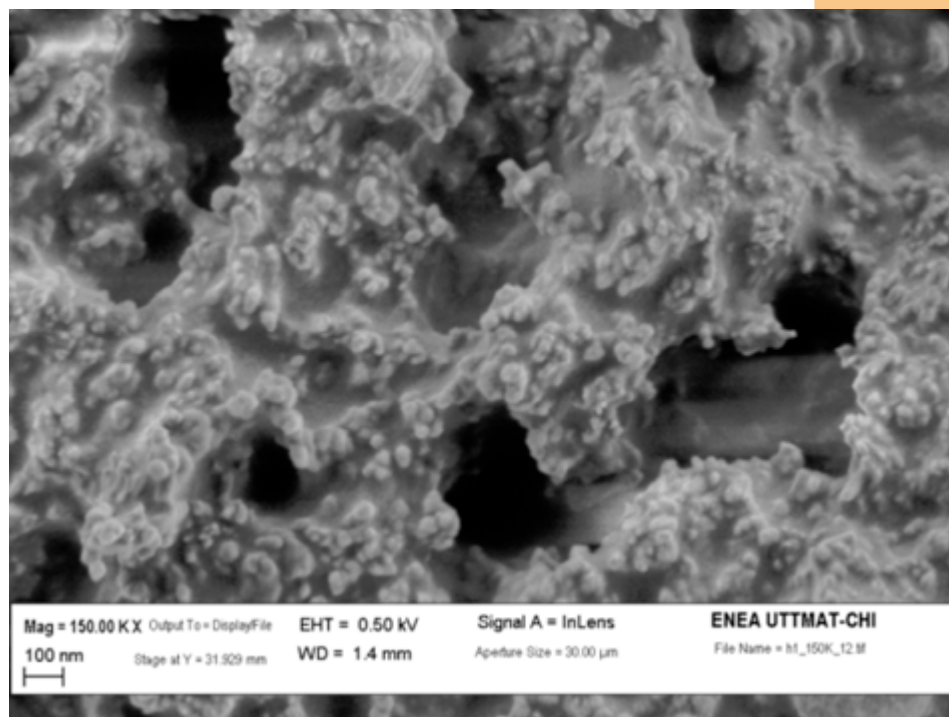


Fig.4.18 - SEM image of statuary Carrara marble treated with RC80-SiO₂ (0.2%)/TiO₂ (0.2%). Nano-mixtures form homogeneous coatings, with aggregates embedded inside a continuous protective film.

5. RADIATION SOURCES LABORATORY

5.1 Mission and infrastructures

The Radiation Sources Laboratory (UTAPRAD-SOR) performs R&D work in the fields of coherent radiation sources and in the acceleration of charged particles. Research activities include emerging technologies in photonics and microlithography, development of laser systems and accelerators for scientific, industrial and medical applications. Current activities are focussed on the development of:

- High energy-per-pulse excimer lasers, plasma driven X-ray sources and their applications;
- Free Electron Laser (FEL) sources for the generation of electromagnetic radiation in the Far InfraRed and in the Terahertz region;
- Low-energy electron accelerators for material processing, medical applications and as a driver for FELs;
- Medium-energy proton accelerators for cancer therapy
- Cybernetic models, artificial vision and automation systems.

These research areas are undergoing a rapid development worldwide with an increasing number of applications such as microlithography in the extreme ultraviolet, X-ray microscopy of biological systems, effects of electromagnetic radiation, imaging systems applied to material characterization, biology, biomedicine and, more recently, art conservation studies. The facilities developed by UTAPRAD-SOR and utilized for current activities include:

- Excimer laser laboratory
- Soft X-ray plasma sources laboratory
- Compact FEL (90 – 150 GHz)
- FEL-CATS (400 – 700 GHz)
- TOP-LINAC
- 5 MeV Electron LINAC

Funding and projects

In 2013 important steps forward were made in the launch of new projects in the field of nano-fabrication and “nano-patterning” by EUV radiation, in the field of the applications of THz radiation to art conservation and in the field of biological effects of THz radiation. In the frame of an agreement with the Regional Government of Lazio, the construction of the new accelerator for proton therapy TOP-IMPLART, a project in collaboration with the National Institute of Health (ISS) and the Physiotherapy Institute Hospital, Rome (IFO), progressed towards the achievement of the first milestone at 35 MeV and allowed the first radiobiology experiments to be carried out. In the following a brief review of the above activities is reported together with the most recent results and perspectives.

5.2 Short-wavelength Sources and Applications

In the extreme ultraviolet (EUV) spectral region (20 eV – 280 eV) laser-plasma and discharge-plasma sources can produce energies per pulse and repetition rates sufficient to be considered a valuable alternative to synchrotrons and short-wavelength free-electron lasers (X-FELs) in many applications, namely when the peak power and the brightness are more important than the average power and when a narrow spectral band is not required.

In past years the SOR Laboratory has developed the laser-driven plasma source EGERIA, a facility that has been used by biologists (in vivo X-ray microscopy of bacteria, DNA repair, micro-radiography), physicists (heavy ions generation, X-ray atomic spectroscopy, micro-devices for photonics, contact-lithography, imaging of sub-micrometric structures on optically active materials) and industry (writing arbitrary pattern on anti-

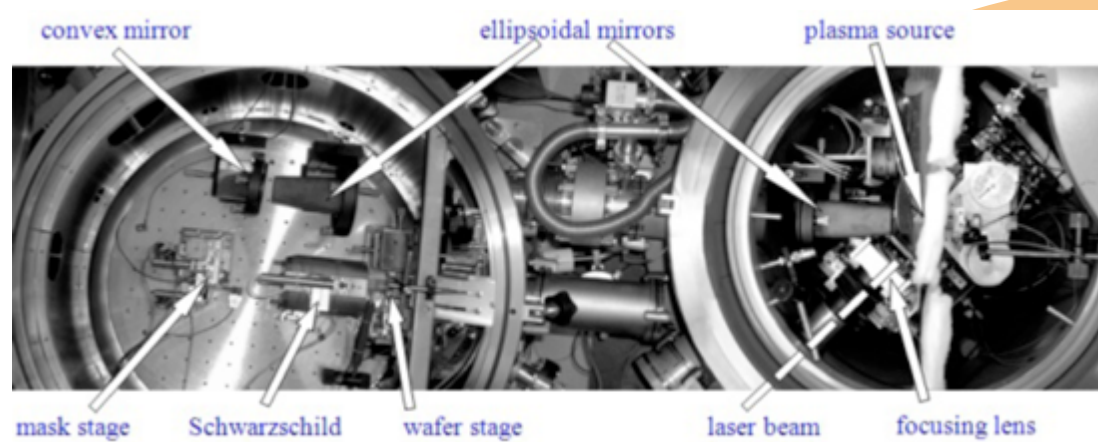


Fig. 5.1 - Top picture of the EGERIA vacuum chamber (right), where the laser-plasma is generated, and of the Micro Exposure Tool high-vacuum chamber (left), where high-resolution patterns are written either on a photoresist or on a fluorescent material.

counterfeiting tags). A Micro-Exposure-Tool (MET) for micro- and nano-lithography has been developed to be used with the plasma source EGERIA. The MET is a complex apparatus comprising a debris mitigation system, an optical collector and an optical projection system able to print a pattern with a spatial resolution better than 100 nm. Figure 5.1 shows a top view of the EGERIA source chamber and of the MET chamber. Since November 2010 a xenon Discharge Produced Plasma (DPP) soft X-ray/EUV source, jointly designed by ENEA Frascati and the Physics Department of LAquila University, is operating

at the SOR Laboratory. A photo of the DPP is shown in Figure 5.2. In the following we describe the experimental activities carried out in 2013, concerning, on one side, the EUV radiation generation and its applications, and, on the other side, the development of devices for the positioning of concentrating solar systems, exploiting the laboratory expertise in lasers and optics.

Discharge-plasma source of EUV radiation

In the framework of the project “New materials for direct nanopatterning and nanofabrication by EUV and soft X-rays

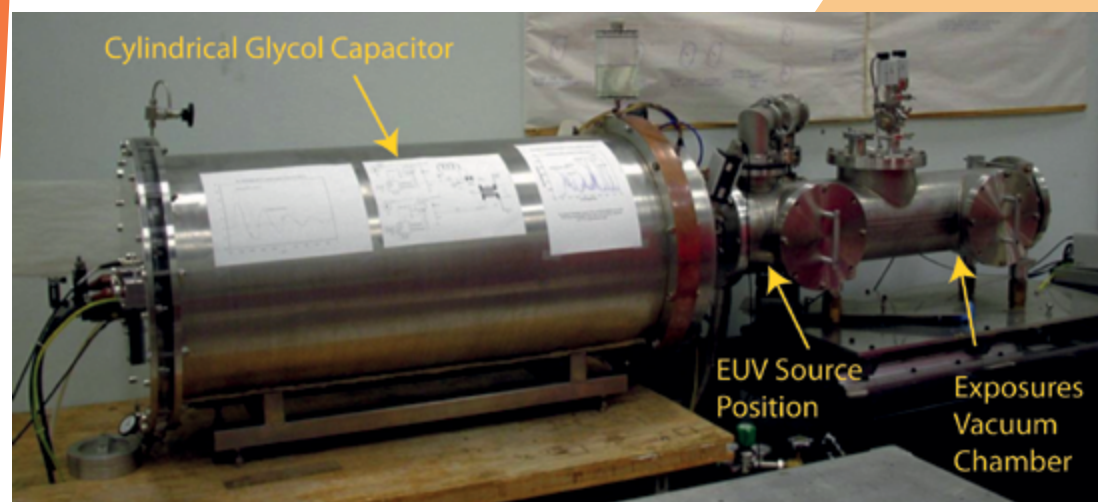


Fig. 5.2 - The DPP (Discharge Produced Plasma) EUV/soft X-ray source operative at the ENEA Frascati Research Centre.

exposures”, funded by the CARIPLO Foundation (April 1st 2013 – December 31st 2015), different photoresists prepared by the Material Engineering Department of Padova University, were deposited on silicon wafers and exposed to the EUV radiation generated by the DPP (Discharge Produced Plasma) source at the ENEA Frascati Laboratories. Samples of photoresists with particular optical/mechanical properties loaded with zirconia, alumina or titania nanoparticles have been exposed. As an example, the zirconia loaded sample imaged under optical microscope after development is shown in Figure 5.3. These tests are part of a process of characterization of different resist materials and optimization of both the EUV exposure conditions and the subsequent development process, as scheduled in the project objectives. The following step of the project activity will be the patterning of the photoresists at high spatial resolution. For this task it is crucial to optimize the source size and its spatial stability. These parameters mainly depend on the source geometry and on the discharge evolution. As already described in former ENEA Activity Reports, the DPP source is supplied by two electric discharges: an initial low-current (~20÷30 A, few microseconds in duration) preionization discharge followed by the high-current main discharge (~ 10 kA for few hundreds nanoseconds) which leads to the high temperature plasma formation. In order to characterize the DPP EUV source size and position during the main discharge, the plasma column has been observed in the visible range by a gated camera (DICAM-2, PCO Computer

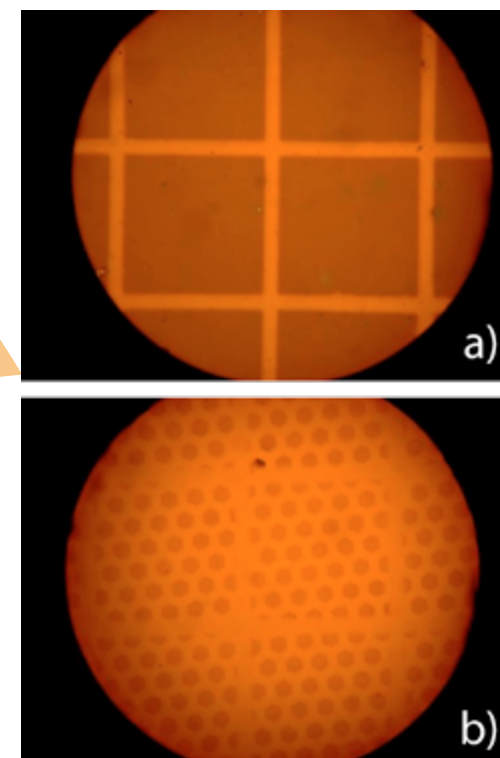


Fig. 5.3 - Zirconia loaded photoresist exposed to 0.6 J/cm² (a) and 0.4 J/cm² (b) of EUV radiation filtered by a 150 nm thick zirconium filter supported by a nickel wires mesh, developed for 30” in 37% (a) or 18.5% (b) HCl acid solution. In both (a) and (b) the shadow of the nickel wires with 363 μm pitch is well recognizable. In case (b) a copper mesh with 400 hexagonal holes/inch has been overlapped to the zirconium filter. Both samples are here observed by an optical microscope with a 20x objective.

Optics GmbH, 1993) placed at 1 m distance in front of the capillary using a telephoto lens as shown in Figure 5.4a. A representative image is shown in Figure 5.4b.

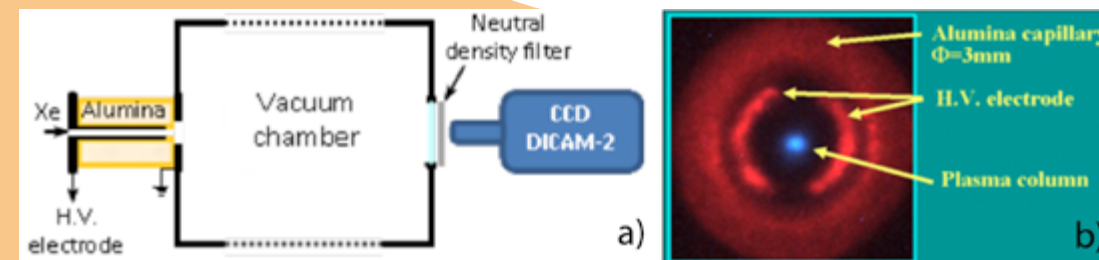


Fig. 5.4 - The DPP plasma source imaged by a gated CCD camera. a) Schematic of the experimental setup (not in scale). b) An example of the acquired images in false colours: the plasma image (blue) is overlapped to the source structure image (red) in order to distinguish each other at the discharge beginning and ending phases, when the plasma is as wide as the H.V. electrode. Plasma image exposure time: 20 ns.

By using a gate time of 20 ns and changing the delay of the camera acquisition with respect to the source discharge (only one image per shot is possible with this camera), the pinch effect due to the magnetic compression is clearly demonstrated and a minimum source size below 300 μm in diameter has been detected as shown in Figure 5.5.

Figure 5.5 shows that, after the collapse, the plasma column is reduced in size by more than a factor 10 with respect to its starting value (which is the capillary internal diameter) and the plasma shot-to-shot position stability is very good. The picture sequence also shows that the plasma collapse and the successive relaxation temporally coincide with the EUV emission rise and fall, respectively, as expected. It is worth noticing that the visible emission power grows both during and after the EUV main pulse so that the optical density of a neutral filter placed in front of the camera had to be increased for longer delays in order to avoid the camera saturation.

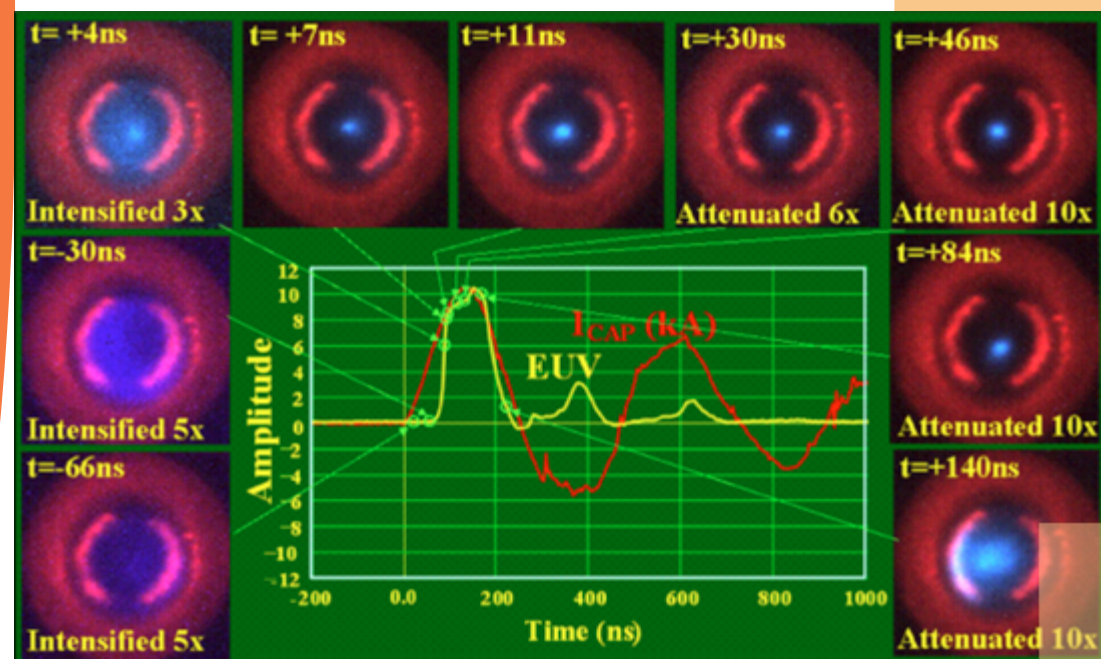


Fig. 5.5 - False colour images of plasma emission in the visible range at different delay times "t" from EUV emission rise (50% of maximum). The temporal position of each image with respect to the EUV power emission (yellow curve) is indicated in the central part of the figure (green circles indicate the time of the 20 ns exposures of the gated camera). The discharge current (ICAP) is also reported (red curve).

This can be related to the fact that the low-charge-state ions population, i.e. the responsible for visible light emission, continuously grows during the main discharge. The gated camera allowed also to analyze the plasma discharge during the low current preionization phase, as shown in Figure 5.6 : at the current onset the discharge clearly occupies only a small portion of the capillary and only after about 2 μs it fills the whole tube. Thus, it is convenient to start the main discharge after more than 2 μs of preionization phase. In this case the gate time has been increased to 100 ns to achieve a correct exposure of the camera.

Figure 5.6 also shows that the onset of the preionization discharge at each shot occurs in a random point of the capillary internal surface. During 2013 the experience acquired on discharge plasma sources at ENEA has also stimulated the beginning of a cooperation with INFN for the development of a low current discharge plasma for wake-field particles acceleration studies.

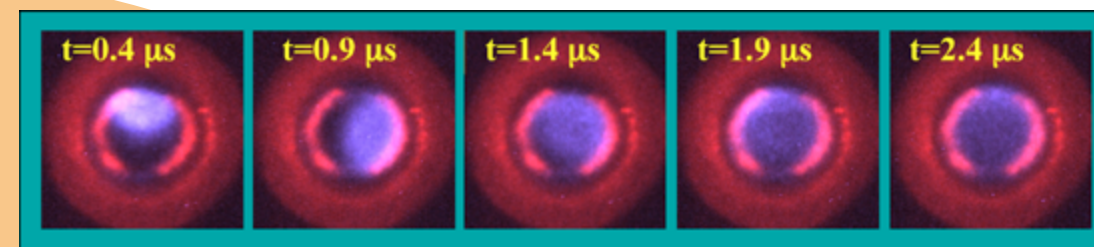


Fig. 5.6 - Sequence of false colour images of the discharge during the preionization current phase (0.1 μs exposure time at a constant step of 0.5 μs , one image/shot). The delay time "t" of each image with respect to the current onset is indicated.

5.3 Optical systems for solar technologies

The Radiation Sources Laboratory has recently applied its expertise in optics to the positioning of concentrating solar systems with respect to the sun and to innovative linear concentration schemes. To this aim, the Laboratory has developed a simplified analytical algorithm that allows the astronomical calculation of the sun position with an accuracy of about 1 minute of arc. Starting from this algorithm, a new high precision solar compass was developed and patented (patent application number RM2012A000664). The innovative sun compass is based on:

- a particular sun image detector;
- a microprocessor connected to a GPS device for accurate knowledge of the local time and geographical coordinates;
- a pointing optics (a telescope with pointing cross).

The research activity in 2013 has concentrated on three main topics:

- Improvements on the structure and on the first prototype of the ENEA solar compass (No 1).
- Development of an upgraded prototype of the sun compass (No 2).
- Contacts and cooperation with external institutes and enterprises aimed at a technological transfer and patent exploitation of the sun compass.

Improvements on the structure and on the calibration of the first prototype

The first prototype of the ENEA solar compass was installed over a telescope with a mechanical goniometer placed between the sun sensor and the telescope. During 2013 the sensor has been integrated into a theodolite with a high precision digital goniometer. This change improved the accuracy of both the vertical alignment of the compass rotation axis and the angular measurement by one order of magnitude, so that their influence on the overall instrument accuracy is now negligible. A picture of the compass integrated on the theodolite is shown in Figure 5.7.



Fig. 5.7 - First ENEA electronic solar compass (prototype No 1) mounted on a theodolite.

A careful calibration of the compass is a crucial task to achieve a high accuracy during the azimuth angles measurements. Generally two alternative principles can be followed for a high precision tool development: either to reduce all construction errors until the accuracy of the instrument is guaranteed (even without any calibration) or to allow a reasonable tolerance on the instrument construction and then measure, through an accurate calibration, the value of all parameters which randomly characterize each realized sample. We followed the second approach since it is simpler than the first one, although it implies an accurate calibration of each sample.

In particular, five main parameters of the compass have been identified: four of them are related to the relative position and orientation of the compass entrance optics with the compass image sensor (optics to sensor distance, lateral shift, horizontal angle, vertical angle), and the last is the compass optics to pointing mean optical device (a telescope, a theodolite, etc.) horizontal angle.

The compass calibration, i.e. the determination of the above mentioned 5 construction parameters, can be obtained by means of a specific optical bench (under development) as well as through a several hours long observation of the sun with the compass together with the observation of a far target whose geographical coordinates are absolutely known.

This last technique was the only one available during 2013 and it resulted to be very effective. After the integration of the compass on a theodolite and its calibration, the compass accuracy improved by approximately a factor two, as derives from the comparison of the results shown in Table 5.8 with respect to those reported in the 2012 Activity Report.

Among the several tests of comparison between the orientation view of surveyed targets as measured by the compass and their theoretical value calculated on the basis of their geographical coordinates, the measurement

Target	Distance from the compass	Experimental azimuth measured by the ENEA compass	Theoretical azimuth from Google maps	Difference in arcminutes
<i>Compass on a panoramic point at the ENEA Research Centre</i>				
Antenna on Monte Mario – Rome	21.9 Km	+120° 52.3'	+120° 51.92'	+0.4'
Cross on the cupola of S. Peter Cathedral in Rome	20.2 Km	+117° 8.8'	+117° 9.45'	-0.7'
Top of Monte Rocca Romana, near Trevignano	54 Km	+137° 58.6'	+137° 58.73'	-0.1'
<i>Compass on a terrace of a building at the ENEA Research Centre</i>				
Telecom tower antenna in Rome EUR	15.3 Km	+80° 38' 28"	+80° 39' 36"	-1.1'
Top of the cupola of S. Peter and Paul church in Rome EUR	17.5 Km	+93° 55' 7"	+93° 56' 57"	-1.8'
Bell tower of the Montecompatri church	3.5 Km	-75° 03' 36"	-75° 04' 18"	+0.7'
<i>Compass at the Doganella spring, near Rocca Priora (Rome)</i>				
Antenna on Monte Artemisio	5.5 Km	+62° 7' 42"	+62° 8' 18"	-0.6'
<i>Compass at the Military Geographic Institute (IGM) Center in Florence to measure the relative orientation of two calibration stones</i>				
IGM stone 2 seen from stone 1	0.1 Km	-57° 02' 36"	-57° 02' 48"	+0.2'

Table 5.8 - View direction of different targets, with respect to true geographic South, experimentally detected by the compass (red values) and comparison with those calculated on the basis of the geographical coordinates given by Google

maps both for the target and for the compass (blue values). An exception is on the last row of the table, where the theoretical azimuth (green value) has been provided by IGM.

done at the Military Geographic Institute (IGM) is particularly significant. In fact, in that case the coordinates of the pointed objects (reference stones) were provided directly by IGM with certified values, i.e. with an accuracy much superior to that generally provided by satellite maps and used for verifying the other measurements.

Another important test of the compass was performed at the parabolic trough solar collector of ENEA Casaccia which nominally has the rotation axis exactly oriented along Est-West direction. The compass has confirmed the mirror axis orientation within an error of 0.4 arc-minutes.

Although the first ENEA sun compass prototype (No 1) demonstrated the performance of the ENEA patented idea, it was somehow different from the structure described in the patent because of the lack of an internal microprocessor, which was simulated by an external computer.

During 2013 a new prototype of the sun compass has been developed (No 2). It differs from the first one in many components:

- a) a cheap microprocessor and a display have been integrated in the compass (as described in the patent) so that the compass can now work standalone, without the assistance of any personal computer.
- b) the optics, constructed at CNR-IFN in Rome, is much more accurate
- c) the image detector has a smaller spatial resolution (5.6 μm rather than 8 μm) and a larger detection area. Consequently, the detector angular resolution is 1.0 arc-minute rather than 1.4 arc-minutes and the sun light acceptance angle is $\pm 5^\circ$ rather than $\pm 4^\circ$.

Furthermore, this prototype has an internal rechargeable battery and an internal memory unit where all data can be saved. A picture of the prototype is shown in Figure 5.9.

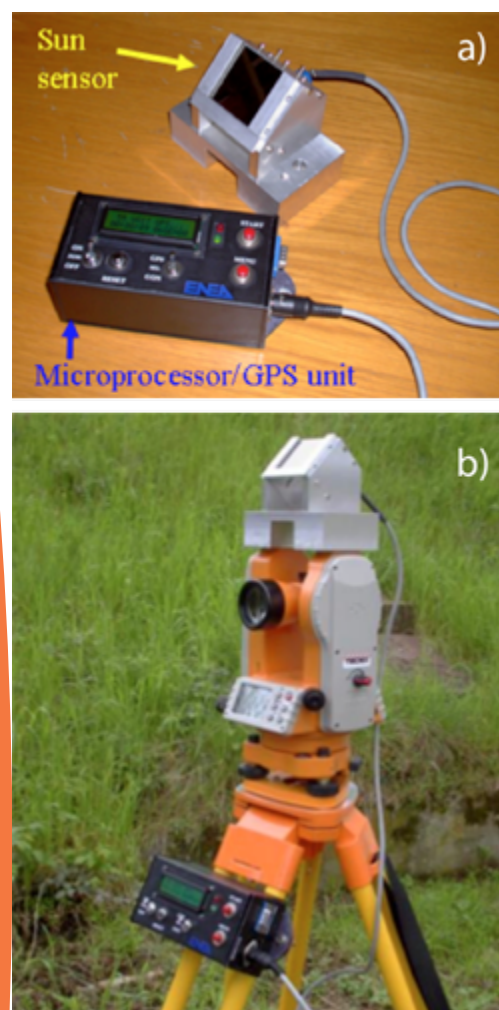


Fig. 5.9 - a) Improved prototype of the ENEA electronic solar compass (No 2). b) Mounted on a theodolite.

Contacts and cooperation with external institutes and enterprises for exploitation of the patent on new compass

Several institutes and enterprises demonstrated an interest for the ENEA compass. On the basis of this manifestations of interest, on December 2013 ENEA has decided to extend the validity of the patent on the solar compass to foreign countries (PCT n° 000365). These manifestations of interest are important for the scientific opportunity of cooperating with industry and improving the compass, and also for the possibility of a future technological

transfer and patent exploitation. In particular:

- A three months scientific collaboration has taken place between ENEA and ACEA LaboratoRi S.p.a. (ACEA is the main Consortium in the Rome area for the state distribution of drinkable water) for the measurement of the orientation of their mobile laboratory equipped with many diagnostics for atmospheric pollution survey, wind speed and direction measurements. In addition, we performed measurements of the reciprocal position of the water springs at the Doganella site in Rocca Priora (Rome), since in that place the use of sophisticated GPS for the determination of accurate geographic coordinates failed. The collaboration has been successful for both applications and ACEA LaboratoRi S.p.a. is now considering the possibility of a long term cooperation with ENEA for the development of a sun compass suitable for any transport mean (cars, boats, airplanes, etc.).
- A meeting with the multinational company Topcon (a global leader for high precision positioning systems and optical instruments for surveying and civil engineering applications) has been held at ENEA Frascati in view of a possible integration of the ENEA compass in Topcon instruments. The dialogue is still underway .
- An agreement with D.D. Costruzioni Meccaniche s.r.l. of Mereto di Tomba (Udine, Italy) has been signed for a 7 months cooperation aimed at the experimentation of the ENEA compass integrated in parabolic trough concentrators for sun power installations (CSP). The cooperation involves also the UT RINN of ENEA Casaccia, where a prototype of thermodynamic solar power parabolic trough system is available. In particular, two identical prototypes of the last version of the ENEA compass (i.e. with internal microprocessor, GPS, etc.) will be realized and implemented both on the D.D. s.r.l. sun power installation and at the ENEA Casaccia installation for preliminary sun

tracking tests and for thermal efficiency measurement respectively. In this case the compass is implemented with an internal inclinometer, which eliminates the need of manual vertical alignment, and by an additional software which can evaluate at any time the parabolic trough mirror angular position to face the sun.

In fact, in the CSP application, the ENEA solar compass has two functions: first the determination of the orientation of the parabolic trough mirror axis, both at the first activation of the solar power installation and at every sunny noon; second, the continuous driving of the mirror rotation to track the sun. The main innovations introduced by the compass integration, compared with the present state of the art, consist of the independent operation of each parabolic through mirror of a sun power installation (typically more than 100 mirrors) and of the automatic compensation of possible axis orientation error. The compass cost is absolutely negligible compared to the cost of each mirror trough and can be recovered thanks to the enhancement in energy production related with its use. The cooperation contract between ENEA and D.D. s.r.l. is planned to begin in spring 2014 and is aimed not only at an experimental proof of principle for the application of the ENEA solar compass to sun power installations, but also at a technology transfer to D.D. s.r.l. and at a final negotiation for the ENEA patent exploitation.

5.4 Terahertz sources and applications

ENEA has a long term expertise in the construction of powerful short-pulse mm-wave and Terahertz free electron sources. Various electron-wave interaction schemes were successfully tested in the past, ranging from Cerenkov to Smith-Purcell radiators and to undulator devices. A variety of applications of millimeter waves and THz radiation have been covered through the years. In 2013 two new projects started in the field of the biological effects and art conservation respectively.

The THz-ARTE project

In the frame of a collaboration with the National Institute for Information and Communications Technology (NICT-Tokyo) and CNR-IFAC (Florence), a three-year bilateral Italy-Japan joint research project on cultural heritage conservation, THz-ARTE, was selected and funded by the Ministry of Foreign Affairs in July 2013. The project is aimed at the study of wall paintings by means of radiation in the spectral range from near infrared to microwaves. Comparison of different spectroscopic techniques in this wide spectral range will lead to the final goal of the project: the realization of a portable iper-spectral imaging system for the analysis of wall paintings. In the second half of the year, different measurements have been jointly preformed with CNR-IFAC and NICT and the mechanical structure of a low cost 3D scanner has been realized. Fresco model samples were prepared at NICT and at CNR-IFAC. Samples prepared at NICT were analyzed utilizing a Picometrix T-Ray 400 pulse-echo imaging system. The effects of different particle size of fillers and of internal layer structures were studied. Transmission properties of the samples from NICT and CNR-IFAC were measured at the ENEA 100 GHz FEL imaging device. Results were used in order to tailor the characteristics of the imaging device prototype, in terms of power of the radiation source and sensitivity of the detectors. Regarding the imaging prototype, in order to reduce the cost of the device, the mechanical structure, including motion devices and control electronics, was directly derived by a commercial 3D printing system, performing some modifications to mount the probe head and related optics (Fig. 5.10). A new control software was designed taking into account the new requirements. The device capabilities, in terms of precision and resolution, were tested, also using a laser triangulation system. The same triangulation system will be used in combination with 2 different sources the first operating at 97 GHz, the second in the range between 20 and 40 GHz, in order to

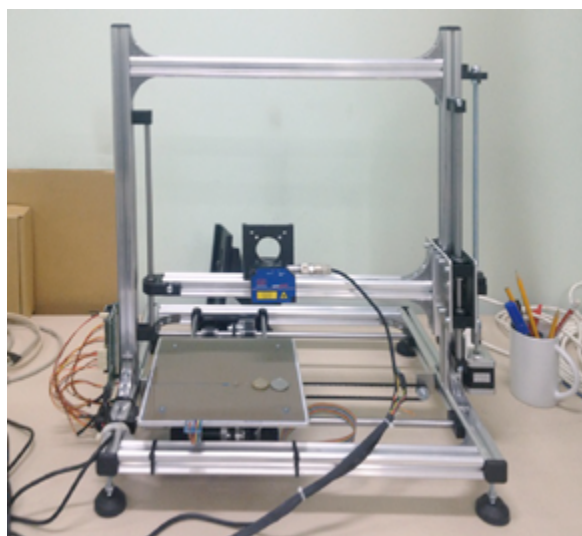


Fig. 5.10 - Prototype of the 3D THz imaging scanner. Radiation source and probe head are not shown.

extract the topological information from the sample to obtain the phase change due to the spectroscopic behavior of the sample. Waveguide components have been acquired to build up the source/probe system to perform phase measurements of the reflected radiation.

The GREAM project

The biological effects of THz radiation are currently arising a growing interest because of their relevance in the medical, security, telecommunications and military areas. After the pioneering proactive studies conducted in the frame of the THz-BRIDGE project in the years 2001- 2009, several research groups have addressed various biological endpoints in a wide range of frequencies worldwide to investigate the mechanism of interaction and the presence of specific frequencies, which may induce a response on biological systems. In the frame of collaboration between the Radiation Source Laboratory and the Army Medical and Veterinary Research Center - Rome, the Department of Science University of "Roma Tre", and the Department of Clinical Sciences and Translational Medicine - University of Rome "Tor Vergata", the

GREAM project has been recently funded by the Ministry of Defense to evaluate potential genotoxic effects associated with the exposure of living cells "in vitro" to high-frequency electromagnetic radiation, such as microwave and THz radiation.

The GREAM project employs the analysis of cytogenetic and molecular markers, indicators oxidative stress, apoptosis and cell death assays, on two distinct human cellular models (peripheral blood lymphocytes and human fibroblasts). Fibroblasts are particularly important in this study since they are the most common cells of connective tissue in animals. Fibroblasts synthesize the extracellular matrix and collagen and play a critical role in wound healing. The ENEA Compact Free Electron Laser has been used to irradiate biological samples in the frequency range 130 - 150 GHz. Due to the peculiar characteristics of the electron accelerator driving the FEL, the radiation pulse is composed by a "train" of micropulses, each 50 ps long, with 330 ps spacing between adjacent micropulses. The overall duration of the train (macropulse) is 4 μ s. Macropulses can be produced at a repetition rate that can be typically varied between 1 and 10 Hz. The peculiar temporal structure of the emitted radiation allows the investigation of the effects of high peak power, while maintaining a low average power, typically few mW, incident on the sample, thus avoiding heating effects. The FEL spectrum consists of several emission lines, spaced at 3 GHz intervals corresponding to the period of the radio-frequency driving the accelerator. For the irradiation of fibroblasts the Compact-FEL has been operated in the so called "wide-bandwidth" mode, with the emission showing a typical relative bandwidth of around 20% (see Fig. 5.11).

The FEL radiation is transported to the exposure set-up by means of a special mm-wave transmission line composed of a copper light pipe with 25 mm clear aperture and appropriate delivery optics. For the genotoxic evaluations on fibroblasts, a specific THz Delivery System (TDS) was designed to irradiate samples from

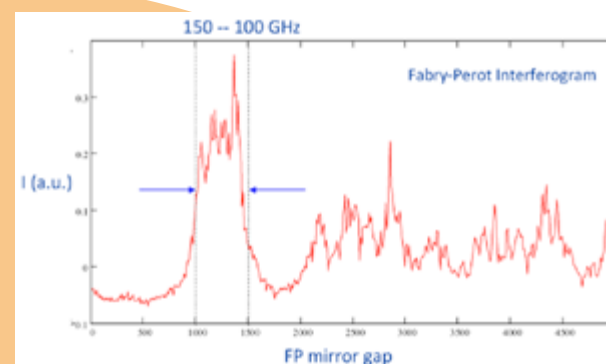


Fig. 5.11 - Fabry-Perot Interferogram of the Compact-FEL wide bandwidth radiation (100 - 150 GHz)

the bottom of polystyrene Petri dishes. An upper limit to the irradiation area is set by the maximum feasible expansion of the THz beam needed to get a uniform power density at the sample surface. Petri dishes with an internal diameter of 5.2 cm, containing a single layer of fibroblasts adherent to the bottom of the Petri dish and immersed in 4ml of culture medium (serum) resulted the best choice to perform THz irradiation. A technical drawing of the TDS is reported in Figure 5.12.

The THz beam coming from the light pipe into the TDS is first focused down to a 17.5 mm diameter aperture by means of a conical section and is then let expand by diffraction to about 52 mm diameter to match the required irradiation area. Calculations have been performed in order to minimize internal reflections in the cone, making the beam expansion similar to the free space expansion. In Figure 5.12 b) the longitudinal section of the cone is shown, together with the

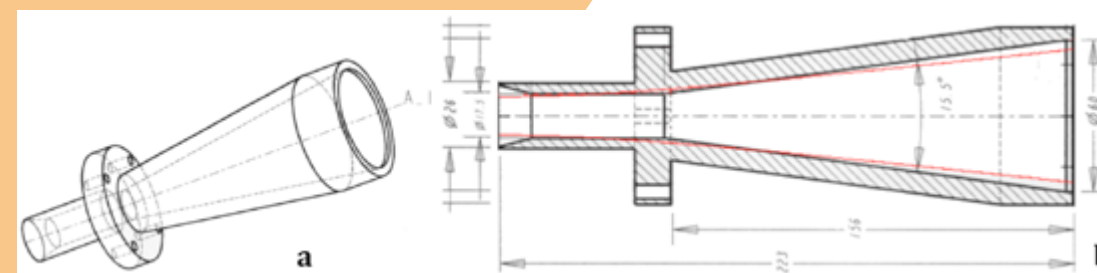


Fig. 5.12 - a) Technical Drawings of the TDS. The red lines in b) indicate the beam waist profile for free space expansion

beam waist profile (red lines) for free space propagation. The Petri dish with sample was directly placed on top of the TDS as shown in Figure 5.13. Sham-exposed samples were placed on the same working plate as the THz exposed samples.

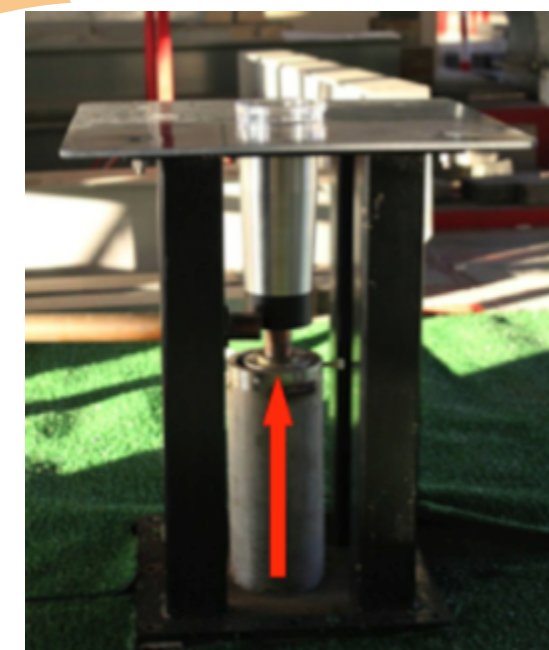


Fig. 5.13 - Photo of the exposure set-up installed on the roof of the Compact-FEL, showing the light pipe output, the THz Delivery System (TDS) and the Petri dish containing the biological sample.

The ENEA CARM Source for Nuclear Fusion

Plasma heating systems based on the electron cyclotron resonance (ECRH) mechanism have been used in different fusion devices exploiting the intrinsic potential capabilities of this technique, i.e. localized energy delivery and use of quasi-optical launching systems.

In the case of the international Tokamak experiment ITER, which operates at a magnetic field of 5.7 Tesla, Gyrotron sources are in an advanced phase of development and can provide a heating power of approximately 1 MW CW at a frequency of 170 GHz. The further step in fusion, DEMO, and any future fusion reactor, due to the high temperatures associated with the plasma, require higher ECRH frequencies to obtain a central Radio-Frequency (RF) power deposition, avoiding downshifted absorption on the distribution function tails.

It will be therefore necessary to develop high-power sources (≥ 1 MW) in the frequency range of 200–300 GHz. A high frequency ECRH system would also find a direct application in heating the plasma of FAST, the “Fusion Advanced Study Torus” proposed by the EURATOM-ENEA as a ITER satellite experiment capable to deal with some aspects of DEMO.

An alternative to gyrotrons for high frequency RF sources is given by the Cyclotron Auto-Resonance Maser (CARM); this source is based on a slightly different type of interaction between the wave and the electron beam. In this case, the electromagnetic radiation is produced by a relativistic electron beam, which remains in synchronism with the RF field during the entire process of electron-wave energy transfer. This mechanism permits an efficient generation of radiation, at high frequencies, and allows the excitation of low order transverse modes and thus reducing the undesired instability given by the cavity mode competition. The ENEA Fusion Technical Unit (UTFUS) in collaboration with the Radiation Sources Laboratory (UTAPRAD-

SOR) and the Theoretical Physics Laboratory (UTAPRAD-MAT) have set up a joint Task-Force for the preliminary design and a prototype realization of a CARM to be tested on the Frascati Tokamak (FTU). The high magnetic field (up to 8T) and the FTU plasma density (10^{21} m^{-3}), represent ideal parameters for a prototype to be tested.

The newly-formed Task Force has as its long-term goal the construction of a prototype CARM providing approximately 200kW of RF power in pulses of duration between 0.1 and 0.2 seconds, which can be effectively used on FTU in heating experiments at the first and second harmonics, i.e. at frequencies in the range 200-240 GHz for magnetic field values ranging between 7-8 Tesla and 3-4 Tesla respectively. The long term objective of the project is the design, realization and test of a CARM with an output power $P \geq 500\text{kW}$ CW (0.5 seconds of pulse duration) and an operating frequency range of 250–300 GHz.

The work-plan is broken down in four interdependent phases covering an overall time period of about five years. In the first phase, the modeling of all components will be completed and benchmarked with analytical models and numerical codes (see also sect. 3.2). The cathode and the electron gun will be further optimized to achieve an electron beam with a velocity spread lower than 1%. At the same time the theoretical study of the resonant cavity, based on Bragg reflectors, will allow the choice of the operating mode for the maximum efficiency of energy exchange between electron beam and electromagnetic field in the cavity region.

This phase will be followed by the practical realization and test of an electron gun and a resonant cavity able to operate at reduced specifications ($P_{\text{min}} \geq 100 \text{ kW}$, $f_{\text{max}}=300 \text{ GHz}$) for pulse lengths limited to 1 μs . The pulse length will then be extended to 100 μs in the second phase of development.

5.5 Accelerators development

The field of particle accelerators involves a variety of multidisciplinary technologies and is cross-sectional to many activities. Accelerator R&D deals with physical technologies based on ionising particles and X rays, which are employed in special applications ranging from materials science to medicine. Electron accelerators are also used as a powerful driver of non-ionising radiation source, such as Free Electrons Laser (FEL).

In the following we briefly describe the main results of the activities carried out in the field of protons and electrons accelerators at the ENEA Frascati Centre for different applications: industrial and medical applications, and generations of FEL radiation.

Electron accelerators at ENEA-Frascati

The Radiation Sources Laboratory currently operates three electrons accelerators:

- 5.3 MeV linac for irradiation with electrons and X-rays from “Bremsstrahlung”;
- 5 MeV microtron used as a driver for the Compact-FEL
- 3 MeV Linac used as a driver for the THz radiation source FEL-CATS

The 5 MeV linac is a S band (3 GHz) standing wave linear accelerator with electron energy in the range 3 to 5 MeV and a current of 0.2 A in 4 μs macropulses. During 2013 it has been mainly used in the framework of the development of dosimeters in collaboration with the National Institute of Health. It has been also employed for X-ray production in collaboration with IFO (Istituti Fisioterapici-Rome) for medical applications and in collaboration with NRT R&D (Aprilia) for industrial applications (radiographic inspection of materials defects).

The 5 MeV microtron operating in S-band (3 GHz) continued to be used as a driver for the Compact-FEL for the generation of electromagnetic radiation in the millimetre-

wave region (90–150 GHz). A stable performance was obtained with 0.3 A, 4 μs pulses at a repetition frequency in the range 2 to 10 Hz. The Compact-FEL was used for irradiation experiments on biological samples.

The 3 MeV linac, equipped with a particular device for the manipulation of the e-beam, used as pilot for the generation of electromagnetic radiation in the sub-millimeter (0.4 – 0.8 THz) by means of a magnetic undulator (FEL-CATS) is currently being refurbished.

Proton accelerator facility

1) The TOP-IMPLART project

The TOP-IMPLART project, carried out by ENEA in collaboration with ISS (Italian National Institute of Health and IFO-IRE (Regina Elena National Cancer Institute in Rome) is devoted to the realization of a new proton therapy center planned to be built in Rome at IFO. The project is centered on a proton accelerator designed as a sequence of linear accelerators. Two phases of construction are foreseen: the first, funded by the “Regione Lazio”, with a maximum energy of 150 MeV, and the second one up to 230 MeV. The segment up to 150 MeV is under construction and will be tested at the ENEA Research Center in Frascati before the transfer to IFO, which is the clinical user.

The low energy part is completely operative (Fig. 5.14) and consists of a 3 MeV RFQ and a DTL up to 7 MeV (PL-7 ACCSYS-HITACHI model), both operating at 425 MHz, followed by a beam transport line with four electromagnetic quadrupoles, to match the beam to the high frequency (2997.92 MHz) linac booster under realization. Accurate beam based alignment of the quadrupoles has been performed in order to center the beam at the end of the transport line with a precision within 100 μm .

In 2013 the variable energy (3-7 MeV) and pulsed current (0.1 – 100 μA) proton beam furnished by the injector has been

made available for different applications (radiobiology experiments, detectors development, material studies). An auxiliary vertical beam transport line has been installed suitable for radiobiology in vitro studies, allowing to irradiate besides cell monolayers also cells growing in suspension culture. This line is based on a 90° bending magnet placed between the two quadrupoles doublets, and includes a collimator (2 mm of diameter) and a 2 μm Au scattering foil producing a uniform proton beam distribution at the end of a 70 cm long vacuum tube.

The uniformity on the area of interest (a circular area of 13 mm diameter equal to the size of the PETRI dish where cells to be irradiated for “in vitro” radiobiology experiments are deposited) has been verified irradiating GAFCHROMIC films (HD-V2 and EBT3 type). The image of a gafchromic film irradiated by a 3 MeV proton beam from the injector acquired by a EPSON Expression 11000 XL scanner and analyzed by the PICODOSE commercial software is shown in Figure 5.15.

The experimental activity on the horizontal beamline included the propagation of the 7MeV proton beam in a magnetic channel (6 mm diameter) with four short (33 mm) high gradient (196 T/m) PMQs arranged in a DOFO lattice scheme placed after the four electromagnetic quadrupoles (Fig.5.16). This experiment is preliminary to the acceleration tests in the first module of the high frequency

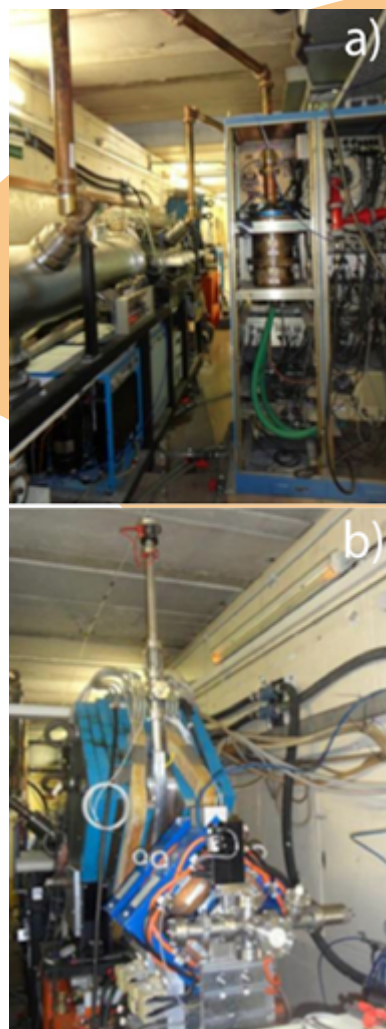


Fig. 5.14 - a) The 3-7 MeV proton beam injector - b) The low energy beam horizontal and vertical transport lines following the injector

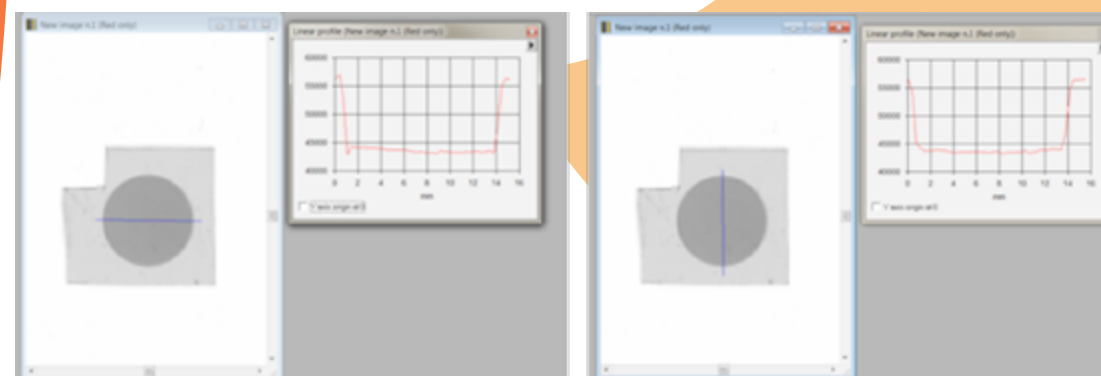


Fig. 5.15 - Gafchromic film HD-V2 type irradiated by the proton beam on the vertical beam line with the horizontal and vertical profile analyzed by PICODOSE software

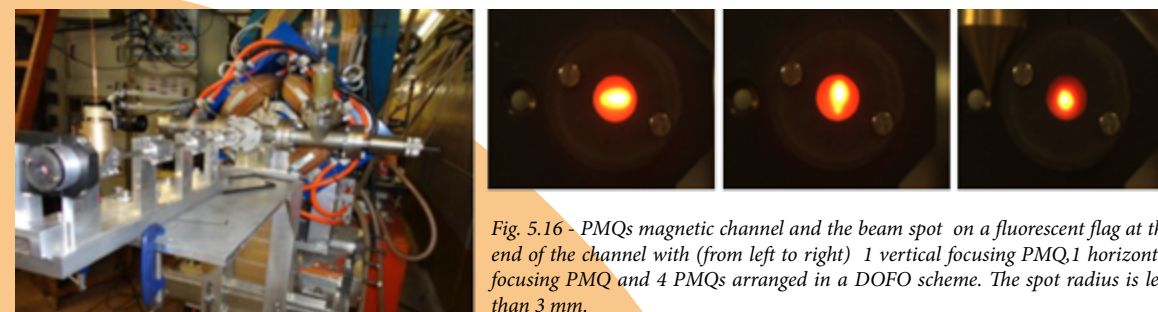


Fig. 5.16 - PMQs magnetic channel and the beam spot on a fluorescent flag at the end of the channel with (from left to right) 1 vertical focusing PMQ, 1 horizontal focusing PMQ and 4 PMQs arranged in a DOFO scheme. The spot radius is less than 3 mm.

booster where the PMQs will be mounted in the inter-tanks spaces to focus the beam during the acceleration.

The medium-energy section of the proton linear accelerator from 7 to 35 MeV is a SCDTL (Side Coupled Drift Tube Linac) structure made of 4 modules supplied by one 10 MW klystron. In 2013 the klystron has been ordered to THALES (TH2175-A model, 4 μsec, 100 Hz). The first module up to 11.6 MeV has been built and the second and third modules are under realization at CECOM.

The module has been completely characterized on the RF bench and is ready for the hot tests (Fig. 5.17).

2) Collaboration with ITEL company

In 2013 the Radiation Sources Laboratory thanks to its expertise in the design of proton accelerators carried out a study commissioned by ITEL Telecomunicazioni s.r.l. (Ruvo di Puglia, BA, Italy), a company offering products and services for high tech in medical, pharmaceutical and EMC sectors. The study concerns the feasibility of a proton accelerator for the therapy of the uveal melanoma in the framework of a Project funded to ITEL by Regione Puglia. Different layouts have been compared based on different accelerator schemes (full linear accelerator with various choices for the injection energy or the hybrid solution “cyclotron+linac”) by extensive beam dynamics and RF properties analysis.

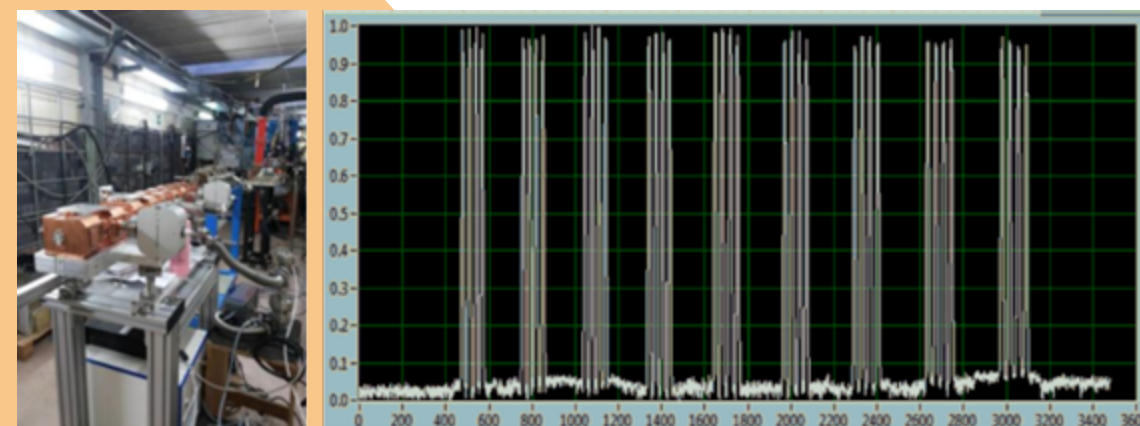


Fig. 5.17 - a) SCDTL 7-11.6 MeV module in the ENEA Frascati bunker, b) Bead pull measurement of the squared electric field along the axis.

5.6 “Olocontrollo emulativo” technology

This activity is dedicated to the development of a cybernetic model of synthetic intelligence. During 2013, the GIASONE model has been integrated with a new implementation concerning the aspects of the mental process that, starting from an external clue, triggers the re-emergence of sedimentary memories that give rise to imaginative configurations. Such configurations concern the entire body in his neurological-physical reality as well as in its endocrine-chemistry. The studies and researches underlying this implementation have led to the development of the concept “De ubiqutate mentis”, which considers the whole body as the protagonist of any mental process.

The summary of the results is described in the paper “De ubiqutate mentis: Giasone modello cibernetico di processi mentali” published by one of the academic journal of the Italian Physical Society (Nuovo Saggiatore, Vol. 29, anno 2013). Contacts with experts of the “Policlinico di Roma Umberto I” and the “Ospedale Pediatrico Bambino Gesù” were also initiated for the use of fMRI (Functional Magnetic Resonance Imaging), in order to detect peripheral neurological activity stimulated by mental processes.

In 2013, as part of the Project FLEX-PROD, in collaboration with the “CALEF Consortium”, hardware and software platforms have been developed, which are needed to realize emulative levels of environmental reality, and to manage the movements of a manipulator, capable of moving autonomously in the environment until the target is reached.

The realized emulator has been tested in the following applications:

- laboratory tests for checking the correct environmental reconstruction including the objects to select for the taking by the manipulator (Fig. 5.18);
- field tests through the use of a physical demonstrator, and in specific case is an existing overhead travelling crane, but

suitably reconfigured, whose movements in the environment are managed by the emulation system realized (Figs. 5.19 - 2a, 2b, 2c, 2d).

There are three video recordings concerning the progress of the project activities FLEX-PROD, until final functioning of the physical demonstrator.



Fig. 5.18 - Project FLEX PROD laboratory tests

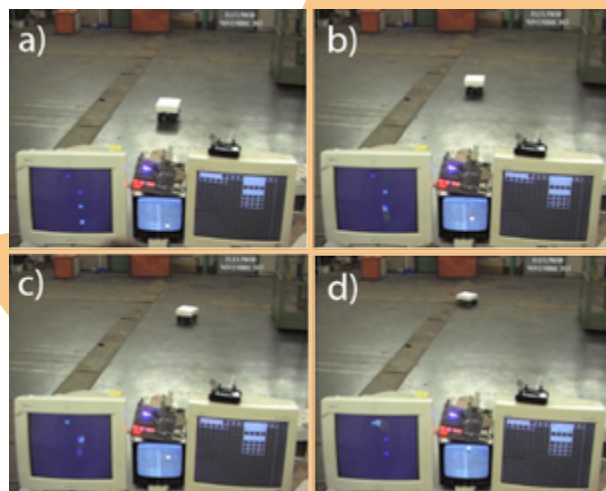


Fig. 5.19 - Project FLEX PROD field test. Sequence of positioning (a, b) and recognition (c, d) of a target object

5.7 Contributions to other projects

FORLAB Project – LIF sensor design

Within the European project FORLAB, ENEA has to develop a sensor based on laser-induced fluorescence (LIF) for in-situ fast screening of post-blast evidences, in order to collect the information provided by the evidences left by the explosion. The sensor must be fast and reliable in selecting/identifying signals ascribable to improvised explosive devices (IEDs) components, which must also be precisely localized. The main sensor components are: a laser source, a laser beam delivery optics, a fluorescence collecting optics, a spectral discriminating system, a UV-VIS sensitive CCD camera, a mechanical system for scene scanning, a computer-based system for process control, data acquisition, data analysis and coordination with other sensors.

In 2013 the Radiation Sources Laboratory has contributed to the design of the LIF sensor components related to the scene illumination, that is the choice of the laser source, the design of the laser beam delivery optics, the selection of the collecting optics features and the scanning parameters. The chosen laser source is a commercial very compact KrF excimer laser (system dimensions: 57×25×25 cm³, weight: 15 kg) emitting 248-nm-wavelength pulses with 16 mJ energy at a maximum repetition rate of 500 Hz. The 248-nm ultraviolet radiation can efficiently excite most substances of interest and the high repetition rate allows a fast scanning of the surveyed area. Moreover, the rectangular beam shape (output beam dimensions: 6×3 mm²) well fits with a flat surface covering. Therefore, this laser system satisfies all the requirements expected by the project: portability, efficient excitation, fast scanning capability. Also, the laser coupling with both the beam delivery optics and the signal collecting CCD camera has been analysed: an optical arrangement has been proposed where a wide-angle-lens CCD camera observes and records the overall scene, while the laser beam, properly enlarged by a

telescope and directed by a two-axes rotating mirror, performs a scan on the same field of view, allowing the illumination of the full area in few minutes. The selected laser beam shape permits an efficient excitation of the scene at least up to 20 m distance from the LIF sensor, giving rise to fully detectable potential fluorescence signals. Since the whole system stands at given height and distance from the area of interest, the analysis took into account the image deformation on the CCD camera due to perspective and the distortion of the beam dimensions when projected on the ground at different distances from the source.

6. LIST OF PERSONNEL

Technical Unit for the Development of Applications of Radiations (UTAPRAD)

Director Roberta Fantoni (roberta.fantoni@enea.it)

Direction staff members

Fabio Avello, Emilia Batisti, Elisabetta Borsella, Paola Chiappini, , Giorgio Fornetti, Anna Pagliardini, Luigi Picardi, Giulio Tuccinardi.

Laboratory for Ultrafast Laser Spectroscopy

Mauro Falconieri, Fabio Fabbri

UTAPRAD-DIM (Diagnostics and Metrology Laboratory)

Director Antonio Palucci (antonio.palucci@enea.it)

DIM staff members

Lorella Addari, Salvatore Almaviva, Federico Angelini, Paolo Aristipini, Florinda Artuso, Rodolfo Borelli, Luisa Caneve, Andrea Capriccioli, Roberto Carletti, Dario Cataldi, Roberto Chirico, Massimiliano Ciaffi, Francesco Colao, Luigi De Dominicis, Antonella De Ninno, Giovanni Dipoppa, Mario Ferri De Collibus, Luca Fiorani, Massimo Francucci, Gianfranco Giubileo, Massimiliano Guarneri, Antonia Lai, Violeta Lazic, Giovanni Leggeri, Giacomo Lorenzoni, Salvatore Marullo, Ivano Menicucci, Marcello Nuvoli, Marco Pistilli, Valeria Spizzichino, Laura Teodori.

DIM research fellows

Adriana Puiu

UTAPRAD-MAT (Mathematical Modelling Laboratory)

Director Giuseppe Dattoli (giuseppe.dattoli@enea.it)

MAT staff members

Franco Ciocci, Emanuele Di Palma, Luca Giannessi, Alberto Petralia, Elio Sabia, Ivan Panov Spassovsky, Amalia Torre.

UTAPRAD-MNF (Photonics Micro and Nano-structures Laboratory)

Director Rosa Maria Montereali (rosa.montereali@enea.it)

MNF staff members

Francesca Bonfigli, Sabina Botti, Luciano Cantarini, Michele Arturo Caponero, Rosaria D'Amato, Stefano Libera, Valerio Orsetti, Massimo Piccinini, Andrea Polimadei, Flaminia Rondino, Antonino Santoni, Gaetano Terranova, Maria Aurora Vincenti.

UTAPRAD-SOR (Radiation Sources Laboratory)

Director Gian Piero Gallerano (gianpiero.gallerano@enea.it)

SOR staff members

Alessandro Ampollini, Rosanna Balvetti, Maria Laura Bargellini, Marco Battaglia, Sarah Bollanti, Ezio Campana, Mariano Carpanese, Gemma Casadei, Domenico De Meis, Paolo Di Lazzaro, Andrea Doria, Antonio Fastelli, Alessandra Filippini, Francesco Flora, Emilio Giovenale, Francesca Maria Marracino, Luca Mezi, Daniele Murra, Paolo Nenzi, Emanuela Pancotti, Loredana Puccia, Concetta Ronsivalle, Vincenzo Surrenti, Monia Vadrucci, Davide Vicca, Giuseppe Vitiello, Consuelo Zampetti.

UTAPRAD-STG (Administration and Management Service)

Director Tiziana Giuli (tiziana.giuli@enea.it)

STG staff members

Maria Luisa Mori, Tiziana Pigiani, Rossella Ester Repetto, Tiziana Vari

*) List of personnel - last updated in december 2013

7. RESEARCH PRODUCTS

7.1 Patents

1. Italian patent n. RM2013A000296, Fiorani L., Menicucci I., Pistilli P., Puiu A. Dispositivo subacqueo per il rilevamento di sostanze naturali e/o antropiche in acqua (in Italian) (2013)
2. Depositated 15/4/2013 at Spanish Patent Office, number P201300359 - J. J. Laserna, F. J. Fortes, S. Giurado, V. Lazic, Sistema portátil de espectroscopia de plasmas inducidos por láser para análisis de sólidos sumergidos en líquidos;
3. Italian Patent - No. RM2013A000462 - Mario Ferri De Collibus, Giorgio Fornetti, “Dispositivo ottico per eliminare la luce non voluta in un sistema ottico e sistema ottico utilizzando tale dispositivo”
4. Italian patent - No. RM2013A000461 - Mario Ferri De Collibus, Giorgio Fornetti, “Metodo e sistema di autofocus per sistema ottico di scansione”
5. Italian patent “Dispositivo Semplice ad Elevata Efficienza per la Rivelazione di Radiazione Ionizzante Basato su Film Sottile di Fluoruro di Litio Luminescente, e Relativi Metodi di Preparazione e Lettura del Dispositivo”, inventori: Rosa Maria Montereali, Francesca Bonfigli, Enrico Nichelatti e Maria Aurora Vincenti.. Numero Deposito nazionale No. RM2013A000123 (01-03-2013)
6. International extension of Italian patent del brevetto ENEA 769 F. Flora, S. Bollanti, D. De Meis, P. Di Lazzaro, A. Fastelli, G.P. Gallerano, L. Mezi, D. Murra, A. Torre, D. Vicca: “High Precision Electronic Solar Compass”, PCT 29379

7.2 Peer review papers with impact factor (I.F.)

1. Crippa M., Canonaco F., Slowik J.G., El Haddad I., DeCarlo P.F., Mohr C., Heringa M.F., Chirico R., Marchand N., Temime-Roussel B., Abidi E., Poulain L., Wiedensohler A., Baltensperger U., Prevot A.S.H. - “Primary and secondary organic aerosol origin by combined gas-particle phase source apportionment”, *Atmos. Chem. Phys.*, 13, 8411–8426, 2013. Impact Factor:5.51
2. Crippa M., El Haddad I., Slowik J.G., De Carlo P.F., Mohr C., Heringa M.F., Chirico R., Marchand N., Sciare J., Baltensperger U., Prévôt A.S.H. - “Identification of marine and continental aerosol sources in Paris using high resolution aerosol mass spectrometry”, *J. Geophys. Res. Atmos.*, 118, 1950-1963, 2013. Impact Factor:3.174
3. Chou C., Stetzer O., Tritscher T., Chirico R., Heringa M., Weingartner E., Prevot A., Baltensperger U., Lohmann U.: “Effect of photochemical aging on the ice nucleation efficiency of diesel and biomass burning particles”, *Atmos. Chem. Phys.*, 13, 761–772, 2013. Impact Factor:5.51
4. Crippa M., De Carlo P.F., Slowik J.G., Mohr C., Heringa M.F., Chirico R., Poulain L., Wiedensohler A., Freutel F., Drewnick F., Schneider J., Di Marco C.F., Nemitz E., Zimmermann R., Elsasser M., Cozic J., Jaffrezo J.-L., Sciare J., Prévôt A.S.H., Baltensperger U.: “Wintertime aerosol chemical composition and source apportionment of the organic fraction in the metropolitan area of Paris”, *Atmos. Chem. Phys.*, 13, 961–981, 2013. Impact Factor:5.51
5. Martin M., Tritscher T., Juranyi Z., Heringa M.F., Sierau B., Weingartner E., Chirico R., Gysel M., Prevot A.S.H., Baltensperger U., Lohmann U.: “Hygroscopic properties of fresh and aged wood burning particles”, *Journal of Aerosol Science*, 56, 15-29, 2013. Impact Factor:2.686
6. Malanotte-Rizzoli P., Artale, Borzelli-Eusebi G. L., Brenner S., Civitarese G., Crise A., Font J., Gacic M., Kress N., Marullo S., Ozsoy E., Ribera d’Alcalà M., Roether W., Schroeder K., Sofianos S., Tanhua T., Theocharis A., Alvarez M., Ashkenazy Y., Bergamasco A., Cardin V., Carniel S., D’Ortenzio F., Garcia-Ladona E., Garcia-Lafuente J. M., Gogou A., Gregoire M., Hainbucher D., Kontoyannis H.,

- Kovacevic V., Krasakapoulou E., Krokos G., Incarbona A., Mazzocchi M. G., Orlic M., Pascual A., Poulain P.-M., Rubino A., Siokou-Frangou J., Souvermezoglou E., Sprovieri M., Taupier-Letage I., Tintoré J., and Triantafyllou G.: “Physical forcing and physical/biochemical variability of the Mediterranean Sea: a review of unresolved issues and directions for future research”, *Ocean Sci. Discuss.*, 10, 1205-1280, doi:10.5194/osd-10-1205-2013, 2013. Impact Factor: 2.164
7. Matteo Rinaldi, S. Fuzzi, S. Decesari, S. Marullo, R. Santolero, A. Provenzale, J. von Hardenberg, D. Ceburnis, A. Vaishya, C. D. O’Dowd and M. C. Facchini: Is chlorophyll-a the best surrogate for organic matter enrichment in submicron primary marine aerosol?, *JOURNAL OF GEOPHYSICAL RESEARCH: ATMOSPHERES*, VOL. 118, 1–10, doi:10.1002/jgrd.50417, 2013 Impact Factor: 3.174
8. Iacono R., E. Napolitano, S. Marullo, V. Artale, A. Vetrano, “2013: Seasonal Variability of the Tyrrhenian Sea Surface Geostrophic Circulation as Assessed by Altimeter Data”. *J. Phys. Oceanogr.*, 43, 1710–1732. doi: <http://dx.doi.org/10.1175/JPO-D-12-0112.1> Impact Factor: 3.179
9. Fortems-Cheiney A., F. Chevallier, M. Saunois, I. Pison, P. Bousquet, C. Cressot, H. J. Wang, Y. Yokouchi, F. Artuso; “ HCFC-22 emissions at global and regional scales between 1995 and 2010: Trends and variability, *Journal of Geophysical Research: Atmospheres*”, vol. 118, issue 13, p.7379-7388, 16 July 2013. Impact factor: 3.174.
10. Hall B. D., A. Engel, J. Mühle, J. W. Elkins, F. Artuso, E. Atlas, M. Aydin, D. Blake, E-G. Brunke, S. Chiavarini, P. J. Fraser, J. Happell, P. B. Krummel, I. Levin, M. Loewenstein, M. Maione, S. A. Montzka, S. O’Doherty, S. Reimann, G. Rhoderick, E. S. Saltzman, H. E. Scheel, L. P. Steele, M. K. Vollmer, R. F. Weiss, D. Worthy, Y. Yokouchi; “Results from the International Halocarbons in Air Comparison Experiment (IHALACE)”, *Atmospheric Measurement Techniques*, accepted on the 18th of December 2013. Impact factor: 3.205.
11. Fiorani L., Saleh W. R., Burton M., Puiu A., Queißer M. “Spectroscopic considerations on DIAL measurement of carbon dioxide in volcanic emissions”. *Journal of Optoelectronics and Advanced Materials* 15, 317-325 (2013) Impact Factor: 0.516
12. Fiorani L. “Laser remote sensing of particulate, vapor and gas in volcanic plumes”. *Bollettino di Geofisica* 54, Supplement 2, 152-154 (2013) Impact Factor: 0.646
13. A. Kiros, V. Lazic, G. E. Gigante, A.V. Gholap, Analysis of rock samples collected from rock hewn churches of Lalibela, Ethiopia using laser-induced breakdown spectroscopy, *J. Archaeological Sci.* 40 (2013) 2570-2578, Impact Factor: 1.89
14. Fantoni R., Caneve L., Colao F., Fiorani L., Palucci A., Dell’Erba R., Fassina V. “Laser induced fluorescence study of medieval frescoes by Giusto De’ Menabuoi” - *Journal of Cultural Heritage* 14, S59-S65(2013) Impact Factor: 2.519
15. Caneve L., Colao F., Fantoni R., Fiorani L. “Scanning lidar fluorosensor for remote diagnostic of surfaces” *Nuclear Instruments and Methods in Physics Research A* 720, 164-167 (2013) Impact Factor 1.142
16. Malaquias, V. Philipps, A. Huber, A. Hakola, J. Likonen, J. Kolehmainen, S. Tervakangas, M. Aints, P. Paris, M. Laan, A. Lissovski, S. Almaviva, L. Caneve, F. Colao, G. Maddaluno, M. Kubkowska, P. Gasior, H.J. van der Meiden, A.R. Lof, P.A. Zeijlmans van Emmichoven, P. Petersson, M. Rubel, E. Fortuna, Q. Xiao, “Development of ITER relevant laser techniques for deposited layer characterisation and tritium inventory” *Journal of Nuclear Materials* 438 (2013) S936–S939 Impact factor 1.211
17. Roberta Fantoni, Salvatore Almaviva, Luisa Caneve, Francesco Colao, Andrey M. Popov, Giorgio Maddaluno “Development of Calibration-Free Laser-Induced-Breakdown-Spectroscopy based techniques for deposited layers diagnostics” on ITER-like tiles *Spectrochimica Acta Part B* 87 (2013) 153–160 - Impact factor 3.141
18. V. Philipps, A. Malaquias, A. Hakola, J. Karhunen, G. Maddaluno, S. Almaviva, L. Caneve, F. Colao, E. Fortuna, P. Gasior, M. Kubkowska, A. Czarnecka, M. Laan, A. Lissovski, P. Paris, H.J.

- van der Meiden, P. Petersson, M. Rubel, A. Huber, M. Zlobinski, B. Schweer, N. Gierse, Q. Xiao, G. Sergienko. "Development of laser-based techniques for in situ characterization of the first wall in ITER and future fusion devices". *Nucl. Fusion* 53 (2013) 093002 Impact factor 2.734
19. V. Lazic, J. J. Laserna, S. Jovicevic, "Insights in the laser-induced breakdown spectroscopy signal generation underwater using dual pulse excitation — Part I: Vapor bubble, shockwaves and plasma", *Spectrochim. Acta Part B* 82 (2013) 42–49, Impact Factor 3.14
 20. V. Lazic, J. J. Laserna, S. Jovicevic, "Insights in the laser induced breakdown spectroscopy signal generation underwater using dual pulse excitation — Part II: Plasma emission intensity as a function of interpulse delay", *Spectrochim. Acta Part B* 82 (2013) 50–59, Impact Factor 3.14
 21. A. De Ninno and A. Congiu Castellano - "Influence of magnetic fields on the hydration process of amino acids: Vibrational spectroscopy study of L-phenylalanine and L-glutamine Bioelectromagnetics", article first published online: 6 NOV 2013 | DOI: 10.1002/bem.21823 Impact Factor 2
 22. L. Teodori, A. Giovanetti, M. C. Albertini, M. Rocchi, B. Perniconi, M. G. Valente and D. Coletti - "Static magnetic field modulates X-ray-induced DNA damage in human glioblastoma primary cells". *Journal of Radiation Research*, 2013, Impact Factor 3,9.
 23. F. Ciocci et al. "Two Color Free-Electron Laser and Frequency Beating" - *Physical Review Letters* 12/2013; 111(26):264801 (Impact Factor 7.94)
 24. Petralia et al. "Chirped seeded free-electron lasers: self-standing light sources for two-color pump-probe experiments." - *Physical Review Letters* 02/2013; 110(6):064801 Impact Factor 7.94
 25. L. Giannessi et al. "Superradiant Cascade in a seeded Free Electron Laser" - *Phys. Rev. Lett.* 02/2013;110(6):064801 Impact Factor 7.94
 26. L. Giannessi et al. "Two-colour generation in a chirped seeded free-electron laser: a close look" - *Optics Express* 09/2013; 21(19):022728. · Impact Factor 3.55
 27. L. Giannessi, "Two-colour pump-probe experiments with a twin-pulse-seed extreme ultraviolet free-electron laser." - *Nature Communications* 09/2013; 4:2476. · 10.02 Impact Factor
 28. L. Giannessi, "Two-stage seeded soft-X-ray free-electron laser" - *Nature Photonics* 10/2013; 7(11):913-918. · Impact Factor 27.25
 29. E. Sabia et al. "Bunching Coefficients in echo enabled harmonic generation" - *Phys. Rev. ST Accel. Beams* 16, 070702 (2013) - Impact factor 1.536
 30. G. Dattoli et al. "Longitudinal dynamics of high gain free electron laser amplifiers" - *Physical Review Special Topics – Accel. Beams*, 16, 030704 Impact Factor 1.536
 31. Torre et al. "Double free-electron laser oscillator for photon–photon collisions" - *JOSA B*, Vol. 30, Issue 11, pp. 2906-2914 (2013) - Impact Factor 2.210
 32. G. Dattoli et al. "The higher order heat equations via signed Levy stable and Airy Generalized Distributions" - *J. Phys. A* 46, 425001 (2013) - Impact Factor 1.766
 33. E. Di Palma et al. "Electron Beam Longitudinal Dynamics for SASE FEL Operation" - *IEEE-JQE*, 49, 267 (2013) - Impact Factor 1.83.
 34. E. Di Palma et al., "Quasi Exact Solution of the Fisher Equation", - *Applied Mathematics* Vol. 4 n. 8A through *Scientific Research (Open Access Journal)* - <http://www.scirp.org/journal/am/> - Impact Factor 0.19
 35. G. Dattoli et al. "Symbolic methods for the evaluation of sum rules of Bessel functions" - *Journal of Mathematical Physics*, Volume 54, Issue 7, pp. 073501-073501-6 (2013) - Impact Factor 1.3
 36. G. Dattoli et al. "Relativistic harmonic oscillator, the associated equations of motion, and algebraic integration methods" - *Phys. Rev. E* 87, 033202 – Published 21 March 2013 - Impact Factor 2.307
 37. G. Dattoli et al. "The Second Solution of the Hermite Equation and the Monomiality Formalism" - *Pure Mathematical Sciences*, Vol. 2, 2013, no. 4, 147 - 152 - HIKARI Ltd, www.m-hikari.com - Impact Factor 0.335
 38. R.M. Montereali, F. Bonfigli, E. Nichelatti, M.A. Vincenti, "Versatile lithium fluoride thin-film solid-state detectors for nano scale radiation imaging", *Nuovo Cimento C* 36 (2) (2013) 35-42 - Impact Factor 0.32
 39. F. d'Acapito, P. Pochet, F. Somma, P. Aloe, R.M. Montereali, M.A. Vincenti, S. Polosan, "Lead incorporation mechanism in LiF crystals". *Appl. Phys. Lett.* 102 (2013) 08107, doi: 10.1063/1.4793751 - Impact Factor: 3.794
 40. S. Heidari Bateni, F. Bonfigli, A. Cecilia, T. Baumbach, D. Pelliccia, F. Somma, M.A. Vincenti, R.M. Montereali, "Optical characterization of lithium fluoride detectors for broadband X-ray imaging", *Nuclear Instruments & Methods In Physics Research A* 720 (2013) 109-112 - Impact Factor: 1.142
 41. D. Hampai, F. Bonfigli, S.B. Dabagov, R.M. Montereali, G. Della Ventura, F. Bellatreccia, M. Magi, "LiF detectors-polycapillary lens for advanced X-ray Imaging", *Nuclear Instruments & Methods In Physics Research A* 720 (2013) 113-115 - Impact Factor: 1.142
 42. F. Bonfigli, A. Cecilia, S. Heidari Bateni, E. Nichelatti, D. Pelliccia, F. Somma, P. Vagovic, M.A. Vincenti, T. Baumbach and R.M. Montereali, "In-line X-ray lensless imaging with lithium fluoride film detectors", *Radiation Measurements* 56 (2013) 277-280 - Impact Factor: 0.861
 43. M. Piccinini, F. Ambrosini, A. Ampollini, M. Carpanese, L. Picardi, C. Ronsivalle, F. Bonfigli, M. A. Vincenti, S. Libera and R.M. Montereali, "Optical spectroscopy and imaging of colour centres in lithium fluoride crystals and thin films irradiated by 3 MeV proton beams", *Nuclear Instruments and Methods B*, in press. DOI: 10.1016/j.nimb.2013.09.036 - Impact Factor: 1.266
 44. R. Francini, R.M. Montereali, E. Nichelatti, M.A. Vincenti, N. Canci, E. Segreto, F. Cavanna, F. Di Pompeo, F. Carbonara, G. Fiorillo, F. Perfetto, "Optical characterization at liquid Argon temperature of Tetraphenyl-butadiene films on glass and specular reflector substrates in the VUV-VIS range of wavelengths" - *Journal of Instrumentation*, *JINST* 8 (2013) P09006,1-22, doi:10.1088/1748-0221/8/09/P09006 - Impact Factor: 1.656
 45. A.P. Voitovich, V.S. Kalinov, L.P. Runets, A.P. Stupak, E.F. Martynovich, R.M. Montereali, G. Baldacchini, "Color centers aggregation kinetics in lithium fluoride after gamma irradiation", *J. Lumin.* 143 (2013) 207-214 - Impact Factor: 2.144
 46. A. Santoni, F. Biccari, C. Malerba, M. Valentini, R. Chierchia, A. Mittiga, "Valence band offset at the CdS/Cu₂ZnSnS₄ interface probed by x-ray photoelectron spectroscopy", *J. Phys. D: Appl. Phys.* 46 (2013) 175101 - Impact Factor: 2.528
 47. F. Rondino, D. Catone, G. Mattioli, A. Amore Bonapasta, P. Bolognesi, A.R. Casavola, M. Coreno, P. O'Keefe, L. Avaldi, "Competition between electron-donor and electron-acceptor substituents in nitrotoluene isomers: a photoelectron spectroscopy and ab initio investigation", *RSC Advanced*, DOI:10.1039/C3RA45705B - Impact Factor: 2.66
 48. A. Filippi, C. Fraschetti, F. Rondino, S. Piccirillo, V. Steinmetz, L. Guisoni, M. Speranza, "Protonated pyrimidine nucleosides probed by IRMPD spectroscopy", *Int. Journal of Mass Spectrometry*, Vol. 354-355, 2013, 54-61 - Impact Factor: 2.142
 49. S. Piccirillo, A. Ciavardini, E. Bodo, F. Rondino, D. Scuderi, V. Steinmetz, A. Paladini, "Probing the competition among different coordination motifs in metal-ciprofloxacin complexes through IRMPD spectroscopy and DFT calculations", *Inorganic Chemistry*, Vol. 52, Issue 1, 2013, 103-112 Impact Factor: 4.593
 50. A. Ciavardini, F. Rondino, A. Paladini, M. Speranza, S. Fornarini, M. Satta, S. Piccirillo, "The effect of fluorine substitution on chiral recognition: Interplay of CH... π , OH... π and CH...F interactions in gas-phase complexes of 1-aryl-1-ethanol with butan-2-ol", - *Physical Chemistry Chemical Physics*, Vol. 15, Issue 44, 2013, 19360-19370 - Impact Factor: 3.829
 51. S. Turchini, D. Catone, N. Zema, G. Contini, T. Prosperi, P. Decleva, M. Stener, F. Rondino, S. Piccirillo, K.C. Prince, M. Speranza, "Conformational Sensitivity in Photoelectron Circular

- Dichroism of 3-Methylcyclopentanone”, *ChemPhysChem*, Vol.14, 2013, 1723–1732 - Impact Factor: 4.22
52. E. Borsella, R. D’Amato, M. Falconieri, E. Trave, A. Panariti, I. Rivolta, “An outlook on the potential of Si nanocrystals as luminescent probes for bio-imaging”, *Journal of Materials Research* 28 (2013) 193-204, DOI: 10.1557/jmr.2012.295 - Impact Factor: 1.87
 53. G.P. Celata, F. D’Annibale, A. Mariani, L. Saraceno, R. D’Amato, R. Bubbico, “Heat Transfer in Water-based SiC and TiO₂ Nanofluids”, *Heat Transfer Engineering* 34 (2013) 1060-1072 - Impact Factor: 0,694
 54. R. D’Amato, M. Falconieri, F. Fabbri, E. Borsella, “Perspectives of application for nanoparticles prepared by CO₂ laser pyrolysis: from ceramic nanocomposites to nanofluids”, *Il Nuovo Cimento C, Colloquia and communications in physics* 36 C (2013) 11-22 - Impact Factor: 0.32
 55. M. Falconieri, E. Trave, R. D’Amato, and E. Borsella, “Study of defect-related light emission in oxidized Silicon nanocrystals”, *Physica Status Solidi B-Basic Solid State Physics* 250 (2013) 831-836. DOI: 10.1002/pssb.201200893 - Impact Factor: 1.489
 56. R. D’Amato, M. Falconieri, S. Gagliardi, E. Popovici, E. Serra, G. Terranova, E. Borsella, “Synthesis of ceramic nanoparticles by laser pyrolysis: from research to applications”, *Journal of Analytical and Applied Pyrolysis* 104 (2013) 461-469, DOI: 10.1016/j.jaap.2013.05.026 - Impact Factor: 2.6
 57. S. Almaviva, S. Botti, L. Cantarini, R. Fantoni, S. Lecci, A. Palucci, A. Puiu, A. Rufoloni, “Ultrasensitive RDX detection with commercial SERS substrates” - *J. Raman Spectrosc.* 2013, (wileyonlinelibrary.com) DOI 10.1002/jrs.4413 - Impact Factor: 2.679
 58. P. Saccomandi, E. Schena, F. Giurazza, R. Del Vescovo, M.A. Caponero, et al - “Temperature monitoring and lesion volume estimation during double-applicator laser-induced thermotherapy in ex vivo swine pancreas: a preliminary study”, *Lasers Med. Sci.* (2013) Jun 19, DOI: 10.1007/s10103-013-1360-z - Impact Factor: 2.402
 59. E. Schena, P. Saccomandi, F. Giurazza, M. A. Caponero, L. Morto, F. M. Di Matteo, F. Panzera, R. del Vescovo, B. Beomonte Zobel, S. Silvestri “Experimental assessment of CT-based thermometry during laser ablation of porcine pancreas” *Physics in Medicine and Biology*, 58 (16), (2013) pp. 5705-5716. DOI: 10.1088/0031-9155/58/16/5705 - Impact Factor: 2.701
 60. M.A. Caponero, A. Polimadei, L. Benussi, S. Bianco, S. Colafranceschi, L. Passamonti, D. Piccolo, D. Pierluigi, A. Russo, F. Felli, G. Saviano, C. Vendittozzi “Monitoring relative humidity in RPC detectors by use of fiber optic sensors” (2013) *Journal of Instrumentation*, 8 (3), art. no. T03003, DOI: 10.1088/1748/-0221/8/03/T03003 - Impact Factor: 1.656
 61. S. Botti, S. Almaviva, L. Cantarini, A. Palucci, A. Puiu, A. Rufoloni, “Trace level detection and identification of nitro-based explosives by surface-enhanced Raman spectroscopy” - *J. Raman Spectrosc.* 2013, 44, 463–468 (nella lista dei most accessed 10/2012- 09/2013) - Impact Factor: 2.679
 62. V. Petrillo, M. P. Anania, M. Artioli, A. Bacci, M. Bellaveglia, E. Chiadroni, A. Cianchi, F. Ciocci, G. Dattoli, E. Giovenale, G. Di Pirro, M. Ferrario, G. Gatti, L. Giannessi, A. Mostacci, P. Musumeci, A. Petralia, R. Pompili, M. Quattromini, J.V. Rau, C. Ronsivalle, A. R. Rossi, E. Sabia, C. Vaccarezza and F. Villa, “Observation of Time-Domain Modulation of Free-Electron-Laser Pulses by Multi-peaked Electron-Energy Spectrum”, *Phys. Rev. Lett.*, PRL 111, 114802 (2013) - Impact Factor: 7.943
 63. E. Chiadroni, M. Bellaveglia, P. Calvani, M. Castellano, L. Catani, A. Cianchi, G. Di Pirro, M. Ferrario, G. Gatti, O. Limaj, S. Lupi, B. Marchetti, A. Mostacci, E. Pace, L. Palumbo, C. Ronsivalle, R. Pompili, and C. Vaccarezza “Characterization of the THz radiation source at the Frascati linear accelerator”, *Rev. Sci. Instrum.* 84, 022703 (2013) - Impact Factor: 1.602
 64. E. Chiadroni, A. Bacci, M. Bellaveglia, M. Boscolo, M. Castellano, L. Cultrera, G. Di Pirro, M. Ferrario, L. Ficcadenti, D. Filippetto, G. Gatti, E. Pace, A. R. Rossi, C. Vaccarezza, L. Catani, A. Cianchi, B. Marchetti, A. Mostacci, L. Palumbo, C. Ronsivalle, A. Di Gaspare, M. Ortolani, A. Perucchi, P. Calvani, O. Limaj, D. Nicoletti, and S. Lupi, “The SPARC linear accelerator based terahertz source”, *Appl. Phys. Lett.* 102, 094101 (2013) - Impact Factor: 3.794
 65. A. Bacci, D. Alesini, P. Antici, M. Bellaveglia, R. Boni, E. Chiadroni, A. Cianchi, C. Curatolo, G. Di Pirro, A. Esposito, M. Ferrario, A. Gallo, G. Gatti, A. Ghigo, M. Migliorati, A. Mostacci, L. Palumbo, V. Petrillo, R. Pompili, C. Ronsivalle, A. R. Rossi, L. Serafini, B. Spataro, P. Tomassini, and C. Vaccarezza, “Electron Linac design to drive bright Compton back-scattering gamma-ray sources”, *Journal of Applied Physics / Volume 113 / Issue 19*, 194508 (2013) - Impact Factor: 2.210
 66. V. Petrillo, I. Chaikovska, C. Ronsivalle, A. R. Rossi, L. Serafini and C. Vaccarezza, “Phase space distribution of an electron beam emerging from Compton/Thomson back-scattering by an intense laser pulse”, *EPL*, 101 (2013) 10008 - Impact Factor: 2.260
 67. A. Cianchi M., P. Anania, M. Bellaveglia, M. Castellano, E. Chiadroni, M. Ferrario, G. Gatti, B. Marchetti, A. Mostacci, R. Pompili, C. Ronsivalle, A. R. Rossi, L. Serafini. “Challenges in plasma and laser wakefield accelerated beams diagnostic”, *Nuclear Instruments and Methods in Physics Research A* 671, 56–61 (2013) - Impact Factor: 1.142
 68. M. Ferrario, D. Alesini, M. Anania, A. Bacci, M. Bellaveglia, O. Bogdanov, R. Boni, M. Castellano, E. Chiadroni, A. Cianchi, S.B. Dabagov, C. De Martinis, D. Di Giovenale, G. Di Pirro, U. Dosselli, A. Drago, A. Esposito, R. Faccini, A. Gallo, M. Gambaccini, C. Gatti, G. Gatti, A. Ghigo, D. Giulietti, A. Ligidov, P. Londrillo, S. Lupi, A. Mostacci, E. Pace, L. Palumbo, V. Petrillo, R. Pompili, A.R. Rossi, L. Serafini, B. Spataro, P. Tomassini, G. Turchetti, C. Vaccarezza, F. Villa, G. Dattolib, E. Di Palma, L. Giannessi, A. Petralia, C. Ronsivalle, I. Spassovsky, V. Surrenti, L. Gizzi, L. Labate, T. Levato, J.V. Rau. “SPARC_LAB present and future”, *Nuclear Instruments and Methods in Physics Research B* 309, 183–188 (2013) - Impact Factor 1.266
 69. K.-T. Kim, J. Park, S.-J. Jo, S. Jung, O.-S. Kwon, G.P. Gallerano, W.-Y. Park, G.-S. Park, “High-power femtosecond-terahertz pulse induces a wound response in mouse skin”, *Scientific Reports* 3-2296 (2013) - Impact Factor: 2.927
 70. S. Bollanti, P. Di Lazzaro, F. Flora, L. Mezi, D. Murra, A. Torre: “New technique for aberration diagnostics and alignment of an extreme ultraviolet Schwarzschild objective”, *Nuclear Instruments and Methods in Physics Research A* 720, 168–172 (2013) - Impact Factor: 1.142
 71. M.P. Anania, E. Chiadroni, A. Cianchi, D. Di Giovenale, M. Ferrario, F. Flora, G.P. Gallerano, A. Ghigo, A. Marocchino, F. Massimo, A. Mostacci, L. Mezi, P. Musumeci, M. Serio: “Design of a plasma discharge circuit for particle wakefield acceleration” *Nuclear Instruments and Methods in Physics Research A* (2013) DOI: <http://dx.doi.org/10.1016/j.nima.2013.10.053> - Impact Factor: 1.142

7.3 Conference presentations and proceedings, other scientific papers

1. Iacono R., E. Napolitano, S. Marullo, V. Artale, A. Vetrano, 2013: Seasonal Variability of the Tyrrhenian Sea Surface Geostrophic Circulation as Assessed by Altimeter Data. *J. Phys. Oceanogr.*, 43, 1710–1732. doi: <http://dx.doi.org/10.1175/JPO-D-12-0112.1>
2. A. Garibbo and A. Palucci. “Photonics for Detection of Chemicals, Drugs and Explosives”. *Photonics for Safety and Security* edited by: Antonello Cutolo (University of Sannio, Italy) edited by: Anna Grazia Mignani (CNR – Institute of Applied Physics ‘Nello Carrara’, Italy) edited by: Antonella Tajani (CNR, Italy). 2013 World Scientific Publishing Co. ISBN: 978-981-4412-96-4
3. S. Almaviva, S. Botti, L. Cantarini, A. Palucci, A. Puiu, F. Schnuerer, W. Schweikert, F.S. Romolo. “Raman Spectroscopy for the detection of explosives and their precursors on clothing in fingerprint concentration: a reliable technique for security and counterterrorism issues”. *Proc. of SPIE* Vol. 8901 890102-9

4. S. Almagia, S. Botti, L. Cantarini, A. Palucci, A. Rufoloni, T. Moller, F.S. Romolo. "Trace detection of explosives by Surface Enhanced Raman Spectroscopy" Proc. of the 2nd EUCDE Conference March 13/15, 2013, Rome (Italy)
5. Chirico, R., Almagia, S., Colao, F., Botti, S., Fiorani, L., Nuvoli, M., Cantarini, L., Palucci, A. - "Stand-off detection of traces of explosives and precursors on fabrics by UV-Raman spectroscopy". 2nd European Conference on Detection of Explosives, Rome, Italy
6. L. Caneve, F. Colao, A. Palucci, V. Spizzichino, "Development of an innovative LIF sensor for post-blast detection of plastic debris in the frame of FORLAB project" – EUCDE 2013 - Roma (Italy), 13-15 March 2013
7. V. Spizzichino, A. Lai, F. Angelini, and A. Palucci "Application Of Raman Spectroscopy For Analysis Of Pollen" "Secondo Workshop Gruppo Biosensori Ottici e Biofotonica" Sestri Levante 19-20 Settembre 2013
8. G. Giubileo, A. Puiu, "Recognition of IED Precursors by Infrared Photoacoustic Spectroscopy combined with PCA", 2nd EUCDE,.
9. G. Giubileo, A. Puiu, "Detectability of melamine in milk by LPAS", 22nd International Laser Physics Workshop – LPHYS'13, Praga (Repubblica Ceca), 15-19 Luglio 2013.
10. G. Giubileo, A. Puiu, "FTIR and Raman spectroscopy for diagnostic of olive oil adulteration", 3rd International Conference on Frontiers in Diagnostic Technologies – ICFDT, Frascati (Italia), 25-27 Novembre 2013.
11. G. Giubileo, A. Puiu, "LIAF emission from human thyroid tissue: statistical data treatment", 3rd International Conference on Frontiers in Diagnostic Technologies – ICFDT, Frascati (Italia), 25-27 Novembre 2013.
12. G. Giubileo, A. Puiu, "LPAS based detectability of methanol in alcoholic beverages", 6th International Symposium on Recent Advances in Food Analysis – RAFA2013, Praga (Repubblica Ceca), 5-8 Novembre 2013.
13. Puiu A., G. Giubileo, A. Lai, "Investigation on plant pathogen interaction by LPAS sensor", Conference on Photoacoustic and Photothermal Theory and Applications – CPPTA, Warsaw (Polonia), 25-27 Settembre 2013.
14. Puiu A., G. Giubileo, A. Palucci, "Photoacoustic Spectroscopy of Improvised Explosive Device Precursors", Conference on Photoacoustic and Photothermal Theory and Applications – CPPTA, Warsaw (Polonia), 25-27 Settembre 2013.
15. Fiorani L., Puiu A., Rosa O., Palucci A. - "Lidar/DIAL detection of bomb factories" Proceedings of SPIE 8897, paper 7 – 6 pp. (2013)
16. Lai A., Colao F., Sighicelli M., Piccinelli D., Giubileo O. G., Puiu A. "Sistemi Ottici Per La Valutazione Della Qualità Dei Prodotti Ortofrutticoli" Convegno frutticolo nel Lazio: Stato dell'arte della ricerca sulle colture arboree nel Lazio – Viterbo 23 Aprile 2013 (Invited paper).
17. M. Sammartino, A. Di Cicco, S. Marullo, R. Santoleri, F. Artuso, D. Cataldi, "Detecting dominant Phytoplankton Size Classes (micro-, nano- and pico-phytoplankton) from SeaWiFS data in the Mediterranean Sea: spatial and temporal variability", International Ocean Colour Science Meeting, Darmstadt, Germany, 6-8 May 2013.
18. R. Santoleri, F. Bignami, S. Colella, G. Liberti, G. Volpe, S. Marullo, F. Artuso, D. Cataldi, A. Di Cicco, R. Casotti, F. Margiotta, C. Santinelli, "Ocean Colour Validation activities in the Mediterranean Sea", Sentinel-3 Validation Team 1st Meeting, 26-29 November 2013, European Space Agency, Frascati (Rome), Italy
19. Fiorani L., Borelli R., Marullo S., Montes-Hugo M. "Biogeo-optical characterization of the St. Lawrence Estuary by laser-induced fluorescence and satellite radiometry" - 3rd MERIS/(A)ATSR and OCLI-SLSTR (Sentinel-3) preparatory workshop, ESA, Frascati, Italy (2013)
20. Fiorani L., Puiu A., Rosa O., Palucci A. "Stand-off detection of acetone: spectral study, laboratory test and interferent study" - 2nd EU Conference on Detection of Explosives, EC, Brussels, Belgium (2013)
21. Fiorani L., Arnon S., Agboola J. I., Borelli R., Eretz Kedosh A., Giannini E., Green N., Mann D., Marullo S., Menicucci I., Musheyev A., Nuri I., Oved I., Pilipenko V., Pistilli M., Puiu A., Tzidki T., Uzan H. - "SOMBRERO a submersible spectrofluorometer with underwater optical wireless communication" - 6th Workshop on Remote Sensing of the Coastal Zone, EARSeL, Matera, Italy (2013)
22. Fiorani L., Borelli R., Gagné J.-P., Marullo S., Montes-Hugo M. - "Comparison between laser-induced fluorescence and satellite radiometry in the St. Lawrence Estuary" - 6th Workshop on Remote Sensing of the Coastal Zone, EARSeL, Matera, Italy (2013)
23. Fiorani L., Aiuppa A., Angelini F., Borelli R., Del Franco M., Murra D., Pistilli M., Puiu A., Santoro S. "Lidar sounding of volcanic plumes" - Proceedings of SPIE 8894, paper 7 – 10 pp. (2013)
24. Fiorani L., Borelli R., Marullo S., Montes-Hugo M. - "Biogeo-optical characterization of the St. Lawrence Estuary by laser-induced fluorescence and satellite radiometry" "Ouwehand L. (ed.), Proceedings of the 3rd MERIS/(A)ATSR and OCLI-SLSTR (Sentinel-3) preparatory workshop, ESA, Frascati, Italy (2013) 4 pp. in CD-ROM
25. Iocola I., Sighicelli M., Pittalis D., Lugliè A., Padedda B. M., Pulina S., Menicucci I., Marullo S., Fiorani L., Palucci A. "Spectral analysis for assessing photosynthetic pigments and phytoplankton composition by shipboard compact and advanced laser spectrometer in Asinara Gulf (Sardinia)" 6th Workshop on Remote Sensing of the Coastal Zone, EARSeL, Matera, Italy (2013)
26. Queißer M., Burton M., Fiorani L. "Investigating the effect of aerosol droplets in a volcanic plume for increasing sensitivity of a CO₂ DIAL measurement" Proceedings of SPIE 8894, paper 9 – 9 pp. (2013)
27. Mitev V., Babichenko S., Bennes J., Borelli R., Dolfi-Bouteyre A., Fiorani L., Hespel L., Huet T., Palucci A., Pistilli M., Puiu A., "Rebane O. Mid-IR DIAL for high-resolution mapping of explosive precursors" Proceedings of SPIE 8894, paper S – 13 pp. (2013)
28. Pasini A., Fiorani L. "Les enjeux du réchauffement climatique" (in French) Nouvelle Cité 564 7-9 (2013)
29. Pasini A., Fiorani L. "Il dibattito mediatico sui cambiamenti climatici" (in Italian) Landucci C., Mazzola P. (eds.), Cambiamenti – Percorsi formativi su globalizzazione, intercultura, economia, ambiente, Città Nuova, Roma, Italy (2013) pp. 185-187
30. Puiu A., Borelli R., Di Cicco A., Lai A., Menicucci I., Pistilli P., Fiorani L. "Compact submersible spectrofluorometer for environmental and industrial applications" 3rd International Conference on Frontiers of Diagnostic Technologies, ENEA & INFN, Frascati, Italy (2013)
31. L. De Dominicis. "3D vision, ranging and range gating", in Subsea Optics and Imaging, Chapter Book WoodHead publishing, 2013. Edited by J. Watson and O. Zielinski, ISBN-13: 978 0 85709 341 7.
32. L. De Dominicis, A. Al-Obaidi, D. Mcstay, G. Fornetti, M. Guarneri, M. Ferri de Collibus, M. Francucci, M. Nuvoli "Structural monitoring of offshore platforms by 3D subsea laser profilers" Proceedings of Offshore Mediterranean Conference 2013, OMC 2013 (Ravenna, Italia, 20 – 22 Marzo 2013), in press, www.onepetro.org
33. L. De Dominicis, A. Al Obaidi, G. Fornetti, M. Guarneri, M. Ferri de Collibus, M. Francucci, M. Nuvoli "Progress in the structural monitoring of offshore infrastructure by 3D subsea laser profilers" Technical report series on the Optoelectronics for the Oil and Gas Industry (Aberdeen, UK, 6 June 2013)
34. M. Guarneri, A. Danielis, G. Fornetti, M. Ferri De Collibus, M. Francucci, M. Nuvoli. "Experiences from a Research Centre: how science and art can talk together?" 22ND EBN (European Business & Innovation Centre Network) Congress (Derry, Londonderry, Ireland, 29-31 May 2013) -

35. M. Guarneri, A. Danielis, G. Fornetti, M. Ferri De Collibus, L. De Dominicis, M. Francucci, M. Nuvoli, A. Mencattini. "3D laser-coloured scanning technique for automatic frescos defects detection" - 6th International Congress on Science and Technology for the Safeguard of Cultural Heritage in the Mediterranean Basin, Athens (Greece), 22 - 25 October 2013.
36. M. Guarneri, L. De Dominicis, M. Ferri de Collibus, G. Fornetti, M. Francucci, M. Nuvoli. "How the amplitude modulation of n-laser stimuli could change our way to observe submerged and emerged worlds" - 3DTV-CON 2013 Conference, Aberdeen (UK), 7 - 8 October 2013.
37. M. Francucci, L. De Dominicis, M. Ferri de Collibus, G. Fornetti, M. Guarneri, M. Nuvoli "RGB-ITR: a 3D laser scanner for remote colorimetry and structural monitoring in cultural heritage" Proceeding of the Conference Fotonica 2013, 15° Convegno Nazionale delle Tecnologie Fotoniche (Milan, Italy, 21 - 23 May 2013).
38. R. Fantoni, M. Ferri de Collibus, M. Francucci, G. Fornetti, M. Guarneri, L. Caneve, F. Colao, L. Fiorani, A. Palucci, V. Spizzichino "High resolution laser remote imaging innovative tools for preservation of painted surfaces: information from reflectance and fluorescence data" (Invited paper) Proceedings of International Conference Fundamentals of Laser Assisted Micro - and Nanotechnologies (FLAMN-13), section Laser Cleaning and Artworks Conservation (St. Petersburg, Pushkin, Russia, 24 - 28 June 2013). Proceedings of SPIE 9065, paper Z - 10 pp. (2013)
39. Fantoni R., De Dominicis L., Ferri De Collibus M., Francucci M., Fornetti G., Guarneri M., Caneve L., Colao F., Fiorani L., Palucci A., Spizzichino V. "High resolution laser imaging remotely collected from painted surfaces: information from reflectance and fluorescence data" 6th International Congress on "Science and Technology for the Safeguard of Cultural Heritage on the Mediterranean Basin", AIC & Fondazione Roma-Mediterraneo, Athens, Greece (2013)
40. Fantoni R., Caneve L., Colao F., Dell'Erba R., Fiorani L., Palucci A. "Laser-induced fluorescence (LIF) and reflectance measurements of medieval frescoes by Giusto de' Menabuoi in the Padua Baptistery". Saunders D., Strlič M., Korenberg C., Luxford N., Birkhölzer K. (eds.), Lasers in the Conservation of Artworks IX, Archetype, London, UK (2013) pp. 198-200.
41. V. Lazic, S. Jovicevic, J. J. Laserna, M. Carpanese, "Laser induced bubble inside liquids: transient optical properties and their effects on successive plasma formation and LIBS signal". - International conference EMSLIBS, Bari (I), 16-19/9/2013.
42. V. Lazic, A. Palucci, M. Ciaffi, "Efficient LIBS analysis of organic liquids in small volumes". - International conference EMSLIBS, Bari (I), 16-19/9/2013..
43. V. Lazic, "Activities at ENEA relative to LIBS spectroscopy and plasma inside liquids". Oral presentation at Workshop ENEA-CEITEC, 24/6, Rome (I).
44. F. Pollastrone, M. Ferri de Collibus, M. Florean, M. Francucci, G. Mugnaini, C. Neri, P. Rossi, G. Dubus, C. Damiani, "Erosion evaluation capability of the IVVS for ITER applications", - 11th International Symposium on Fusion Nuclear Technology (ISFNT-11, Barcelona, Spain, 16 - 20 September 2013).
45. Elia V, Ausanio G, De Ninno A, Gentile F, Germano R, Napoli E and Niccoli Experimental Evidence of Stable Aggregates of Water at Room Temperature and Normal Pressure After Iterative Contact with a Nafion® Polymer Membrane WATER 5, 16-26, May 4th 2013
46. E. Del Giudice, C. Hison, R. Germano, A. De Ninno "Hydrogen-induced amorphization of intermetallics and QED coherence" Key Engineering Materials Vol. 543 (2013) pp 338-341 © (2013) Trans Tech Publications, Switzerland, doi:10.4028/www.scientific.net/KEM.543.338
47. A De Ninno, A Congiu Castellano and E Del Giudice. "The supramolecular structure of liquid water and quantum coherent processes in biology" Journal of Physics: Conference Series 442 (2013) 012031
48. D Coletti, L Teodori, Z Lin1, J F Beranudin and Se Adamo . "Restoration versus reconstruction: cellular mechanisms of skin, nerve and muscle regeneration compared" Regenerative Medicine Research 2013, 1:4
49. R. Germano, E. Del Giudice, A. De Ninno, V. Elia, C. Hison, E. Napoli, V. Tontodonato, F.P. Tuccinardi and G. Vitiello. "2Oxhydroelectric Effect in Bi-Distilled Water", Key Engineering Materials Vol. 543 (2013) pp 455-459 © (2013) Trans Tech Publications, Switzerland doi:10.4028/www.scientific.net/KEM.543.455
50. De Ninno A.. Invited paper in "Water Conference - Conference on the Physics, Chemistry and Biology of Water". 22-25 October, 2013 Borovets, Bulgaria.
51. R. Fantoni "perspective of LIBS application to archaeometry" - Int. Conf. EMSLIBS - Bari 16-19/09/2013 - Invited paper
52. "Linolenic acid counteracts TNF negative effects on skeletal muscle cells" Felicia Carotenuto, Maria Cristina Albertini, Marco Rocchi, Dario Coletti, Alessandra Costa, Paolo Di Nardo and Laura Teodori, CYTO 2013 Conference, San Diego, CA - May 19-22, 2013: San Diego, CA
53. "Functionalization of decellularized scaffold for skeletal muscle tissue engineering" . Alessandra Costa, Paola Aprile, Paola Aulino, Barbara Perniconi, Sergio Adamo, Dario Coletti and Laura Teodori CYTO 2013 Conference, San Diego, CA - May 19-22, 2013: San Diego, CA
54. "Extracellular matrix in tissue engineering" (invited speaker) Laura Teodori, Alessandra Costa, Barbara Pernigoni, Paola Aprile, Dario Coletti. International Conference on Polymers on the Frontiers of Science & Technology Feb 21-23, 2013 Chandigarh, India
55. Alessandra Costa, Paola Aprile, Paola Aulino, Dario Rossi, Barbara Perniconi, Sergio Adamo, Dario Coletti and Laura Teodori. "Functionalization Of Decellularized Scaffold For Skeletal Muscle Tissue Engineering". World Conference on Regenerative Medicine 2013 (Leipzig)
56. G. Dattoli and E. Sabia - "Bunching Coefficients and the effect of Coulomb effects in FREE Electron laser" - FEL conference New York 2014
57. A. Coricciati, P. Corvaglia, A Largo, M.A. Caponero, "Smart composite device for structural health monitoring" Advances in Science and Technology, 83 (2013) 138, DOI:10.4028/www.scientific.net/AST.83.138
58. M.A. Caponero, F. Bonfigli, S. Libera, A. Polimadei, M.A. Vincenti, A. Zini, R.M. Montereali, "Enhancing temperature sensing features of FBGs by use of thin film aluminium coating", Fifth European Workshop on Optical Fibre Sensors, Ed. Leszek R. Jaroszewicz, Proc. SPIE Vol. 8794 (2013) 87943R, doi: 10.1117/12.2026826.
59. S. Gagliardi, C. Paoletti, R. D'Amato, M. Falconieri, "Characterization of electron transport in titania electrodes for photoelectrochemical applications", Proc. of FEMS-EUROMAT 2013, European Congress and Exhibition on Advanced Materials and Processes, (2013).
60. M.A. Caponero, F. Bonfigli, S. Libera, A. Polimadei, M.A. Vincenti, A. Zini, R.M. Montereali, "Enhancing temperature sensing features of FBGs by use of thin film aluminium coating in EWOF2013", 5th European Workshop on Optical Fibre Sensors, Krakow, Poland, 19-22 maggio 2013, 87943, 8794-184.
61. R. M. Montereali, F. Bonfigli, M. A. Vincenti, E. Nichelatti, "Lira: lithium fluoride radiation imaging thin film detectors with enhanced sensitivity", in Fotonica 2013, 15° Convegno Nazionale delle Tecnologie Fotoniche, Milano, 21-23 Maggio 2013, ISBN 9788887237160.
62. M.A. Caponero, F. Bonfigli, S. Libera, A. Polimadei, M.A. Vincenti, A. Zini, R.M. Montereali, "Uniform Thin Film Aluminium Coating of FBG Sensors for Enhanced Temperature Sensing and Functionalisation", in Fotonica 2013, 15° Convegno Nazionale delle Tecnologie Fotoniche, Milano, 21-23 Maggio 2013, ISBN 9788887237160.
63. F. Francini, R.M. Montereali, E. Nichelatti, M.A. Vincenti, N. Canci, E. Segreto, F. Cavanna, F. Di Pompeo, F. Carbonara, G. Fiorillo, F. Perfetto, "VUV-VIS optical characterization of Tetraphenyl-butadiene films on glass and specular reflector substrates from room to liquid Argon temperature", LIDINE 2013: LIGHT Detection In Noble Elements, May 29-31 2013, Fermi National Accelerator

- Laboratory (One West). Proc. of LIDINE 2013: LIGHT Detection in Noble Elements, 2013 JINST 8 C09010, pp. 1-22, published by IOP Publishing for SISSA Medialab, doi:10.1088/1748-0221/8/09/C09010
64. M. Piccinini, F. Ambrosini, A. Ampollini, M. Carpanese, L. Picardi, C. Ronsivalle, F. Bonfigli, M.A. Vincenti, S. Libera and R.M. Montereali, "Optical spectroscopy and imaging of colour centres in lithium fluoride crystals and thin films irradiated by 3 MeV proton beams", in REI-2013, 7th International Conference on Radiation Effects in Insulators, Helsinki, Finland, 30 giugno - 5 luglio 2013, PB-23.
 65. M.A. Vincenti, F. Bonfigli, G. Messina, R.M. Montereali, A. Rufoloni, E. Nichelatti, "Photoluminescence of colour centres in thermally-evaporated LiF films for radiation imaging detectors", "Ettore Majorana" Foundation And Centre For Scientific Culture, International School of Atomic and Molecular Spectroscopy Nano-structures for optics and Photonics, Optical Strategies for Enhancing Sensing, Imaging, Communication, and Energy Conversion, Erice, Sicily, Italy; July 4-19, 2013.
 66. F. Bonfigli, A. Faenov, F. Flora, M. Francucci, P. Gaudio, A. Lai, S. Martellucci, L. Mezi, R. M. Montereali, A. Poma, L. Reale, M. Richetta, L. Spanò, A. Tucci, M. A. Vincenti, "Contact X-ray microscopy on lithium fluoride using laser-plasma soft X-ray sources", in FisMat 2013, Italian National Conference on Condensed Matter Physics, Milano, 9 - 13 settembre 2013, #511.
 67. F. Bonfigli, D. Hampai, S.B. Dabagov and R.M. Montereali, "High-resolution fluorescence imaging by LiF detectors for characterization of X-ray poly-capillary optics", in FOI 2013, 1st EOS Topical Meeting on Frontiers in Optical Imaging, Murten, Svizzera, 16 - 18 settembre 2013, 1569776863.
 68. F. Bonfigli, A. Cecilia, S. Heidari Bateni, E. Nichelatti, D. Pelliccia, F. Somma, M.A. Vincenti, T. Baumbach, R.M. Montereali, "Rivelatori basati su film sottili di fluoruro di litio per imaging a raggi X senza lenti ed in proiezione", XCIX Congresso Nazionale SIF, Trieste, 23 - 27 settembre 2013, p. 91- 92.
 69. M. Piccinini, F. Ambrosini, A. Ampollini, M. Carpanese, L. Picardi, C. Ronsivalle, F. Bonfigli, S. Libera, M.A. Vincenti and R.M. Montereali, "Spettroscopia e microscopia ottica di centri di colore in cristalli e film di fluoruro di litio irraggiati con protoni di energia 3 MeV" - XCIX Congresso Nazionale SIF, Trieste, 23 - 27 settembre 2013, p. 237.
 70. F. Marracino, F. Ambrosini, A. Ampollini, F. Bonfigli, M. Carpanese, S. Libera, R.M. Montereali, L. Picardi, C. Ronsivalle, M.A. Vincenti, G. Vitiello, M. Piccinini, M. Balduzzi, G. Esposito, A. Tabocchini, "Uso di un Acceleratore Lineare di protoni da 7 MeV per esperimenti di radiobiologia", Use of a 7 MeV proton linear accelerator for radiobiology experiments, in AIFM 2013, 8° Congresso Nazionale Associazione Italiana di Fisica Medica, Torino, 16-19 novembre 2013.
 71. R.M. Montereali, F. Bonfigli, E. Nichelatti, M.A. Vincenti, "Luminescent lithium fluoride thin-film detectors for X-ray spatial metrology", , in ICFDT 2013, 3° International Conference Frontiers in Diagnostic Technologies, Frascati, 25-27 novembre 2013, p. 36-37.
 72. M. Piccinini, F. Ambrosini, A. Ampollini, M. Carpanese, L. Picardi, C. Ronsivalle, F. Bonfigli, S. Libera, M.A. Vincenti and R.M. Montereali, "Solid state detectors based on point defects in lithium fluoride for advanced proton beam diagnostics", ICFDT 2013, 3° International Conference Frontiers in Diagnostic Technologies, Frascati, 25-27 Novembre 2013, p. 6. (Invited paper)..
 73. M. Valentini, C. Malerba, F. Biccari, E. Salza, A. Santoni, C. L. Azanza Ricardo, P. Scardi, A. Mittiga, "Study of CZTS Solar Cells Obtained from Two Different Types of Precursors", 28th EU PVSEC - Parc des Expositions Paris Nord Villepinte, 30/9-4/10 2013.
 74. C. Paoletti, S. Gagliardi, R. D'Amato, M. Falconieri, "Characterization of electron transport in titania electrodes for photoelectrochemical applications", in FEMS-EUROMAT 2013, European Congress and Exhibition on Advanced Materials and Processes, Siviglia (Spagna), 8-13 Settembre 2013.
 75. P. Saccomandi, G. Lupi, E. Schena, A. Polimadei, M. A. Caponero, F. Panzera, M. Martino, F.M. Di Matteo, S. Sciuto, S. Silvestri "Influence of FBG sensors length on temperature measures in laser-irradiated pancreas: Theoretical and experimental evaluation", Proceedings of the Annual International Conference on the IEEE Engineering in Medicine and Biology Society, EMBS, (2013) art. no. 6610356, pp. 3737-3740. DOI: 10.1109/EMBC.2013.6610356
 76. E. Popovici, G. Demian, E. Dutu, A.D. Badoi, R. D'Amato, G. Terranova, E. Borsella, M. Demian, S. Radu, "Studies on thermal processes in the synthesis of nanostructured SiC by laser pyrolysis", 2nd Central and Eastern European Conference on Thermal Analysis and Calorimetry, Vilnius (Lithuania), 27-30 August 2013.
 77. F. Rondino, R. D'Amato, G. Terranova, E. Borsella, M. Falconieri, "Thermal diffusivity enhancement in titania based nanofluids: role of nanoparticles aggregation", European Conference on Nonlinear Optical Spectroscopy (ECONOS) and CARS Workshop 2013, University of Exeter (UK), 22-24 April 2013.
 78. S. Almaviva, S. Botti, L. Cantarini, A. Palucci, A. Puiu, F. Schnuerer, W. Schweikert, F. S. Romolo "Raman Spectroscopy for the detection of explosives and their precursors on cloth in fingerprint concentration: a reliable technique for security and counterterrorism issues" Symposium on Optics and Photonics for a counterterrorism, crime fighting and defence IX, Proc. of SPIE Vol. 8901 890102-9, DOI 10.1117/12.2028855
 79. S. Almaviva, S. Botti, L. Cantarini, A. Palucci, A. Rufoloni, T. Moller, F. S. Romolo "Trace detection of explosives by Surface Enhanced Raman Spectroscopy" "Proc. of the 2nd European Conference on Detection of Explosives: closing the gap
 80. Rosa Maria Montereali, "Le nanotecnologie nella realta' industriale e nella ricerca", Universita' degli Studi di Roma Sapienza, Giornata di presentazione Laurea Magistrale in Ingegneria delle Nanotecnologie, a.a. 2013-2014, Roma, 26 Giugno 2013, Relatore ENEA.
 81. Rosaria D'Amato, "Sintesi e caratterizzazione di nanopolveri per i Beni Culturali", Nanoforum 2013, IX edizione, Micro, nano and advanced technologies: where research meets business, Universita' di Roma "La Sapienza", Roma, 18-20 Settembre 2013.
 82. Antonino Santoni, "XPS spectroscopy of low atomic number elements: B thin films on Al₂O₃ substrates", Helium Replacement in Italy- HeRe in Italy, ENEA Frascati, 2-3 Dicembre 2013
 83. E. MacPherson, G.P. Gallerano, G.-S. Park, H. Hintzsche, G. Wilmsink, "Guest Editorial: Terahertz Imaging and Spectroscopy for Biology and Biomedicine" IEEE J. Biomedical and Health Informatics, 17, n. 4, July, 765 (2013)
 84. P. Di Lazzaro, D. Murra, B. Schwartz: "Pattern recognition after image processing of low-contrast images, the case of the Shroud of Turin" Pattern Recognition 46, 1964-1970 (2013). Published online <http://www.sciencedirect.com/science/article/pii/S0031320312005377>
 85. P. Di Lazzaro, S. Bollanti, F. Flora, L. Mezi, D. Murra, A. Torre: "Mitigation of ion and particulate emission from laser-produced plasmas used for extreme ultraviolet lithography" Applied Surface Science 272, 13-18 (2013). Published online <http://www.sciencedirect.com/science/article/pii/S0169433212005946>
 86. P. Di Lazzaro, S. Bollanti, F. Flora, L. Mezi, D. Murra and A. Torre: "Characterization of sources for extreme ultraviolet lithography" in Handbook of Short Wavelength Laboratory Sources A. Michette Ed. (RSC Publishing, June 2013) ISBN 13: 9781849734561
 87. S. Bollanti, P. Di Lazzaro, F. Flora, L. Mezi, D. Murra, A. Torre: "ENEA Extreme Ultraviolet Lithography Micro-Exposure Tool: main features" in Handbook of Short Wavelength Laboratory Sources A. Michette Ed. (RSC Publishing, June 2013) ISBN 13: 9781849734561
 88. P. Di Lazzaro, D. Murra: "Figurative art, perception and hidden images in inverse perspective" Energia Ambiente e Innovazione 1-2, 42-51 (2013). Available online <http://www.enea.it/it/produzione-scientifica/pdf-eai/n.1-2-gennaio-aprile-2013/10-inverse-perspective-pdf>

89. R. Balveti, A. Botticelli, M. L. Bargellini, M. Battaglia, G. Casadei, A. Filippini, E. Pancotti, L. Puccia, C. Zampetti, G. Bozanceff, G. Brunetti, A. Chiapparelli, A. Guidoni, L. Rubini, A. Tripodo, "De ubiqutate mentis: Giasone modello cibernetico di processi mentali" *Nuovo Saggiatore* Vol. 29, no. 1-2, 17-30 (2013)
90. V. Petrillo, M. Artioli, F. Ciocci, G. Dattoli, A. Petralia, C. Ronsivalle, M. Quattromini, E. Sabia, L. Giannesi, M.P. Anania, G. Gatti, R. Pompili, C. Vaccarezza, F. Villa, A. Bacci, A.R. Rossi, J.V. Rau, P. Musumeci, A. Cianchi, A. Mostacci "Generation of a train of short pulses by means of FEL emission of a combed electron beam". 35th Intern. Free-Electron Laser Conference, New York (Manhattan), USA; 08/2013
91. M. Piccinini, F. Ambrosini, A. Ampollini, M. Carpanese, L. Picardi, C. Ronsivalle, F. Bonfigli, M. A. Vincenti, S. Libera and R.M. Montereali, "Optical spectroscopy and imaging of colour centres in lithium fluoride crystals and thin films irradiated by 3 MeV proton beams", The 17th International Conference on Radiation Effects in Insulators (REI) 30 June -5 July 2013, Helsinki (FI)
92. F. Marracino, F. Ambrosini, A. Ampollini, F. Bonfigli, M. Carpanese, R.M. Montereali, L. Picardi, C. Ronsivalle, M.A. Vincent, G. Vitiello, M. Piccinini, M. Balduzzi, G. Esposito, A. Tabocchini. "Use di un Acceleratore Lineare di protoni da 7 MeV per esperimenti di radiobiologia", Atti dell'ottavo Congresso Nazionale dell'Associazione Italiana di Fisica Medica (AIFM) (16-19 Novembre 2013, Torino).
93. S. Ceccuzzi, G. Dattoli, E. Di Palma, A. Doria, G.P. Gallerano, E. Giovenale, F. Mirizzi, I. Spassovsky, G. Ravera, V. Surrenti, A. Tuccillo, "CARM: a THz source for plasma heating", Proceedings 38th International Conference on Infrared, Millimeter and Terahertz Waves, IRMMW-THz2013, Mainz, Germany, September 1-6, 2013, DOI 10.1109/IRMMW-THz.2013.6665644, Page(s): 1 - 2 (2013)
94. I. Spassovsky, S. Ceccuzzi, G. Dattoli, E. Di Palma, A. Doria, G.P. Gallerano, E. Giovenale, F. Mirizzi, G. Ravera, V. Surrenti, A. Tuccillo, "CARM: a THz source for plasma heating", 6th UK-Europe-China Millimeter Waves and THz Technology Workshop UCMMT-2013, DOI: 10.1109/UCMMT.2013.6641523 Page(s): 1 - 2, (2013)
95. G.P. Gallerano, "THz radiation and its applications: A review of events and a glance to the future", 6th UK-Europe-China Millimeter Waves and THz Technology Workshop UCMMT-2013, DOI: 10.1109/UCMMT.2013.6641531, Page(s): 1 (2013)
96. P. Di Lazzaro, S. Bollanti, F. Flora, L. Mezi, D. Murra, A. Torre, F. Bonfigli, R.M. Montereali, M.A. Vincenti: "Extreme ultraviolet marking system for anti-counterfeiting tags with adjustable security level" XIX International Symposium on High-Power Laser Systems and Applications 2012, Proc. SPIE vol. 8677 (2013) pp. 86770T; doi: 10.1117/12.2010400
97. S. Almaviva, S. Bollanti, F. Bonfigli, P. Di Lazzaro, M. Francucci, A. Lai, L. Mezi, D. Murra, R. M. Montereali, M. A. Vincenti, P. Gaudio, S. Martellucci, M. Richetta, A. Poma, L. Spanò, A. Tucci, L. Reale, A. Faenov, T. Pikuz: "Contact X-ray microscopy on lithium fluoride using laser-plasma soft X-ray sources" FisMat 2013, Italian National Conference on Condensed Matter Physics, Milano (2013) p. 241.
98. R. Balveti, A. Botticelli, M.L. Bargellini, M. Battaglia, G. Casadei, A. Filippini, E. Pancotti, L. Puccia, C. Zampetti, G. Bozanceff, G. Brunetti, A. Guidoni, L. Rubini, A. Tripodo, "Towards the construction of a cybernetic organism: the place of mental processes", Proceedings Int. Conference of Complexity, Cybernetics, and Informing Science and Engineering: CCISE 2013 June 30 - July 6, 2013 Porto, Portugal p. 13-15
99. G.P. Gallerano, "Effetti e applicazioni delle NIR: Il caso della radiazione Terahertz", Convegno Sviluppi nella prevenzione e protezione dalle radiazioni ionizzanti e non ionizzanti, CISAM, S. Piero a Grado (PI) 29-30 Maggio 2013 – Invited paper
100. S. Ceccuzzi, G. Dattoli, E. Di Palma, A. Doria, G.P. Gallerano, E. Giovenale, F. Mirizzi, G. Ravera, I. Spassovsky, V. Surrenti, A. Tuccillo, "MM-Wave Cyclotron Auto-Resonance Maser for Plasma Heating", Proceedings 20th Topical Conference on Radio Frequency Power In Plasmas, Sorrento, Italy, June 25-28, 2013 - P3.10
101. E. Giovenale, A. Doria, G.P. Gallerano, I. Spassovsky: "Phase sensitive mm-wave and Terahertz imaging for art conservation studies", Italian National Conference on Condensed Matter Physics - FisMat2013, Milan, Italy September 9-13, 2013
102. G.P. Gallerano, "THz radiation and its applications: A review of recent literature & events and a glance to the future", 10th International Bioelectrics Symposium (BIOELECTRICS 2013), Karlsruhe, Germany, September 16-19, 2013 – Invited paper
103. P. Di Lazzaro: "A glance at the images on the Shroud of Turin and on the Tilma of Guadalupe: similarities and differences" Tercer encuentro de dos lienzos, Gerusalemme 28 Luglio 2013 – Invited paper
104. D. Murra, P. Di Lazzaro: "Immagine virtuale di specchi conici e anamorfofi: una trattazione esatta" XCIX Congresso nazionale SIF, Trieste 26 Settembre 2013
105. L. Mezi, S. Bollanti, P. Di Lazzaro, F. Flora, D. Murra, A. Torre: "Efficient extreme ultraviolet and soft X-rays plasma sources" at ENEA Frascati Conferenza nazionale di Fisica della Materia FISMAT 2013, Milano, 9-13 settembre 2013.

7.4 Technical reports

1. M.A. Vincenti, R.M. Montereali, G. Messina, E. Nichelatti, A. Mancini, A. Rufoloni, Growth and characterisation of thermally-evaporated lithium fluoride thin films for high-energy radiation detectors, RT ENEA, RT/2013/22/ENEA.
2. R. Francini, R.M. Montereali, E. Nichelatti, M.A. Vincenti, N. Canci, E. Segreto, F. Cavanna, F. Di Pompeo, F. Carbonara, G. Fiorillo, F. Perfetto, VUV-VIS optical characterization of Tetraphenyl-butadiene films on glass and specular reflector substrates from room to liquid Argon temperature, Instrumentation and detectors, arXiv:1304.6117 [physics.ins-det] (2013).
3. F. Rondino, V. Orsetti, A. Rufoloni, A. Santoni, "Preparazione e caratterizzazione morfologica di anodi di silicio nanostrutturati per batterie litio-ione", Report Rds 2013/239.
4. M. Valentini, C. Malerba, F. Biccari, C. Azanza, E. Esposito, R. Chierchia, P. Mangiapane, E. Salza, R. Sensoli, A. Santoni, M. Capizzi, P. Scardi, A. Mittiga, "Realizzazione di celle solari a film sottili policristallini di $\text{Cu}_2\text{ZnSnS}_4$ con efficienza superiore al 5%", Report RDS 2013.
5. F. Rondino, A. Ciavardini, M. Satta, A. Paladini, C. Frascetti, A. Filippi, B. Botta, A. Calcaterra, M. Speranza, A. Giardini, S. Piccirillo, Rendiconti Lincei, Ultraviolet and infrared spectroscopy of neutral and ionic non-covalent diastereomeric complexes in the gas phase, Rendiconti Lincei, Vol. 24, 3, 2013, 259-267.
6. R.M. Montereali e F. Bonfigli Versatile lithium fluoride thin-film solid-state detectors for nanoscale soft X-ray imaging, Laboratorio Elettra-Sincrotrone Trieste, 27 marzo 2013.
7. R.M. Montereali, Light-emitting lithium fluoride thin-films for nanoscale radiation imaging detectors and bio-photonics, Laboratoire de Physique de la Matière Vivante, Ecole Polytechnique Fédérale de Lausanne, EPFL, CH, 09/04/2013.
8. M.A. Vincenti, R.M. Montereali, G. Messina, E. Nichelatti, A. Mancini, A. Rufoloni, Growth and characterisation of thermally-evaporated lithium fluoride thin films for high-energy radiation detectors, RT ENEA, RT/2013/22/ENEA.
9. R. Francini, R.M. Montereali, E. Nichelatti, M.A. Vincenti, N. Canci, E. Segreto, F. Cavanna, F. Di Pompeo, F. Carbonara, G. Fiorillo, F. Perfetto, VUV-VIS optical characterization of Tetraphenyl-butadiene films on glass and specular reflector substrates from room to liquid Argon temperature,

- Instrumentation and detectors, arXiv:1304.6117 [physics.ins-det] (2013).
10. F. Rondino, V. Orsetti, A. Rufoloni, A. Santoni, "Preparazione e caratterizzazione morfologica di anodi di silicio nanostrutturati per batterie litio-ione", Report RdS 2013/239.
 11. M. Valentini, C. Malerba, F. Biccari, C. Azanza, E. Esposito, R. Chierchia, P. Mangiapane, E. Salza, R. Sensoli, A. Santoni, M. Capizzi, P. Scardi, A. Mittiga, "Realizzazione di celle solari a film sottili policristallini di Cu₂ZnSnS₄ con efficienza superiore al 5%", Report RDS 2013.
 12. F. Rondino, A. Ciavardini, M. Satta, A. Paladini, C. Frascchetti, A. Filippi, B. Botta, A. Calcaterra, M. Speranza, A. Giardini, S. Piccirillo, Ultraviolet and infrared spectroscopy of neutral and ionic non-covalent diastereomeric complexes in the gas phase, *Rendiconti Lincei*, Vol. 24, 3, 2013, 259-267.
 13. P. Di Lazzaro, D. Murra: "L'anamorfose tra arte, percezione visiva e prospettive bizzarre" RT/2013/05/ENEA (2013). <http://openarchive.enea.it/bitstream/handle/10840/4479/RT-2013-5-ENEA.pdf?sequence=1>
 14. D. Murra, P. Di Lazzaro: "Immagine virtuale di specchi conici per anamorfose: calcolo analitico ed esperimenti" RT/2013/23/ENEA (2013).
 15. Arnon S., Fiorani L., Agboola J. I., Borelli R., Eretz Kedosh A., Giannini E., Green N., Mann D., Marullo S., Menicucci I., Musheyev A., Nuri I., Oved I., Pilipenko V., Pistilli M., Puiu A., Tzidki T., Uzan H. - UNELAS 2012 Report "Report to the Italian Ministry of Foreign Affairs for the Unelas Project", Italian National Agency for New Technologies, Energy and Sustainable Economic Development, Frascati, Italy, 192 pp. (2013)
 16. Colao F., Fiorani L., Palucci A., Angelini F., Marullo S. - "Descrizione del sistema lidar pre-esistente sulla base del quale verrà progettato il nuovo lidar" - Report to the Italian Ministry of Education, Universities and Research (in Italian) for the Ritmare Project, Italian National Agency for New Technologies, Energy and Sustainable Economic Development, Frascati, Italy, 12 pp. (2013)
 17. Colao F., Fiorani L., Palucci A., Angelini F., Marullo S. - "Rapporto con le specifiche iniziali per un lidar idrografico e lista delle misure in situ effettuate fino al Dicembre 2012 rese disponibili al progetto" Report to the Italian Ministry of Education, Universities and Research (in Italian) for the Ritmare Project, Italian National Agency for New Technologies, Energy and Sustainable Economic Development, Frascati, Italy, 37 pp. (2013)
 18. Colao F., Fiorani L., Palucci A., Angelini F., Marullo S. - "Prototipo microsensore ottico e risultati campagne di misura preliminari" Report to the Italian Ministry of Education, Universities and Research (in Italian) for the Ritmare Project, Italian National Agency for New Technologies, Energy and Sustainable Economic Development, Frascati, Italy, 30 pp. (2013)

7.5 Prizes

1. Prize from Science and Technology of Homeland Security Department USA for the contribution with RADEX Project (Raman Detection of Explosives), in the special program of NATO STANDEX (Standoff Detection of Explosives).
2. DigiBIC Award 2013 for Digital Technologies concerning the category "Research Institutes" for the ENEA technology "3D color Laser Scanner" for outdoor use and for the underwater 3D Laser Scanner (EBN Annual Congress, European Business & Innovation Centre Network, Derry, Londonderry, Ireland, 31 May 2013).
3. Luca Giannessi - International FEL Prize 2013.

FRONT COVER :

Color center photoluminescence 3D plot, stored in a solid state lithium fluoride radiation imaging film detector, showing the Bragg peak energy release after exposure to the TOP-IMPLART linac 7 MeV proton beam.

BACK COVER :

(left): Bragg peak fluorescence optical image, stored by radiation-induced color centers in a 1 μm thick LiF film detector, after exposure to the TOP-IMPLART linac 3 MeV proton beam at grazing incidence.

(right): Bragg peak fluorescence optical image, stored by radiation induced color centers in a LiF crystal, after exposure to the TOP-IMPLART linac 7 MeV proton beam.



Italian National Agency for New Technologies, Energy and Sustainable Economic Development